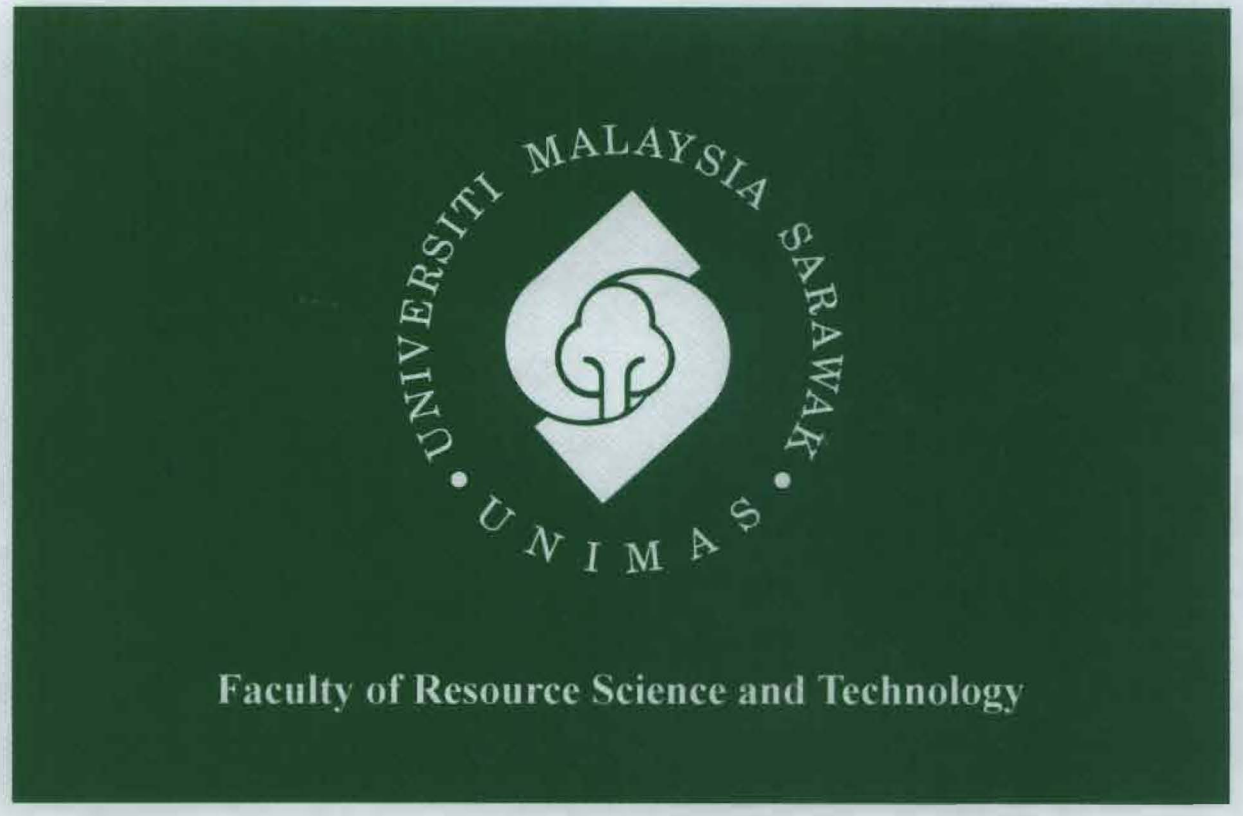

Magnetic Hybrid Alg/TiO_2/FeNPs Triads for the Efficient Removal of Pollutants in Water

Nurfatyha Rusydah Bt Mohamad Shahdad

Master of Science
2018

UNIVERSITI MALAYSIA SARAWAK

Grade: _____

Please tick (√)
Final Year Project Report ☐
Masters ☑
PhD ☐

DECLARATION OF ORIGINAL WORK

This declaration is made on the ....18.....day of..SEPTEMBER.....2018.

Student's Declaration:

I Nurfatyha Rusydah Bt Mohamad Shahdad, 15020871, Faculty of Resource Science and Technology
(PLEASE INDICATE STUDENT'S NAME, MATRIC NO. AND FACULTY) hereby declare that the work entitled, Magnetic Hybrid Alg/TiO_2/FeNPs Triads for the Efficient Removal of Pollutants in Water is my original work. I have not copied from any other students' work or from any other sources except where due reference or acknowledgement is made explicitly in the text, nor has any part been written for me by another person.

18/9/2018
Date submitted

Nurfatyha Rusydah Bt Mohamad Shahdad (15020871)
Name of the student (Matric No.)

Supervisor's Declaration:

I Dr. Devagi Kanakaraju (SUPERVISOR'S NAME) hereby certifies that the work entitled, Magnetic Hybrid Alg/TiO_2/FeNPs Triads for the Efficient Removal of Pollutants in Water (TITLE) was prepared by the above named student, and was submitted to the "FACULTY" as a * partial/full fulfillment for the conferment of ---------- (PLEASE INDICATE THE DEGREE), and the aforementioned work, to the best of my knowledge, is the said student's work

Received for examination by: Dr Devagi (Name of the supervisor)

Date: 19/9/18

I declare this Project/Thesis is classified as (Please tick (√)):

☐ **CONFIDENTIAL** (Contains confidential information under the Official Secret Act 1972)*
☐ **RESTRICTED** (Contains restricted information as specified by the organisation where research was done)*
☑ **OPEN ACCESS**

Validation of Project/Thesis

I therefore duly affirmed with free consent and willingness declared that this said Project/Thesis shall be placed officially in the Centre for Academic Information Services with the abide interest and rights as follows:

- This Project/Thesis is the sole legal property of Universiti Malaysia Sarawak (UNIMAS).
- The Centre for Academic Information Services has the lawful right to make copies for the purpose of academic and research only and not for other purpose.
- The Centre for Academic Information Services has the lawful right to digitise the content to for the Local Content Database.
- The Centre for Academic Information Services has the lawful right to make copies of the Project/Thesis for academic exchange between Higher Learning Institute.
- No dispute or any claim shall arise from the student itself neither third party on this Project/Thesis once it becomes sole property of UNIMAS.
- This Project/Thesis or any material, data and information related to it shall not be distributed, published or disclosed to any party by the student except with UNIMAS permission.

Student's signature: _____ (18/9/2018)
(Date)

Supervisor's signature: _____
(Date) 19/9/18

Current Address:
No.279, Kampung Haji Baki, Blok C, Lorong 16, 93250 Kuching, SARAWAK.

Notes: * If the Project/Thesis is **CONFIDENTIAL** or **RESTRICTED**, please attach together as annexure a letter from the organisation with the period and reasons of confidentiality and restriction.

[The instrument was duly prepared by The Centre for Academic Information Services]

Magnetic Hybrid Alg/TiO_2/FeNPs Triads for the Efficient Removal of Pollutants in Water

Nurfatyha Rusydah Bt Mohamad Shahdad

A thesis submitted

In fulfillment of the requirement for the degree of Master of Science

(Environmental Chemistry)

Faculty of Resource Science and Technology
UNIVERSITI MALAYSIA SARAWAK
2018

DECLARATION

I hereby declare that the work in this thesis was carried out in accordance with the regulations of Universiti Malaysia Sarawak. It is original and is the result of my work, unless otherwise indicated or acknowledged as referenced work. The thesis has not been accepted for any degree and is not concurrently submitted in candidature of any other degree.

Nurfatyha

Nurfatyha Rusydah Bt Mohamad Shahdad (15020871)

Faculty of Resource Science and Technology

Universiti Malaysia Sarawak

Date: 14h September 2018

ACKNOWLEDGEMENT

First and foremost, I would like to thank God Almighty for the strength, knowledge, ability and opportunity to undertake this research study and to persevere and complete it satisfactorily. Without His blessing, this achievement would not have been possible.

In my journey towards this master, I have found an inspiration, a role model and a pillar of support in my Guide, Dr. Devagi Kanakaraju. She has been there providing her heartfelt support and guidance all times and has given me invaluable guidance, inspiration and suggestions in my quest for knowledge.

My sincere thanks also goes to Professor Wan Azelee Wan Abu Bakar from Universiti Teknologi Malaysia, for sharing his knowledge and technique on response surface methodology (RSM). I have great pleasure in acknowledging my gratitude to my fellow labmates, Wong Soon Pang and Mohamad Hazim Bin Ya, for their advices and suggestion along this journey. Their support, encouragement and brilliant ideas have been great contributors in the completion of the thesis.

I would also like to thank Mr. Tomy Bakeh, Mr. Shafri Bin Semawi, Mr. Wahap Bin Marni for their kind guidance and assistance in instrumentation analysis. I would also like to acknowledge Dr Lim Ying Chin from UiTM Shah Alam for analysing XRD. Without her help, the quality of this thesis would be insufficient. It would not be appropriate if I omit the names of my dear friends Jennifer Jalan, Mohamad Amirul Bin Azmi and Malcolm Jeremiah, who have, in their own ways, kept me going on path to success, assisting me as per their abilities, in whatever manner possible and for ensuring that good times keep flowing.

Last but not least, my endless appreciation and love to my strength, my family. The blessing of my parents Mr. Mohamad Shahdad bin Yusup and Mrs. Suriani Bt Suhud and the love and care of my sister and brother Ifa'Iza and Muhammad Syafiq, have all made a tremendous contribution in helping me reach this stage in my life.

ABSTRACT

Nanocomposite materials have been receiving considerable attention in wastewater treatment due to their improved photocatalytic efficiency. However, solutions are needed to cope with problem arise from the formation of titanium dioxide (TiO_2) slurry in the treated water. In this context, the possibility to use photocatalytic magnetic nanoparticles to ease separation from the treated water offers an appealing solution. A facile non-thermal method was applied to synthesize a hybrid nanocomposite consisting of TiO_2/calcium alginate (Alg) and magnetite nanoparticles (FeNPs) referred to as Alg/TiO_2/FeNPs. The efficiency of Alg/TiO_2/FeNPs was assessed for the removal of methylene blue (MB) and a mixture of three heavy metals (MHM) consisting of Cr(III), Cu(II) and Pb(II) ions in aqueous solutions under ultraviolet (UVC) irradiation (λ=254 nm). The potential of adsorbent Alg as a barrier to prevent direct contact between magnetic core and TiO_2 was investigated by varying the concentrations of sodium hydroxide (NaOH) and Alg. The performance of four different synthesized Alg/TiO_2/FeNPs samples (Alg/TiO_2/Fe-1, Alg/TiO_2/Fe-2, Alg/TiO_2/Fe-3 and Alg/TiO_2/Fe-4) was found to be fairly comparable and stable based on their efficiency in removing MB from aqueous solution due to the physico-chemical characterization (surface morphology, functional groups, and elemental analysis) which supports the performance of Alg/TiO_2/FeNPs. For the optimization study using the response surface methodology (RSM) with three factorial Box-Behnken experimental designs, 0.2 g of Alg/TiO_2/Fe-2 was chosen as it exhibited the highest MB removal of 97.6% for an initial concentration of 5 ppm of MB after 120 min treatment under UVC irradiation. Among the three independent variables studied (i.e., pH, contact time and initial MB concentration), the initial concentration of MB had significant effect towards the MB removal performance. A recycling study was done and confirmed the stability of Alg/TiO_2/Fe-2 up to 3 cycles, with only a slight drop in the removal efficiency from 93.1% to

88.5%. For MHM removal, 0.6 g of Alg/TiO_2/Fe-2 was selected as the optimized adsorbent dosage. Similar parameters as in MB removal were investigated for the removal of MHM using RSM *via* Box-Behnken design. Removal percentages of Pb(II), Cr(III), and Cu(II) ions in the aqueous solution mixture solution were 99.6%, 98.6%, and 98.4%, respectively under optimized conditions of pH 6.80 and 44 ppm within 72 min of irradiation. The removal of Pb(II) ions was the highest as it exhibited the smallest degree of hydration of metal ions precursor compared to Cr(III) and Cu(II) ions. Thus, this made Pb(II) ions to be easily adsorbed onto the surface of Alg/TiO_2/Fe-2. The recycling experiments showed no significant changes with only slight increment of Pb(II) ions in the second cycle when the Alg/TiO_2/Fe-2 beads were retrieved and reused in three consecutive cycles of the heavy metals removal. This finding again confirmed the stability of Alg/TiO_2/Fe-2 when reused repeatedly in the photocatalytic treatment of multi-heavy metals solution. Hence, the fabricated Alg/TiO_2/FeNPs nanocomposites could be a potential functional material for treating artificial dye and heavy metals laden wastewater.

Keywords: Photocatalysis, adsorbent, response surface methodology, Fe_3O_4 nanoparticles, titanium dioxide, heavy metals, dye

Kecekapan Hibrid Magnetik Alg/TiO_2/FeNPs bagi Penyingkiran Bahan Pencemaran Air

ABSTRAK

Peningkatan kecekapan pemfotomangkin dalam bahan komposit-nano melalui rawatan air sisa telah menerima perhatian yang menggalakkan. Walaubagaimanapun, beberapa kaedah diperlukan bagi mengatasi masalah pembentukan ampaian titanium dioksida (TiO_2) dalam air yang telah dirawat. Bagi memudahkan pengasingan daripada air yang telah dirawat, zarah-nano magnetik pemfotomangkin berpotensi menawarkan kaedah yang bersesuaian. Satu kaedah bukan-termal yang mudah telah diaplikasikan untuk mensintesis komposit-nano hibrid, terdiri daripada TiO_2/kalsium alginat (Alg) dan zarah-nano magnetik (FeNPs) atau lebih dikenali sebagai Alg/TiO_2/FeNPs. Keberkesanan Alg/TiO_2/FeNPs telah dikaji melalui penyingkiran metilena-biru (MB) dan campuran antara tiga jenis logam berat (LBC) iaitu ion Cr(III), Cu(II) dan Pb(II) dalam larutan akueus di bawah penyinaran ultralembayung (λ=254 nm). Potensi zat penjerap Alg sebagai sempadan hubungan langsung antara teras magnetik dan TiO_2 telah dikaji dengan mengubah kepekatan natrium hidroksida (NaOH) dan Alg. Berdasarkan kecekapan sampel Alg/TiO_2/FeNPs (Alg/TiO_2/Fe-1, Alg/TiO_2/Fe-2, Alg/TiO_2/Fe-3 dan Alg/TiO_2/Fe-4) dalam penyingkiran MB daripada larutan akueus, semua sampel telah menunjukkan prestasi yang hampir sama dan stabil disebabkan oleh ciri-ciri fisio-kimia Alg/TiO_2/FeNPs (sifat permukaan, kumpulan fungsi, dan komposisi analisis). Kajian pengoptimuman melalui kaedah Gerak Balas Permukaan (GBP) dengan rekaan eksperimen Box-Behnken tiga faktorial telah menggunakan 0.2 g Alg/TiO_2/Fe-2 kerana ia menunjukkan penyingkiran MB yang tertinggi iaitu 97.6% selepas 120 minit pada kepekatan 5 ppm MB. Dalam tiga pembolehubah bebas yang telah dikaji (seperti pH, tempoh masa, dan kepekatan awal MB), kepekatan awal MB mempunyai kesan signifikan terhadap prestasi penyingkiran

MB. Kajian kitar semula yang telah dijalankan telah membuktikan kestabilan Alg/TiO_2/Fe-2 melalui tiga kitaran, dengan hanya sedikit penurunan penyingkiran MB daripada 93.1% kepada 88.5%. Bagi penyingkiran LBC, 0.6 g Alg/TiO_2/Fe-2 telah dipilih sebagai dos optimum. Kajian penyingkiran LBC menggunakan parameter yang sama dengan penyingkiran MB iaitu malalui RSM dengan reka bentuk Box-Behnken. Pada tahap optimum iaitu pH 6.80 dan 44 ppm dalam tempoh masa penyinaran selama 72 min, kadar penyingkiran logam campuran ion Pb(II), Cr(III) dan Cu(II) dalam larutan akueus adalah masing-masing 99.6%, 98.6%, dan 98.4%. Penyingkiran ion Pb(II) adalah yang tertinggi kerana ia menunjukkan tahap penghidratan ion prekursor logam yang paling rendah berbanding ion Cr(II) dan Cu(II). Dengan ini, ion Pb(II) boleh menjerap dengan mudah ke atas permukaan Alg/TiO_2/Fe-2. Kajian kitaran semula mendapati bahawa tiada perbezaan yang ketara dengan hanya sedikit peningkatan peratusan penyingkiran ion Pb(II) pada kitaran yang kedua apabila Alg/TiO_2/Fe-2 diambil dan digunakan semula dalam tiga kitaran berturut-turut bagi penyingkiran logam berat. Hasil kajian ini telah membuktikan kestabilan Alg/TiO_2/Fe-2 setelah digunakan berulangkali di dalam rawatan pemfotomangkin untuk larutan pelbagai logam berat. Oleh hal yang demikian, komposit-nano Alg/TiO_2/FeNPs ini boleh menjadi salah satu bahan yang berpotensi untuk merawat pewarna tiruan dan logam berat di dalam air sisa.

***Kata kunci**: Pemfotomangkin, penjerap, gerak balas permukaan, zarah-nano Fe_3O_4, titanium dioksida, logam berat, pewarna*

TABLE OF CONTENTS

LIST OF TABLES

LIST OF FIGURES

LIST OF ABBREVIATIONS

λ	Wavelength
ANOVA	Analysis of Variance
AOPs	Advanced Oxidation Processes
Alg/TiO_2/FeNPs	Alginate titanium dioxide magnetite nanoparticles
Alg	Alginate
BBD	Box-Behnken Design
e^-	Electron
EDX	Energy-Dispersive X-ray Spectroscopy
FTIR	Fourier Transform Infra-Red Spectroscopy
h^+	hole
hv	Photon energy
MHM	Mixed heavy metal
NPs	Nanoparticles
pH_{PZC}	Point of Zero Charge
RSM	Response Surface Methodology
SEM	Scanning Electron Microscope
UV	Ultraviolet
UV-Vis	Ultraviolet Visible
VB	Valence Band

CHAPTER 1

INTRODUCTION

1.1 General Introduction

Water pollution has been recognized as one of the major global environmental issues due to its considerable impacts to the aquatic ecosystems and human health. In light of water pollution, it is becoming extremely difficult to ignore the existence of two types of water pollutant namely dyes and heavy metals. The existence of dyes and heavy metals in the environmental components are typically resulted and heightened from various industrial activities such as textiles, printing, electroplating, industrial wastes, agricultural and mining activities (Rafatullah *et al.*, 2010; Onundi *et al.*, 2011; Zeitoun & Mehana, 2014). As both dyes and heavy metals are known for their persistent and non-biodegradable characteristics when present in the aquatic environment, the arising toxicity and carcinogenicity of these toxic pollutants remains of a great concern (Aguedach *et al.*, 2005; Nassar *et al.*, 2015; Edokpayi *et al.*, 2016). As such, the removal of these pollutants from wastewater has been attracting a lot of interest.

Conventional wastewater treatments such as flocculation, coagulation, precipitation, membrane filtration, and adsorption have been reported to produce low efficiency in removing contaminated wastewater consisting of dyes and heavy metals (Roussy *et al.*, 2005; Behbahani, 2013; Dargo *et al.*, 2014). Several limitations commonly encountered when using these conventional water treatment technologies are incomplete removal of organic compounds, since they are only converted from liquid phase into the solid phase (Bet-moushoul *et al.*, 2016), high operating costs (Boczkaj & Fernandes, 2017), high chemical consumption (Fu & Wang, 2011), and also the formation of toxic by-products (Gaya & Abdullah, 2008; Dong *et al.*, 2015).

However, among the conventional wastewater treatment methods, adsorption has been recognized as one of the most efficient and practical ways to eliminate both dye and heavy metals from wastewater (Forgacs *et al.*, 2004; Kalantari *et al.*, 2014). Adsorbents such as alum, ferric chloride, and activated carbon have been typically applied for the removal of water pollutants. Nonetheless, this method is also confined to several drawbacks, such as the continuous accumulation of pollutants or adsorbate on the surface of the adsorbents without decomposition, generation of toxic secondary pollutants, and also incomplete pollutant removal (Costa *et al.*, 2012). Therefore, most of the afore-mentioned processes are restricted to their own limitations to remediate dye and heavy metals contaminated wastewaters. A new approach or an improvised adsorption process becomes necessary to overcome these limitations.

In this context, titanium dioxide (TiO_2) photocatalysis, an advanced oxidation process (AOP) has been regarded as a promising alternative approach in various wastewaters purification due to its ability to mineralize recalcitrant pollutants into non-toxic products such as CO_2, H_2O and mineral acids (Narayana *et al.*, 2011; Costa *et al.*, 2012; Baloyi *et al.*, 2014; Kanakaraju *et al.*, 2015). Typically, AOPs are based on the utilization of powerful oxidants such as hydroxyl radicals (•OH), ozone and fluorine. Series of oxidation-reduction processes resulting from TiO_2 photocatalysis are able to degrade the organic pollutant like dyes into a simpler compounds and even mineralizing the parent dye compounds into CO_2 and H_2O (Boczkaj & Fernandes, 2017). In the case of inorganic metal ions in water, TiO_2 photocatalysis has been reported to be able to reduce the metal ions to its lower valence state (Farzana & Meenakshi, 2015). TiO_2 is said to be one of the most effective semiconductor photocatalysts because it exhibits higher photocatalytic behaviour compared to its counterparts, such as ZnO and SiO_2 (Shi *et al.*, 2012). Additionally, TiO_2 properties, such as high surface to volume ratio,

non-toxic, low cost and photochemical stability have considerably contributed to its wide application in water treatment (Nasikhudin *et al.*, 2017).

Albeit being considered as one of the most preferable semiconductors in wastewater purification, TiO_2 has several drawbacks such as the quick recombination of the photo-created electron-hole pairs, low electrochromic efficiency and large band gap (3.2 eV for anatase and 3.0 eV for rutile) which absorbs only 3–5% of solar light and can be excited only by ultraviolet (UV) light ($\lambda \leq 400$ nm) (Jiang *et al.*, 2007; Kumar & Devi, 2011; Nasirian & Mehrvar, 2016). Modifications of the electronic and optical properties of titania have been the main interest among researchers to deal with these prevailing limitations. Another well recognized drawback of TiO_2 is the fine or nanosized particles which has restricted its application to small-scale water treatment due to the difficulty encountered in recovering the nanoparticles after treatment (Kanakaraju *et al.*, 2015). The reclamation of TiO_2 fine powders at the post-treatment stage often incurs additional cost.

One approach that has been adopted to improve TiO_2 separation from water is by immobilizing TiO_2 photocatalyst on suitable supports or adsorbents. Several supports that have been used, thus far, to immobilize TiO_2 are chitosan, alginate, glass substrate, and agarose (Kimling & Caruso, 2012). Among them, alginate (Alg), which is a natural adsorbent, has recently caught the attention of researchers due to its effectiveness in the adsorption of water pollutants (Kanakaraju *et al.*, 2017). This polysaccharide is abundantly available in nature, non-toxic, and an inexpensive biopolymer. Many researchers have utilized this material as an immobilization carrier for enzyme and biomass (Kanakaraju *et al.*, 2017). Therefore, its ability to form hydrogels with controlled shapes has made it a potential adsorbent to immobilize or encapsulates TiO_2.

An increasing number of studies have been conducted on magnetite nanoparticles (MNPs) primarily magnetite (Fe_3O_4) nanoparticles (NPs) in wastewater treatment (Xu *et al.*, 2012; Villa *et al.*, 2016). Fe_3O_4 nanoparticles have high adsorption capacity due to their high surface area to volume ratio. Indeed, one might anticipate that combining TiO_2 and Fe_3O_4 NPs would offer a more sustainable application for water treatment compared to the suspended form of TiO_2. As incorporation of Fe_3O_4 NPs with TiO_2 making the process of recovering and recycling TiO_2 easier thus reducing cost (Harifi & Montazer, 2014). However, one of the limitations of this approach is that the direct contact between the Fe_3O_4 NPs cores with TiO_2 shell may lead to low photoactivity because Fe_3O_4 NPs core could react as the recombination center for electron and positive holes (Lucas *et al.*, 2013).

Based on the above considerations, this study was designed to synthesize a multifunctional composite based on Alg/TiO_2/FeNPs where adsorption capability of Alg is combined with mineralization capability of TiO_2 associated with magnetic separation of iron-based nanoparticles. This multifunctional material is needed to combine adsorption with degradation capabilities by following a "catch and destroy" approach. Since direct contact between TiO_2 and Fe_3O_4 nanoparticles could potentially affect the photocatalytic activity, the role of Alg as a barrier between TiO_2 and Fe_3O_4 nanoparticles has been investigated to enhance the performance efficiency of the nanocomposite material.

The efficiency of the TiO_2 photocatalysis is known to be affected by various parameters such as solution pH (Akpan & Hameed, 2009), initial concentration of solution, contact time (Reza *et al.*, 2017), and the adsorbent dosage (Kumar, 2017). The importance of these operating parameters have been confirmed in various photodegradation studies (Saien *et al.*, 2014;

Aljuboury *et al.*, 2015). Therefore, it is important to obtain an optimization of these parameters in related studies to achieve a maximum degradation efficiency for the desired pollutant.

In this study, the efficiency of Alg/TiO_2/FeNPs was investigated on two model pollutants namely methylene blue (MB) and mixture of three heavy metals (MHM) solution consisting of Pb(II) ions, Cr(III) ions and Cu(II) ions. The removal of MB has been reported using alginate-clay quasi-cryogel beads (Uyar *et al.*, 2016), magnetic microsphere with sodium alginate and activated carbon (Li *et al.*, 2017), chemical activated carbon prepared from jackfruit (Artocarpus heterophyllus) peel waste (Hasbullah *et al.*, 2014), and TiO_2/Ca-Alg beads (Albarelli *et al.*, 2009). In contrast to studies on single heavy metal species, removal of MHM has received scant attention. Only several reports on the removal of MHM can be found in literature. For instance, removal of multi heavy metals have been reported using carbon nanotubes-granular activated carbon for the removal of Pb(II) ions, Cu(II) ions and Ni(II) ions (Onundi *et al.*, 2011), Alg-goethite beads for the removal of Cr(III) ions and Cr(IV) ions (Lazaridis & Charalambous, 2005), and polysaccharides for the removal of Hg(II) ions and Pb(II) ions (Son *et al.*, 2004).

Thus far, no report has investigated the use of trifunctional Alg/TiO_2/FeNPs composite beads for the removal of both MB and MHM. Response surface methodology (RSM) which is a great tool for rapidly optimizing the parameters to obtain the highest photodegradation efficiency of MB and MHM. RSM also allows optimization of multiple independent variables through different level combinations of the variables studied with limited number of trials (Bezerra *et al.*, 2008; Aravind *et al.*, 2015). This could reduce the number of experiments to be conducted and thus provide more efficient and economical way to obtain optimized condition for an experimental design (Toemen *et al.*, 2014).

1.2 Problem Statements

TiO_2 photocatalyst is regarded as one of the most promising heterogeneous photocatalysts owing to its high photocatalytic activity, low cost and strong oxidizing power. Although application of TiO_2 in a suspension is known to be efficient for photocatalytic oxidation of various recalcitrant compounds, such an approach requires post separation method at the end of the treatment process. Additional separation methods besides time consuming can also be uneconomical due to high cost involved in catalyst recycling. To overcome the separation of TiO_2 nanoparticles, immobilization of TiO_2 has been proposed as one of the viable options. Nevertheless, the efficiency of supported TiO_2 may lead to a decrease in the photocatalytic efficiency of the catalyst due to a mass transfer limitation as a result of a reduction in the specific surface area. Alg, a natural biopolymer which is capable of forming stable hydrogels was used as a support and immobilization carrier as its potential for these purposes have not been well explored. Among magnetic photocatalytic systems developed so far, TiO_2/Fe_3O_4 has drawn much attention due to the high magnetic properties and low toxicity of Fe_3O_4. However, the direct contact between the TiO_2 shell and Fe_3O_4 magnetic cores have been reported to cause low photoactivity. TiO_2 can oxidize Fe_3O_4 thus reducing the magnetic moment. Thus, this study was proposed to prepare photocatalyst, Alg/TiO_2/FeNPs with triad functions through the incorporation of magnetic property, photocatalytic activity, and adsorption. The Alg/TiO_2/FeNPs beads which was synthesized by employing a facile non-thermal method was further investigated for its efficiency in removing MB and MHM from the aqueous solution.

1.3 Research Question

a. Can the Alg/TiO_2/FeNPs beads effectively remove MB and MHM from the aqueous solution?

b. What is the correlation between physico-chemical properties of combined Alg/TiO_2/FeNPs beads with its photocatalytic activity?

1.4 Objectives

The main objective of this study was to synthesize Alg/TiO_2/FeNPs beads for the removal of MB and MHM in the aqueous solution.

The specific objectives of this study were to:

a. prepare Alg/TiO_2/FeNPs beads by varying the synthesis conditions such as concentrations of NaOH and Alg,

b. characterize the synthesized Alg/TiO_2/FeNPs beads for crystal structure, surface morphology, and functional groups,

c. optimize the independent variables for the removal of MB and MHM such as pH, initial concentrations and contact time by Alg/TiO_2/FeNPs beads in the aqueous solution by employing RSM,

d. compare the efficiency of the optimized Alg/TiO_2/FeNPs beads to remove MB and MHM under different conditions,

e. study the reusability of Alg/TiO_2/FeNPs beads under optimum condition up to three cycles.

CHAPTER 2

LITERATURE REVIEW

2.1 Advanced Oxidation Processes (AOPs) for Wastewater Treatment

Existing conventional wastewater treatment methods have been labelled as inefficient in removing myriads of harmful, toxic, and stable compounds such as heavy metals, dyes, and pharmaceuticals originating from industrial effluents. The contaminated industrial effluents are usually discharged into the water system untreated or inadequately treated (Krishnan *et al.*, 2016). Conventional water treatment methods such as filtration and flocculation, ion exchange, solvent extraction, activated carbon adsorption, and membrane separation have been applied with the aim to improve the quality of the contaminated effluents (Tabatabaee *et al.*, 2014). However, these methods seem not to be economically viable due to their high operating costs (Wahi *et al.*, 2010). Besides, incomplete removal or degradation of toxic water pollutants can cause the accumulation of contaminants that require additional post-treatment processes (Mota *et al.*, 2008).

The adsorption method has been widely applied in wastewater treatment compared to the other conventional methods due to its efficiency in removing both inorganic and organic water pollutants (Rafatullah *et al.*, 2010). The most commonly used adsorbents are activated carbon, zeolite, and biomass (Wan Ngah *et al.*, 2011; Zheng *et al.*, 2013). However, the adsorption technology merely transfer the pollutants from the aqueous phase to the adsorbent phase (Wahyuni *et al.*, 2015). As a consequence, the pollutants will accumulate on the adsorbent surface to form more toxic waste which is usually disposed to the landfills and the regeneration of the adsorbent can become more tedious (Lam *et al.*, 2012; Qiusheng *et al.*, 2015). In view of these drawbacks, an emerging method known as advanced oxidation processes (AOPs) has been

recognized for its efficiency to remove various carcinogenic and persistent pollutants that are present in wastewater (Stasinakis, 2008).

AOPs consist of several methods including radiation, photolysis, photocatalysis, sonolysis, electrochemical oxidation, Fenton, photo-Fenton, and ozonation (Wang & Xu, 2012). The effectiveness of AOPs in removing water pollutants such as dyes and heavy metals has already been proven by existing studies (Kansal *et al.*, 2007; Ajmal *et al.*, 2014). AOPs can be defined as a redox process that involves the generation of reactive oxygen species (ROS) such as hydroxyl radical (•OH), O_3, H_2O_2 and superoxide anion radical ($O_2^{\bullet -}$) (Krzemińska *et al.*, 2015). These ROS, primarily •OH radicals serve as a strong oxidant that can oxidize organic compounds into shorter and simpler molecules like CO_2, H_2O, and inorganic salts (Fox & Dulay, 1993; Wahyuni *et al.*, 2015; Boczkaj & Fernandes, 2017). On the other hand, reduction of heavy metal ions can also occur through AOPs, thus producing a non-toxic metal form (Barakat, 2011).

Among the ROS, •OH radical is the most reactive free radical. It exhibit distinctive properties such as short half-life, can be easily generated with a strong oxidant and electrophilic behaviour, ubiquitous in nature, and practically non-selective (Boczkaj & Fernandes, 2017). Moreover, high oxidation potential (E^o = 2.80 V) of •OH radicals are able to speed up the oxidation reaction rates of compounds compared to its other counterparts except fluorine, which has a higher oxidation potential (E^o = 3.03 V) (Krzemińska *et al.*, 2015). Although fluorine exhibit a higher oxidation potential, its high toxicity has made •OH radicals to be more preferred in wastewater treatment (Yonar, 2011). Table 2.1 shows the oxidation potential of oxidants involved in AOPs.

Table 2.1: The oxidation potential of several chemical oxidants

Oxidant	Oxidation potential (V)
Fluorine (F_2)	3.03
Hydroxyl radical (•OH)	2.80
Atomic oxygen (O)	2.42
Ozone (O_3)	2.07
Hydrogen peroxide (H_2O_2)	1.70
Hypobromous acid (HBrO)	1.59
Chlorine dioxide (ClO_2)	1.50
Chlorine (Cl_2)	1.36
Oxygen (molecular) (O_2)	1.23
Bromine (Br_2)	1.09

Source: Krzemińska *et al.* (2015)

The main advantage of AOPs over conventional methods is the conversion of organic and inorganic pollutants to a simple form of compounds or CO_2 and H_2O with no sludge production, which eliminates the requirement of other treatment stages (Elmoubarki *et al.*, 2017). The oxidation process can occur in three ways including radical addition (Eq. 2.1), hydrogen abstraction (Eq. 2.2), and electron transfer (Eq. 2.3) (Stasinakis, 2008).

$$R + \bullet OH \rightarrow ROH \quad (2.1)$$

$$R + \bullet OH \rightarrow R\bullet + H_2O \quad (2.2)$$

$$R^n + \bullet OH \rightarrow R^{n-1} + OH^- \quad (2.3)$$

AOPs used in wastewater treatment can be classified into two main classes namely photochemical and non-photochemical (Table 2.2) (Buthiyappan *et al.*, 2016). Photochemical is a reaction which includes the generation of free radicals in the presence of UV light, while non-photochemical is the generation of free radicals without the presence of UV light (Quiroz *et al.*, 2011). Titanium dioxide/UV light process, hydrogen peroxide/UV light process, and Fenton's reaction are among the most popular AOPs used in wastewater treatment, due to their efficiency in generating •OH radicals (Munter, 2001). It has been reported that these methods

exhibit high oxidation rates and generates more •OH radicals to mineralize organic and inorganic water pollutants (Stasinakis, 2008; Vilhunen & Sillanpää, 2010).

Table 2.2: Classification of AOPs

Non-photochemical AOPs	Photochemical AOPs
Alkaline media ozonation	Fenton and Fenton-like reactions
Fenton reaction	Heterogeneous photocatalysis
O_3/H_2O_2	UV/H_2O_2
Electrochemical oxidation	UV/O_3
Hydrodynamic/ultrasonic cavitation	
Sub/super critical water	

Source: Quiroz *et al.* (2011)

2.1.1 TiO_2 Photocatalysis

In 1972, Fujishima and Honda reported the photoelectrochemical decomposition of water under UV irradiation using rutile TiO_2 as the anode and Pt as the cathode (Carp *et al.*, 2004). Their findings revealed that oxidation occurred at the TiO_2 electrode while the reduction reaction at the Pt electrode. Subsequently, in 1977, a photocatalytic approach was first employed by Frank and Bard for the photodegradation of cyanide in water by utilizing TiO_2 powder as the photocatalyst (Fujishima & Zhang, 2006). This discovery gained the interest of other researchers to use the electron splitting mechanism in environmental applications, primarily wastewater treatment.

Photocatalysis can be defined as a photoreaction that is accelerated with the aid of catalysts (Deng & Zhao, 2015). A catalyst is a material that will not be consumed in a reaction but is utilized to lower the activation energy in order to increase the rate of the reaction. Photocatalysis degrade the pollutants by the following steps (Herrmann, 1999):

1. Transfer of the reactants in the fluid phase to the surface

2. Adsorption of a least one of the pollutants

3. Reaction in the adsorbed phase (photocatalytic reaction taking place)

4. Desorption of the product(s)

5. Removal of the products from the interface region

TiO_2 photocatalytic reaction occurs upon the UV (photon) irradiation absorbs an energy with energy equal or higher than the band gap energy, E.g. (3.2 eV for anatase), resulting electron-hole pairs. Figure 2.1 shows the mechanism of the excitation of electron from the valence band to the conduction band and a positive hole in the valence band (Dong *et al.*, 2015).

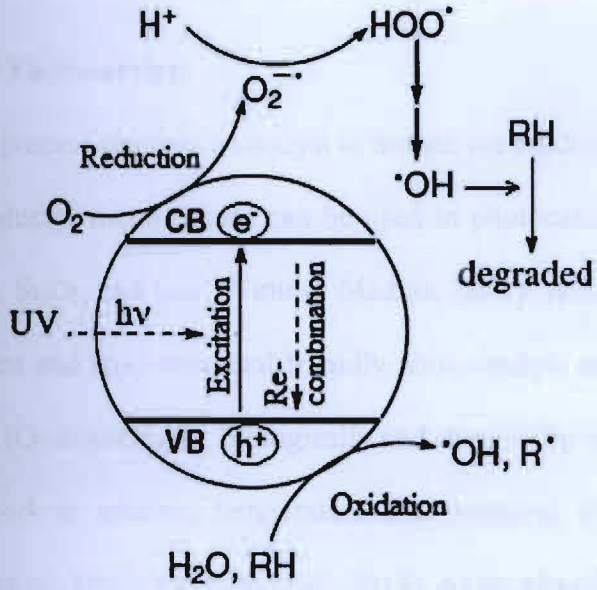

Figure 2.1: Schematic diagram demonstrating the principle of TiO_2 photocatalysis with the presence of water pollutant (RH) (Source: Dong *et al.*, 2015).

The electron-hole pair will eventually react with OH^-, H_2O and O_2 that are present on the surface of TiO_2 to form •OH and $O_2^{\bullet-}$ radicals. These radicals will consequently degrade the

adsorbed organic pollutant present on the photocatalysts surface (Lan *et al.*, 2013). The series of reactions that are involved in the photocatalytic reactions are shown below (Eqs. 2.4 – 2.7):

$$TiO_2 + h\nu \rightarrow e^-_{CB} + h^+_{VB} \quad (2.4)$$

$$h^+_{VB} + OH^- (surface) \rightarrow \bullet OH \quad (2.5)$$

$$h^+_{VB} + H_2O (absorbed) \rightarrow \bullet OH + H^+ \quad (2.6)$$

$$e^-_{cb} + O_2 (absorbed) \rightarrow O_2^{\bullet -} \quad (2.7)$$

However, some of the electron-hole pairs may eventually recombine and the input energy may be lost as heat, get trapped in metastable surface states, or react with electron donors and electron acceptors that are adsorbed on the semiconductor surface or within the surrounding electrical double layer of the charged particles (Zaleska, 2008).

2.2 Titanium Dioxide Photocatalyst

Photocatalysis process requires a catalyst to initiate the reaction (Yasmina *et al.*, 2014). A number of semiconductor metal oxides can be used in photocatalytic reactions, including ZnO, ZnS, WO_3, CdS, SnO_2, and GaP (Vinu & Madras, 2011). Among them, TiO_2 has been regarded as an excellent and environmental-friendly photocatalyst compared to others due to its unique properties. TiO_2 is non-toxic, biologically and chemically inert, resistant to chemical corrosion, and can work at ambient temperature and pressure, without addition of other chemical species (Lan *et al.*, 2013; Yasmina *et al.*, 2014). As for physical properties, TiO_2 exists as a white fine powder form that is insoluble and odourless, with a molecular weight of 79.9 g/mol (Shi *et al.*, 2013). High surface area of TiO_2 enhances the light absorption rate and photo-reduction rate, leading to high photocatalytic reactions (Lan *et al.*, 2013). When the diameter of the crystalline TiO_2 falls below a critical radius of about 10 nm, the charge carrier exhibits

quantum mechanical behaviours. As a result, their band gap increases and the band edges shift leading to an increase of their redox potentials (Gupta & Tripathi, 2012).

TiO_2 exists in three crystalline structures namely anatase, rutile and brookite (Figure 2.2) (Pelaez *et al.*, 2012). Among these crystal phases, only rutile and anatase show photocatalytic behaviours (Pelaez *et al.*, 2012). Table 2.3 shows the properties of each crystal phase of TiO_2. Anatase possesses a wider band gap of 3.2 eV, with an absorption edge at 386 nm, while rutile has a band gap of 3.02 eV and an absorption edge in the visible range at 416 nm. Lower calcination temperatures ranging from 250 to 500°C and temperature higher than 600°C are commonly applied to form anatase and rutile TiO_2, respectively (Chen *et al.*, 2003).

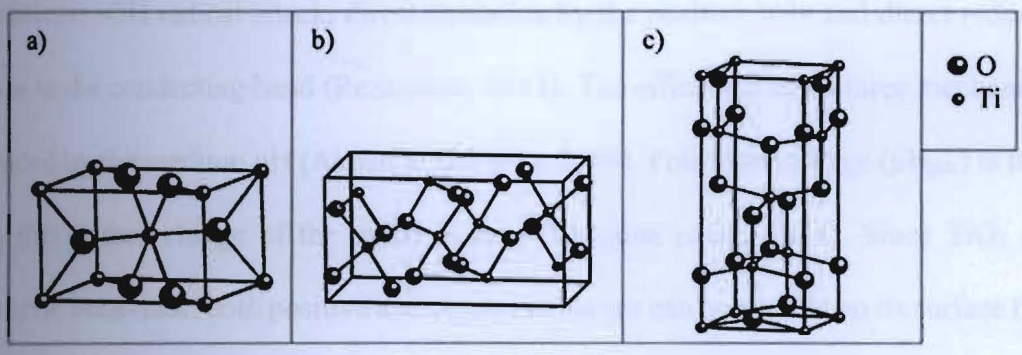

Figure 2.2: Crystalline structures of TiO_2: a) rutile, b) brookite, and c) anatase (Source: Bagheri *et al.*, 2015).

Table 2.3: Properties of the crystalline forms of TiO_2

Crystalline phase	Descriptions
Anatase	-Stable at low temperature -Greater photocatalytic activity because of its band gap, number of -OH groups, porosity and surface area
Brookite	-Discovered in minerals -Has orthorhombic crystal structure
Rutile	-Has orthorhombic crystal structure -Excellent stability under high temperature

Source: Bagheri & Julkapli (2015)

2.3 Parameters Affecting Photocatalytic Degradation

The photocatalytic degradation of organic and inorganic pollutants can be enhanced by controlling a number of parameters such as solution pH, initial concentration of the pollutant, photocatalyst dosage, contact time, reaction temperature, light intensity, and the presence of electron acceptors. However, in this study, only pH, initial concentration, contact time, and photocatalyst dosage were focused due to their significant effects on the photocatalytic degradation efficiency (Wahyuni *et al.*, 2015; Reza *et al.*, 2017).

2.3.1 Solution pH

The pH of the medium has been identified as one of the most critical parameters that affect photocatalytic degradation (Vaez *et al.*, 2012). There are three possible photodegradation mechanisms: •OH radical attack, direct oxidation by the positive hole and direct reduction by electron in the conducting band (Reza *et al.*, 2017). The efficiency of all three mechanisms are influenced by the medium pH (Akpan & Hameed, 2009). Point zero charge (pH_{pzc}) is the pH at which the surface charge of the oxide is zero (Yasmina *et al.*, 2014). Since TiO_2 exhibits amphoteric behaviour, both positive and negative charges can be present on its surface (Pekakis *et al.*, 2006). When the pH of the medium is lower than the pH_{pzc}, the TiO_2 surface charge is positively charged while the surface oxide become negatively charged when the pH of the medium is higher than the pH_{pzc}. The reactions below depict the influence of pH medium on the ionization state of the TiO_2 surface (Eqs 2.8 & 2.9) (Konstantinou & Albanis, 2004).

$$TiOH + H^+ \rightarrow TiOH_2^+, \qquad pH < pH_{pzc} \text{ (acidic medium)} \tag{2.8}$$

$$TiOH + OH^- \rightarrow TiO^- + H_2O, \; pH > pH_{pzc} \text{ (alkaline medium)} \tag{2.9}$$

Typically, in an acidic medium, the TiO_2 surface is protonated, while in the alkaline medium the TiO_2 surface is hydroxylated (Guillard *et al.*, 2003). The adsorption efficiency of

a pollutant onto the active sites of TiO_2 could be either high or low depending on their nature (Konstantinou & Albanis, 2004). For instance, MB removal will be more favoured in basic medium due to their cationic property. In a study by Salehi *et al.* (2012), the pH_{pzc} of the TiO_2 was determined as 6.80. When the pH of the MB solution was adjusted to basic pHs (e.g. 11.40 and 13.30), the negatively charged TiO_2 surface enhanced the adsorption of MB onto the TiO_2 surface and ultimately the percentage removal of MB from 50.0% to 90.0%.

However, for the anionic pollutants, their adsorption is more favoured at acidic medium (Lachheb *et al.*, 2002; Kabra *et al.*, 2007; Salamat & Younesi, 2017). Guillard *et al.* (2003) investigated the photodegradation of methylene blue, orange G, Alizarin S, Azo-Methyl Red and Congo red at pH 3.00, 6.00, and 9.00. It was noted that the increase of pH enhanced the photodegradation of all dyes except for orange G. The adsorption of orange G was inhibited at high pHs due to the presence of negatively charged sulfonate (SO_3^-).

2.3.2 Initial Concentration of Water Pollutant

Generally, when the initial concentration of the pollutants increases and others parameters are kept constant, the photodegradation is expected to be decreased (Kansal *et al.*, 2007). This can be explained by the saturation of the adsorption sites on the surface of the adsorbent with the molecules of the pollutant. The adsorption equilibrium can be achieved as the adsorbent surface is saturated with the pollutants (Rahman *et al.*, 2012) eventually contributing to the low photodegradation efficiency. In contrast to high initial concentration, there will be more unoccupied active sites at low initial concentration. Therefore, more pollutants can be adsorbed and result in high photodegradation of the pollutant. However, an increase in the loading capacity of the adsorbent occurs as the initial concentration of the water pollutants increases, due to the high driving force mass at a high initial concentration (Reza *et*

al., 2017). For instance, in the photodegradation of Acid Red 27 (AR27), as the initial concentration increased from 10 ppm to 80 ppm, the adsorption capacity of P25 TiO_2 increased as well. This is believed due to the high driving force for mass transfer of AR27 onto P25 TiO_2 surface (Behnajady *et al.*, 2014).

2.3.3 Contact Time

Contact time is also one of the important factors that enhance the photodegradation of water pollutants. By increasing the contact time of treatment, more ions can be adsorbed onto the TiO_2 surface and react with the free radicals that are present on the surface (Joshi *et al.*, 2011). Shrivastava (2012) studied the photocatalytic degradation of MB and Cr(IV) from wastewater with nanocrystalline TiO_2 semiconductor at different time intervals (30 to 195 min) and observed that as time progressed, the photodegradation also increased. The highest photodegradation was achieved at 150 min and remained constant after 180 min. This indicated that 180 min was the optimal contact time for the photodegradation of MB and Cr(IV). Benjwal *et al.* (2015) reported the photocatalytic degradation of methylene blue and arsenite using reduced graphene oxide-ferric oxide-titania nanocomposite. Contact time positively influenced the photodegradation of these pollutants by allowing more molecules to be adsorbed onto the surface of TiO_2 when the treatment time was increased.

2.3.4 Photocatalyst Dosage

The photocatalytic degradation could be affected by the photocatalyst dosage used in a treatment. Increasing the photocatalyst dosage generally increases the photocatalytic degradation. This could be explained due to the abundance of available active sites for the pollutants to be adsorbed and be degraded by the •OH radicals. However, at certain extent, as the active sites are saturated with the pollutants, the photodegradation might be reduced due to

the inhibition of light penetration through the photocatalyst. A review by Răileanu *et al.* (2013) indicated that the dosage of TiO_2 is directly proportional to the overall photocatalytic reaction. A study by Yang *et al.* (2015) reported that when the TiO_2 dosage was increased from 0.01 to 0.15 g, acceleration of the photodegradation of MB was observed due to the increased in the active sites of TiO_2. However, constant increase in the dosage led to the aggregation of TiO_2 particle which is known to reduce the efficiency of TiO_2 photocatalytic reaction due to the increase in opacity and light scattering of the catalyst particles.

2.4 Shortcomings of TiO_2 and Ways to Overcome

Despite being the preferred semiconductor photocatalysts, TiO_2 is also bound to several limitations that hinder its application in large-scale water treatment. The AOP method is known to have a poor adsorption capacity towards hydrophobic contaminants, high aggregation tendency, inefficient absorption of visible light due to the large band gap, and difficult to separate and recover after treatment (Habib *et al.*, 2013; Mohapatra *et al.*, 2014; Dong *et al.*, 2015). In light of these limitations, several approaches have been established, including doping with metal, non-metals and carbon-based NPs, surface organic modification, immobilization on support structures, and incorporation of magnetic property to ease separation (Dong *et al.*, 2015).

2.4.1 Doping with Metals

Metal-doped TiO_2 particularly with transition metals such as Cu, Co, Ni, Cr, Mn, Fe, Ru, Au, Ag, and Pt has been reported to affect the band gap energy, surface area, particle size, and thermal property of the photocatalyst (Mogal *et al.*, 2013). The anatase phase of TiO_2 photocatalyst which is commonly used in many photocatalytic reactions, can only be activated under the UV light (<387 nm) as a result of its wide band gap energy (3.2 eV) (us Saqib *et al.*,

2016). Doping the TiO_2 photocatalyst with transition metals reduced the band gap energy through the formation of a new energy level between the valence band and conduction band (Figure 2.3). Such an approach results in novel TiO_2 materials that can be photo-induced under the visible light range (>400 nm) (Chong *et al.*, 2010; Pelaez *et al.*, 2012; Dong *et al.*, 2015; Nasirian & Mehrvar, 2016).

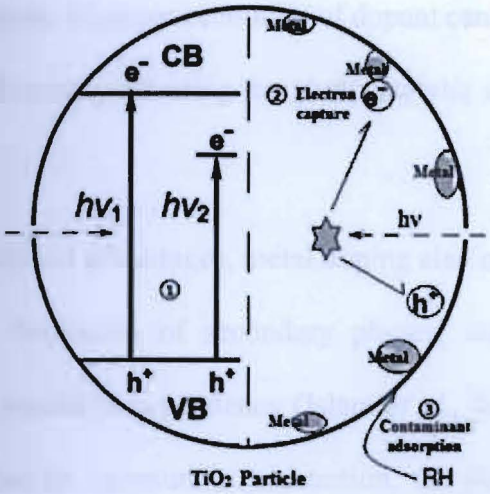

Figure 2.3: Mechanism of metal-doped TiO_2 photocatalysis: 1) narrowing band gap (hv_1: pure TiO_2; hv_2: metal-doped TiO_2); 2) retarding electron-hole recombination; and 3) enhancing adsorption of contaminants (RH) (Source: Dong *et al.*, 2015).

The recombination of electron-hole pairs during photocatalytic reactions lead to the dissipation of stored energy in only a few nanoseconds, hence reducing the photocatalytic efficiency (us Saqib *et al.*, 2016). The incorporation of transition metals in the crystal structure of TiO_2 may act as a photo-generated electron trapper and reduce the recombination of electron-hole pairs (Khairy & Zakaria, 2014). The formation of Schottky barrier at the metal-TiO_2 interface causes the decrease in the charge carriers recombination (Dong *et al.*, 2015).

A number of studies have utilized various transition metals for the purpose TiO_2 doping (Li *et al.*, 2008; Dimitrov *et al.*, 2011; Khairy & Zakaria 2014). For example, the removal of methyl orange using Cu-doped TiO_2 and Zn-doped TiO_2 reduced the recombination rate of electron-hole pairs and simultaneously enhanced the photocatalytic removal of methyl orange by 50.0% and 40.0%, respectively (Khairy & Zakaria., 2014). One important factor that has been highlighted in these studies is the dependence of the recombination rate on the concentration of the metal dopant. High concentration of dopant can either decrease or increase the recombination rate and ultimately affecting the photocatalytic activity of the metal doped TiO_2 (Zhang *et al.*, 2006).

Besides the aforementioned advantages, metal doping also restricted to few drawbacks such as thermal instability, formation of secondary phases, dopant insolubility, surface aggregation, and dopant concentration dependency (Islam *et al.*, 2017). When the amount of the dopant used is higher than its optimum concentration, the photodegradation rate could decrease instead of yielding the desired effect (Thu *et al.*, 2016). For this reason, non-metal doping can be an alternative approach to reduce the band gap of TiO_2 photocatalyst.

2.4.2 Doping with Non-Metals

Similar to their metal counterparts, non-metal dopants also work by introducing dopants into the lattice crystal structure of TiO_2 or the impurity states in the band gap of the system. The objective is to ensure the doped TiO_2 is activated under the visible light region and eventually enhance the photodegradation of pollutants by favouring the charge transfer and separation in the lifetime (Long & Cai, 2011).

There are several non-metals such as C, N, S, B, P, F, and I that are commonly used as dopants to dope TiO_2 NPs. Among them, N stands out as one of the most excellent dopant

candidate (Chong *et al.*, 2010; Pelaez *et al.*, 2012; Ibhadon & Fitzpatrick, 2013; Bagheri *et al.*, 2015) for its smaller atomic size as compared to oxygen, low ionization potential, and high stability (Islam *et al.*, 2017). The incorporation of N atoms are known to be through either interstitial type doping (N-O bonding) or substitutional type doping (replacement of O with N atoms) in TiO_2 (Di Valentin & Pacchioni, 2013). Xu *et al.* (2015) observed an enhanced reduction of multiple organic water pollutants (methyl orange, rhodamine B, methylene blue, Cr(IV)) under visible-light irradiation using tri-doped TiO_2 that incorporated metal iron (Fe) and non-metal nitrogen (N) and sulphur (S). In comparison with undoped TiO_2 and single non-metal doped N-P25, tri-doped TiO_2 exhibited better photocatalytic efficiencies and good recyclability for the reduction process.

To enhance the thermal stability of TiO_2, phosphorus (P) is used as the non-metal dopant in the formation of titanyl phosphate (Fagan *et al.*, 2016). Additionally, P provides a larger specific surface area and smaller crystalline size compared to pure titania that favours the adsorption of pollutants onto TiO_2 surface (Tan *et al.*, 2011). Non-metal dopants have significantly enhanced the photocatalytic activity of TiO_2 by improving their morphology and increasing the percentage of anatase phase (Tan *et al.*, 2011; Daghrir *et al.*, 2013). This helps to hinder the growth of the crystalline size of TiO_2 and subsequently increases the specific surface area of the photocatalyst (Daghrir *et al.*, 2013).

Nevertheless, non-metal doping technique involve high cost for its preparation and the formation of oxygen vacancies in bulk increases the recombination of electron-hole pairs (Dong *et al.*, 2015). These limitations will somehow limit the visible light photocatalysis efficiency of non-metal doped TiO_2 and its industrial applications.

2.4.3 Immobilization on Support Structures

In photocatalytic reactions, surface area is one of the determining factors that increase the reaction rate by adsorbing more organic molecules onto TiO_2 surfaces. TiO_2 NPs are known for their (i) large surface areas (Tan *et al.*, 2011), and (ii) ability to adsorb organic molecules and simultaneously degrade them (Reza *et al.*, 2017). However, NPs often encounter aggregation issue as they exhibit high surface energies and the particles tend to agglomerate to diminish this energy (Bhuiyan *et al.*, 2015). The possible solutions that have been proposed are to embed or anchor the NPs onto a support structure and to modify their surfaces using organic coating.

Organic materials such as carboxylic acid and humic acid could stabilize the NPs by reducing the aggregations. As for the modification by carboxylic acid, Weng *et al.* (2003) proposed a surface binding using carboxylic group to modify the TiO_2 surface *via* an interface-sensitive molecular probe.

Although surface modification of TiO_2 NPs is one of the dominant factors that enhance photocatalytic activity, their application in the slurry form is limited. Among the limitations are the need for post-treatment of treated wastewater, high cost for the regeneration of TiO_2 NPs and a decrease in the photocatalytic activity due to agglomeration of NPs (Dong *et al.*, 2015). Hence, it is not realistic in real wastewater treatment. A new approach is to immobilize the TiO_2 NPs onto fixed supports. A number of supports have been explored by researchers; these include bio-polymers, glass beads, fiber glass, glass pellets, glass sheets, silica, organo-clays, stainless steel, activated carbon and zeolites (Jobanputra *et al.*, 2011; Topkaya *et al.*, 2014; Hendrix *et al.*, 2015).

The incorporation of these supports increases the illuminated specific catalyst area, adsorption capacity and surface area of the photocatalyst as well as the selectivity of the photocatalytic reaction (Dong *et al.*, 2015). Immobilization of TiO_2 using alginate was attempted by Albarelli *et al.* (2009). Although the suspended TiO_2 demonstrated better photocatalytic degradation of methylene blue compared to the immobilized TiO_2, the latter facilitated recovery and recycling of the material. In a separate study, Samadi *et al.* (2014) synthesized Cu-TiO_2/chitosan hybrid film for the removal of Pb(II) ions by varying the sorbent surface area, contact time, and solution pH. Synergistic effect between the investigated parameters enhanced the photocatalytic degradation of Pb(II) ions.

Although there is a claim that not all the active sites on the immobilized TiO_2 are exposed to irradiation during treatment, this approach appears to be the more viable and economical for industrial application compared to slurry-type approach (Delnavaz *et al.*, 2015).

2.4.4 Magnetic Separation

Another economical way to improve the separation and recyclability of TiO_2 NPs is by incorporating magnetic materials such as magnetite (Fe_3O_4) and maghemite (γ-Fe_2O_3) into TiO_2 matrices. Numerous studies have been reported on the positive enhancement of magnetic materials into TiO_2. Ljubas *et al.* (2014) reported a new technique of growing magnetite crystals on aggregated surface-active TiO_2 P25 (MT/P25) NPs and applied an external magnetic field to recover the aggregates from suspension. The initial concentration of tartronic acid was reduced to 60.0% after 60 min of irradiation under UVA in the presence of TiO_2 P25. While, MT/P-25 successfully reduced similar concentration of tartronic acid to approximately 54.0% under similar experimental condition. This finding ascertained that magnetite did not affect the photocatalytic activity of MT/P25.

Behrad *et al.* (2015) coated magnetic particles with TiO_2 NPs *via* the sol-gel method. Fe_3O_4 was employed as seeds for the synthesis of Fe_3O_4/TiO_2 nanocomposites. Fe_3O_4 was first stabilized with trisodium citrate before being introduced into the synthesis of TiO_2 nanocomposites. The synthesis method was successful due to the strong magnetic separation ability and photocatalytic property demonstrated by the Fe_3O_4/TiO_2 nanocomposites. Another study by Tang *et al.* (2013) successfully designed a magnetic TiO_2-graphene photocatalyst, with an excellent electron-capture ability and high adsorptivity of graphene, that is easily separated by an external magnetic field. Moreover, the magnetic TiO_2-graphene completely degraded 2,4-dichlorophenoxyacetic acid, a herbicide under solar light irradiation and allowed rapid recovery after treatment.

Fe_3O_4 appears to be a suitable candidate to be merged with TiO_2 NPs, for both magnetic and photocatalytic properties. This dual nature of the nanocomposite makes it more attractive for industrial applications. The only problem foreseen is the possibility of the magnetic NPs acting as a recombination center for the electron hole pairs (Bagheri & Julkapli, 2015).

2.5 Magnetic NPs

Magnetic NPs (MNPs) have gained considerable attention due to their unique characteristics such as high surface-to-volume ratio, low diffusion rate, high dispersibility in water, and super magnetic properties (Bucak *et al.*, 2012; Lunge *et al.*, 2014). The term NPs correspond to particles with diameters ranging from 1 to 100 nm (Wu *et al.*, 2008). Various applications utilize MNPs as the basis, such as magnetic ferrofluid, catalysis and bioapplications. MNPs in the form of magnetic ferrofluid have open doors to a myriad of commercial applications such as magnetic drug targeting, magnetic separation of cells, and dynamic sealing (Scherer & Figueiredo, 2005).

MNPs are often referred to as iron oxides such as magnetite (Fe_3O_4), maghemite (γ-Fe_2O_3), and hematite (α-Fe_2O_3) (Bucak *et al.*, 2012). Figure 2.4 shows their respective crystal structures (Wu *et al.*, 2015). These three MNPs have their own unique properties that can be exploited for environmental and biomedical applications.

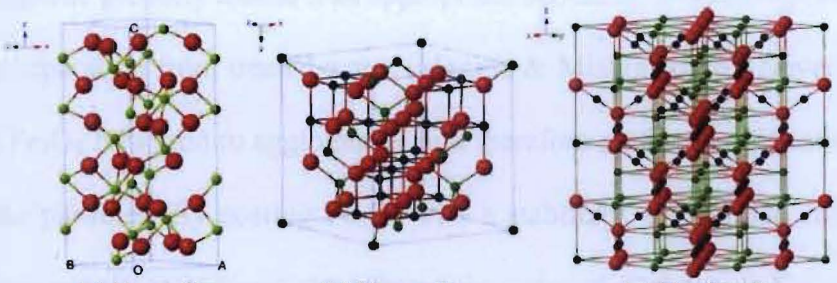

Figure 2.4: Crystal structure and crystallographic data of (a) hematite, (b) magnetite, and (c) maghemite (the black ball is Fe^{2+}, the green ball is Fe^{3+}, and the red ball is O^{2-}) (Source: Wu *et al.*, 2015).

Both α-Fe_2O_3 and γ-Fe_2O_3 are synthesized using only Fe^{3+}. However, to synthesize Fe_3O_4, Fe^{2+}/Fe^{3+} in the ratio of 1 to 2 is used (Teixeira *et al.*, 2012). Hematite possesses the highest band gap of 2.3 eV, followed by maghemite (2.0 eV) and magnetite (0.1 eV). Among these MNPs, magnetite and maghemite appears to be promising candidates for environmental applications as they have been proven safe and biocompatible (Wu *et al.*, 2008). Additionally, their small particle sizes (less than 20 nm) provide them superparamagnetic properties. Nevertheless, magnetite is the most favored one as it can be easily synthesized using simple methods such as co-precipitation method without extreme conditions compared to its counterpart maghemite (Mascolo *et al.*, 2013).

2.5.1 Magnetite NPs (Fe_3O_4-NPs)

Magnetite exhibits the most outstanding properties as it contains both Fe^{2+} and Fe^{3+} in its crystal structure. It has low toxicity, good magnetic and adsorption properties, as well as biocompatibility (Mamba & Mishra, 2016). Many studies have reported the application of Fe_3O_4 in water pollutant removal, especially heavy metals ions (Gómez-Pastora *et al.*, 2014). Moreover, its magnetic property makes it an appropriate candidate to be incorporated into TiO_2 powder for easy separation from treated water (Mamba & Mishra, 2016). Nevertheless, small particle sizes of Fe_3O_4 NPs tend to agglomerate and therefore surface modification is required for stabilizing the particles. By coating Fe_3O_4 with a stabilizer, the surface energy resulting from the electronic repulsion between the NPs can be reduced (Scherer & Figueiredo, 2005). Also, stabilizers provide routes for subsequent functionalization.

Unlike maghemite, magnetite does not undergo photocatalysis hence it can act as the center for electron-hole recombination when combined with TiO_2 (Mamba & Mishra, 2016). The following sections discuss examples of methods that are commonly applied to prepare Fe_3O_4 such as co-precipitation, hydrothermal and microemulsion. In this study, co-precipitation has been chosen over the other methods, as it is effortless and economical. Although this method is known for the aggregation of the NPs, it can be prevented by the addition of organic stabilizers such as sodium citrate (Hasanpour *et al.*, 2012).

2.5.1.1 Co-precipitation

One of the most widely applied methods to synthesize Fe_3O_4 is the co-precipitation method due to its superiority in controlling the size and magnetic properties of Fe_3O_4 (Majidi *et al.*, 2014). This versatile method can be performed either in an inert condition, at room temperature or at high temperature. It involves the addition of a base into a salt solution of Fe^{2+}:

Fe^{3+} with molar ratio 1:2. The resulting size and shape depends on the type of salt used (e.g., chlorides, sulfates, nitrates), the ratio of Fe^{2+} and Fe^{3+}, reaction temperature, and the pH value (Tresilwised *et al.*, 2005). However, for complete precipitation pH is maintained between 8 and 14. The co-precipitation reaction is as shown in Eq. 2.10:

$$Fe^{2+} + 2Fe^{3+} + 8OH^- \rightarrow Fe(OH)_2 + 2Fe(OH)_3 \rightarrow Fe_3O_4 + 4H_2O \quad (2.10)$$

The mean size of the NPs can be controlled to be in the range of 2 to 15 nm by simply adjusting the pH and the ionic strength of the precipitation medium (Majidi *et al.*, 2014).

Mahdavi *et al.* (2013) investigated the effect of pH, temperature and stirring on the particle size of Fe_3O_4 produced *via* the co-precipitation method. When the pH of the precipitation medium was higher than 11.00, the particle size of Fe_3O_4 NPs was found to be large (~10 nm). The growth of the Fe_3O_4 nucleus was also found to be more stable when the pH was greater than 11. At lower pH (<pH 11.00), the particle size of Fe_3O_4 was found to reduce. According to Majidi *et al.* (2014), when the temperature of the reaction is lower than 60°C, amorphous hydrated oxy-hydroxide that can be simply converted to Fe_2O_3 was formed; while higher temperatures (>80°C) led to the formation of Fe_3O_4. In order to prevent the oxidation of Fe_3O_4 to γ-Fe_2O_3, it is important that the reaction is performed under an inert condition (Majidi *et al.*, 2014) .

Mohammad-beigi *et al.* (2011) prepared Fe_3O_4 *via* the co-precipitation method at different pH values (9.00, 10.00, 11.00, and 12.00) and found that the size of the NPs decreased with increasing pH. Citrate coating was employed to stabilize the NPs and a reduction in the saturation magnetization was observed, due to the reduction in the surface energy of the NPs after coating.

2.5.1.2 Hydrothermal Technique

Another method which have been applied to synthesize Fe_3O_4-NPs is the hydrothermal or solvothermal technique (Laurent *et al.*, 2008). Although this technique demands high vapor pressure and temperature, but allow the formation of particles with a better crystallinity compared to other methods (Butter *et al.*, 2005; Majidi *et al.*, 2014). The formation of ferrite in hydrothermal conditions takes place through hydrolysis and oxidation or neutralization of mixed metal hydroxides. The only difference between these routes is the ferrous salts that are used in the hydrolysis and oxidation reaction (Laurent *et al.*, 2008). The parameters that have significant effects on the formation of MNPs include the type of solvent, temperature, and reaction time. Sun *et al.* (2009) synthesized Fe_3O_4 using the hydrothermal method with $FeCl_2$ as the metal precursor and sucrose as the reducing agent without purgation or a protection procedure. It was observed that particles synthesized in the presence of sucrose were much smaller compared to those produced in a sucrose-free condition.

The hydrothermal method is rather economical and enables facile synthesis of high-quality NPs despite the required high pressure and temperature during the reaction (Ozel *et al.*, 2014). Ozel *et al.* (2014) studied the effect of reaction temperature and time on the growth of NPs. The size of the NPs was observed to increase at high temperatures (60 to 180°C) and longer reaction times (12 to 72 h), with a higher likelihood to form magnetite.

2.5.1.3 Microemulsion Technique

Microemulsion technique involves two immiscible liquids to form a thermodynamically stable isotropic dispersion referred to microemulsion which is later stabilized by an interfacial film or surfactant molecules (Bedanta *et al.*, 2013). This technique has been widely used for synthesizing magnetic NPs of uniform size. Surfactant is commonly used to reduce the surface

tension between water and oil. The multiple advantages of microemulsion method include the use of simple equipment and the ability to synthesize Fe_3O_4 NPs with controlled size and shape, which also exhibit high surface areas (Majidi *et al.*, 2014).

The properties of NPs prepared by the microemulsion method are controlled by the type and structure of the surfactant (Sanchez-Dominguez *et al.* 2012). A surfactant is an amphiphilic molecule that lowers the interfacial tension between water and oil, resulting in the formation of a transparent solution (Faraji *et al.* 2010). Lopez-Quintela and Rivas (1993) reported that magnetite NPs with 4 nm in diameter was synthesized by the controlled hydrolysis of $FeCl_2$ with ammonium hydroxide and $FeCl_3$ aqueous solutions, within the inverse micelle.

2.5.2 Prevention of direct contact between magnetite and TiO_2

A number of studies have claimed that the direct contact between the magnetic core and TiO_2 accounted for the poor photocatalytic activity of TiO_2 based nanocomposites (Wei, 2009; Álvarez *et al.*, 2010; Ljubas *et al.*, 2014). Therefore, many studies have been carried out to improve the photocatalytic activity of magnetic TiO_2 based nanocomposites such as addition of inert interlayers and metal doping or deposition (Yao *et al.*, 2015).

The addition of an inert layer to magnetic TiO_2 nanocomposites could reduce the electron-hole recombination in the photocatalytic reaction (Absalan & Nikazar, 2016). Silica is a common intermediate layer used to keep the Fe_3O_4 NPs core and TiO_2 coating apart (Yao *et al.*, 2015). Encapsulating the MNPs with silica before TiO_2 depositions prevents their oxidation and increases their chemical stability (Wu *et al.*, 2008). Figure 2.5 shows the pathway of photogenerated charge transfer when silica is present as the intermediate layer (Yao *et al.*, 2015).

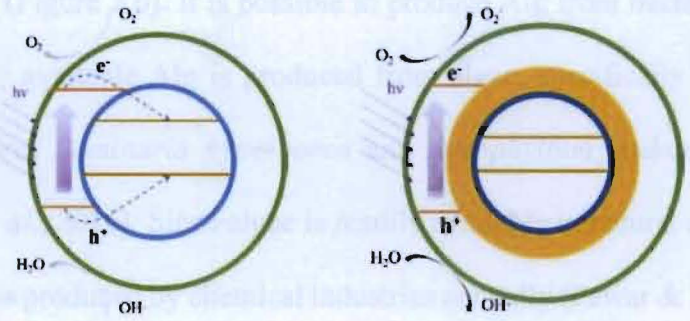

Figure 2.5: Schematic diagram of photo-induced charge transfer for TiO_2 a) without intermedia layer and (b) with inert intermediate layer (Source: Yao *et al.*, 2015).

The SiO_2 layer has been reported to improve the stability of titanium dioxide/silica dioxide/magnetite ($TiO_2/SiO_2/Fe_3O_4$) compared to TiO_2/Fe_3O_4 as it increases the chemical stability (Cheng *et al.*, 2012). Moreover, $TiO_2/SiO_2/Fe_3O_4$ was found to demonstrate a comparable photocatalytic activity with the Degussa P25 TiO_2 photocatalyts in the removal of acetaminophen and pharmaceuticals (Álvarez *et al.*, 2010).

Some authors have argued that SiO_2 may not fully protect the magnetic core which subsequently can cause photodissolution (Dupont *et al.*, 2014). The release of large amounts of chloride and nitrate from iron chloride or iron nitrate during the treatment may cause detrimental effects to the environment (Salamat *et al.*, 2017). Therefore, other alternatives are necessary to prevent the direct contact between the Fe_3O_4 and TiO_2 photocatalyst.

2.6 Alginate (Alg)

Alg is an ideal candidate to immobilize both Fe_3O_4 and TiO_2, as attributed to its inert properties that provide a protective layer to prevent the recombination effect between the TiO_2 and Fe_3O_4 core (K. Y. Lee & Mooney, 2012). Alginates or alginic acid are unbranched polysaccharides consist of 1→4 linked β-D-mannuronic acid (M) and its C-5 epimer α-L-

guluronic acid (G) (Figure 2.6). It is possible to produce Alg from bacterial and algal source. However, currently available Alg is produced from algae, specifically brown algae such as *Macrocystis pyrifera*, *Laminaria hyperborea* and *Ascophyllum nodosum* (Pawar & Edgar, 2012; Szekalska *et al.*, 2016). Since algae is readily available in nature, approximately 30,000 metric tons of Alg is produced by chemical industries annually (Pawar & Edgar, 2012). For this reason, it is practical and economical to design sustainable biomaterials based on Alg. The extraction of Alg from seaweeds is not complicated; diluted mineral acids are added to the raw material, then the alginic acid obtained from purification is converted into a water-soluble sodium salt in the presence of calcium carbonate (Szekalska *et al.*, 2016). Although Alg is produced in the form of different salts, but sodium alginate is the most widely investigated form (Rezende *et al.*, 2007; Szekalska *et al.*, 2016).

The properties of Alg are affected by the distribution and proportion of 1→4 linked β-D-mannuronic acid (M) and its C-5 epimer α-L-guluronic acid (G) in Alg, which are also known as M-block and G-block (Nalamothu *et al.*, 2014). The gelling characteristic is determined by the content of both M-block and G-block. Higher contents of G-block result in stronger and brittle Alg gels, while higher contents of M-blocks produce Alg gels with softer and more elastic features.

Furthermore, Alg gels with more M-block may undergo ion exchange more easily as more water can be absorbed (Szekalska *et al.*, 2016). Three functional groups that are present in Alg include carboxyl (-COO), ether (C-O-C), and hydroxyl (-OH). They may be bound with other metal cations for specific applications such as removal of heavy metals in wastewater treatment.

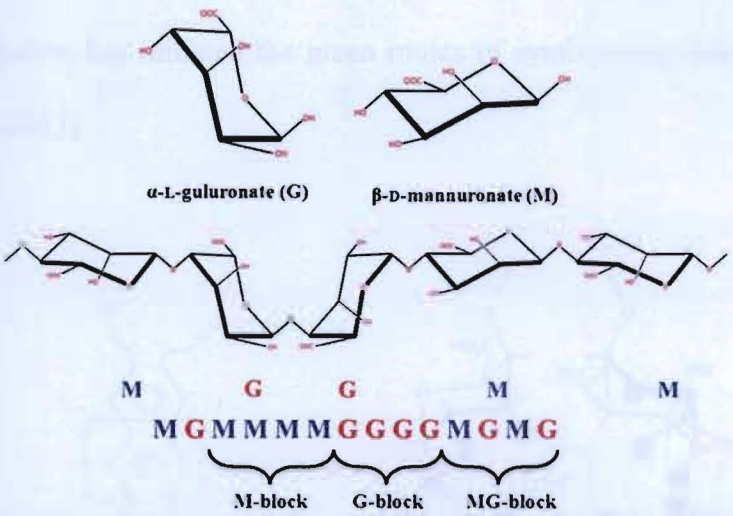

Figure 2.6: Chemical structure of alginate. Linear block polymers of β-D-mannuronate (M) and -L-guluronate (G) with a variation in composition and sequential arrangements (Source: Paredes Juárez *et al.*, 2014).

It is proposed that only G-blocks (Lee & Mooney, 2012) with abundant carboxyl groups participate in the crosslinking process with divalent cations such as calcium ions (Ca^{2+}) to form hydrogels (Bakr *et al.*, 2015).

In order for the gelation process to occur, the presence of cations such as lead, copper, cadmium, calcium and zinc are very important. The gelation process is completed through the crosslinking of Alg with other cations, thus making Alg an excellent immobilization carrier (Daemi & Barikani, 2012). Among the cations, calcium chloride is the most commonly used one due to its non-toxic properties. The calcium ion promotes a cooperative effect between G-blocks to form a 3D network known as the "egg-box" mode (Figure 2.7) (Braccini *et al.*, 2001). Braccini *et al.* (2001) reported that solid Alg-calcium gels maintained their function as a semi-permeable membrane through which low molecular weight and water-soluble molecules can diffuse.

Immobilization of TiO_2 with Alg has gained the interest of many researchers as it enhances the separation of the composite from treated water and can be reused several times.

Besides, Alg utilization has initiated the green routes of synthesizing new supports for TiO_2 (Harikumar *et al.*, 2013).

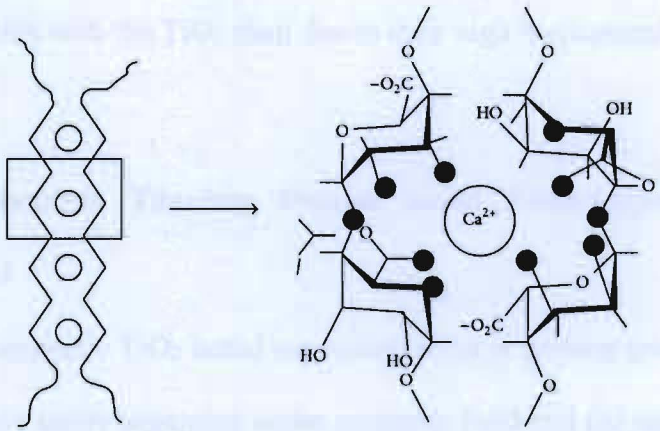

Figure 2.7: The "Eggs-box" model for Alg gelation with calcium ions. Dark circles represent the oxygen atoms involved in the coordination of the calcium ion (Source: Paredes Juárez *et al.*, 2014).

A number of researchers have investigated the ability of Alg as immobilizing carrier (Teoh *et al.*, 2011; Ai *et al.*, 2013). Immobilization in insoluble Alg gel is well known as a rapid, non-toxic and versatile method. Papageorgiou *et al.* (2012) studied the immobilization of TiO_2 photocatalyst into the matrix of calcium alginate for the degradation of methyl orange in polluted water and observed a high removal efficiency of 90.0% within 220 min of treatment.

Meanwhile, Teoh *et al.* (2011) investigated the optimum Alg concentration to synthesize Alg-TiO_2 hydrogels that are stable under UV irradiation. The study indicated that Alg concentrations lower than 2.0% (w/v) were depolymerized from long cross-linked polymer to shorter polymer chain after 3 h of irradiation under UV light. However, by increasing Alg concentration from 2.0 to 2.5% (w/v), its mechanical stability under UV irradiation was found to increase. An enhancement in the mechanical strength of Alg was attributed to the better cross-

linking between Ca^{2+} ions and Alg chain. Additionally, the removal of Pb(II) ions also increased with the increasing Alg concentration in the Alg-TiO_2 hydrogel.

In summary, Alg may be a suitable candidate to be as a barrier to prevent the direct contact between Fe_3O_4 NPs with the TiO_2 shell due to their high mechanical strength and inert properties.

2.7 Application of Magnetic Titanium Dioxide based Nanocomposites for Water Pollutants Removal

The application of magnetic TiO_2 based nanocomposites is gaining great attention as the nanocomposites can be (i) easily separated under magnetic field and (ii) reused several times without any deterioration (Li *et al.*, 2014). The presence of magnetic nanoparticles in the nanocomposite increases the adsorption sites for water pollutants and also the photocatalytic reaction efficiency (Su *et al.*, 2014). Furthermore, TiO_2 based nanocomposites can be used for both organic and inorganic water pollutants such as dyes and heavy metal.

The following section discusses the application of magnetic TiO_2 based nanocomposites for the removal of dyes and heavy metals as a representative of organic and inorganic water pollutant, respectively.

2.7.1 Removal of Dyes

Table 2.4 summarizes selected studies on the magnetic TiO_2 based nanocomposites for the removal of dyes in aqueous solutions or wastewaters under UV or visible light.

TiO_2/silicon dioxide-coated magnetic nanomaterial, $Fe_3O_4@SiO_2@TiO_2$ successfully removed 91.0% of 50 mg/L Reactive Black 5, which was comparable with the efficiencies of TiO_2 (93.0%) and TiO_2 P25 (97.0%) (Lucas *et al.*, 2013). The presence of a silica shell between

Fe_3O_4 and TiO_2 successfully reduce the electron-hole pairs recombination without interfering with the photocatalytic activity. Despite offering desirable advantages, fast recombination of the electron-hole pairs remains as the main drawback of magnetic property in TiO_2 composites, leading to further improvement by means of co-doping (Zhang *et al.*, 2016). For instance, by co-doping cadmium sulfide on TiO_2/Fe_3O_4, an improvement in the photocatalytic removal of 50 mg/L of Reactive Brilliant Red X-3B under visible light source was observed (Dong *et al.*, 2013). Another study reported that co-doping cadmium sulfide on $TiO_2/Fe_3O_4@SiO_2$ provided better removal efficiency of Rhodamine B compared to pure cadmium sulfide and Degussa P25 TiO_2.

Besides, TiO_2 coupled with noble metals such as gold (Au), platinum (Pt) and silver (Ag) also offers a great solution to enhance their photocatalytic activity under visible light as it may hinder the recombination of electrons and holes (Gomes *et al.*, 2017). Ag was incorporated in the Fe_3O_4/TiO_2 nanocomposites for the photodegradation of MB under visible light (Fauzian *et al.*, 2017). An increase in the weight percentage of Ag from 5 to 25 wt% in the $Fe_3O_4/TiO_2/Ag$ nanocomposites produced 85.0% of MB removal within 120 min.

Several other nanocomposites have been reported to successfully remove dye within short period of treatment time mainly due their high surface area available for adsorption (Hu *et al.*, 2005; Dong *et al.*, 2014). Reduced-GO (rGO) supported onto Fe_3O_4/TiO_2 ($rGO/Fe_3O_4/TiO_2$) completely degraded MB under UV light irradiation within 5 min as a result of the synergistic interactions between rGO and Fe_3O_4 which increased the surface area of $rGO/Fe_3O_4/TiO_2$ (Benjwal *et al.*, 2015). Also, functional groups present in the graphene oxide (GO) made it to be highly hydrophilic and water soluble, which may be susceptible for supporting metal or metal oxide particles (Benjwal *et al.*, 2015).

Table 2.4: Selected studies of magnetic TiO_2 based nanocomposites for dye removal

Magnetic titanium dioxide based nanocomposite	Dye	Parameters used	Removal efficiency	Reference
$Fe_3O_4/SiO_2/TiO_2$	RB5	• Concentration of RB5: 50 ppm	Maximum degradation efficiency of MB: (1) under UV lamp = 91.0%	Lucas *et al.*, (2013)
CdS-TiO_2/Fe_3O_4	Reactive brilliant red dye X-3B (X-3B)	• Concentration of X-3B: 50 ppm	Photocatalytic degradation rate of X-3B: (1) under sunlight = 85.0%	Dong *et al.* (2013)
Fe_3O_4/TiO_2/Ag	Methylene blue (MB)	• Catalyst dosage: 0.01 – 0.04 g/L	Removal rate of RhB: (1) under UV lamp = 85.0%	Fauzian *et al.* (2017)
TiO_2/Fe_3O_4	Methylene blue (MB)	• Concentration of MB: 10 ppm • Fe^{2+}/TiO_2 molar ratio: 0.16 – 0.8	Photodecomposition of MB: (1) under UV lamp = 52.0%	Harifi & Montazer (2014)
$rGO/Fe_3O_4/TiO_2$	Methylene blue (MB)	• Contact time: 50 – 100 min	Photodegradation of MB: (1) under UV lamp = 100.0% (2) under visible light = 91.0%	Benjwal *et al.* (2015)
Fe_3O_4@TiO_2 core/shell nanosphere loaded on the reduced graphene oxide sheet (Fe_3O_4@TiO_2/rGO) (FTR ternary nanocomposite)	Methyl orange (MO)	• Concentration of MO: 20 ppm	Photodegradation of MO: (1) FTR = 83.8% (2) Fe3O4@TiO2 = 33.7% (3) TiO2 = 33.0%	Ma *et al.* (2013)
$Fe_3O_4/SiO_2/TiO_2$	Reactive Black B (RBB)	• Catalyst dosage: 50 – 200 mg/L • pH: 3 - 9	Photodegradation of RBB: (1) under UV lamp = 100.0%	Aghel *et al.* (2016)

2.7.2 Removal of Heavy Metals

Magnetic TiO_2 based nanocomposites are also found to be effective to remove heavy metals. The magnetic materials enhance the adsorption of the metal ions onto the surface of the catalysts, enabling them to be readily reduced by the photogenerated electrons of TiO_2 to lower valence states and eventually deposited onto the surface of the catalyst (Kabra *et al.*, 2004). Table 2.5 summarizes the selected studies on the magnetic TiO_2 based nanocomposites for the removal of heavy metals in aqueous solutions or wastewaters under UV or visible light. A study by Sobhanardakani & Zandipak (2017) demonstrated that encapsulation of Fe_3O_4 with SiO_2 prevents the direct contact of Fe_3O_4 with TiO_2 whereby reduced the recombination effect of electron-hole pairs and enhanced the photocatalytic activity for Cd(II), Hg(II), and Ni(II) removal simultaneously. Additionally, the presence of Fe_3O_4 in the nanocomposites also afforded synergistic effects of adsorption and reduction for metal ions in the aqueous solution. SiO_2 is also said to be able to improve the dispersion property of Fe_3O_4 in the magnetic TiO_2 nanocomposite leading to the enhancement of the photocatalytic degradation (Xu *et al.*, 2012).

Graphene oxide has also been used for heavy metals removal due to their large surface which enhance the adsorption of pollutant for the photodegradation (Cui *et al.*, 2015). Reduced graphene oxide-metal oxide (rGO-TiO_2-Fe_3O_4) was investigated for the adsorption of As(III) (Benjwal *et al.*, 2015). 147.05 mg g^{-1} of As(III) was able to be adsorbed when using rGO-Fe_3O_4-TiO_2 nanocomposites. This is believed due to the surface area enhancement of rGO/Fe_3O_4/TiO_2 about 173.10 m^2 g^{-1} which resulted from the synergistic interaction between rGO and Fe_3O_4. Fe_3O_4/TiO_2/graphene (FTG) ternary nanocomposites with high surface area of 422.84 m^2. g^{-1} promoted to a high adsorption capacity of Cu(II) ions, 87.4 mg g^{-1} (Sun *et al.*, 2017). After five cycles of Cu(II) adsorption by the FTG nanocomposite, the adsorption capacity declined only by 7.4% indicating the stability and sustainability of this nanocomposites.

Since most of these nanocomposites exist in powder form studies have sought immobilize Fe_3O_4 NPs into polymeric biomaterials such as alginate, alginate, and chitosan as they exhibit non-toxic and unique biocompatibility and biodegradability properties (Betigeri & Neau, 2002; Lakouraj *et al.*, 2014; Gopalakannan & Viswanathan, 2015; Konwar *et al.*, 2015). For instance, Jiao *et al.* (2014) embedded Fe_3O_4 and TiO_2 into calcium alginate beads for the removal of Pb(II) ions in the mixture of mud. Pb(II) ions demonstrated an increase of adsorption capacity from 25.0 to 95.0 mg/g within 240 min at the medium pH 6.20. To the best of our knowledge, limited number of studies have been conducted on the multi-heavy metals removal by using magnetic TiO_2 based nanocomposite. Studies by Ismail *et al.* (2008) and Jiao *et al.* (2015) have attempted to remove heavy metals using TiO_2/SiO_2 and Fe_3O_4/Alg-polyvinylpyrrolidone (PVP), respectively. Therefore, more studies should be performed on the removal of multi-heavy metals from wastewater as they typically present as mixtures of metals rather than single metal.

Table 2.5: Selected studies of magnetic TiO_2 based nanocomposites for heavy metal removal

Magnetic titanium dioxide based nanocomposite	**Heavy metals**	**Parameters used**	**Removal efficiency**	**Reference**
Fe_3O_4/TiO_2/Graphene	Cu(II)	• Concentration of Cu(II): 50 ppm	Adsorption capacity: (1) 87.4 mg g^{-1}	Sun *et al.* (2017)
$TiO_2/SiO_2/Fe_3O_4$	Cd(II), Hg(II) and Ni(II)	• Concentration of Cd(II): 15-200 ppm • Concentration of Hg(II): 20-25 ppm • Concentration of Ni(II): 20-250 ppm	Maximum degradation efficiency of: (1) Cd(II) =98.0% (2) Hg(II) = 100.0% (3) Ni(II) = 85.0%	Sobhanardakani & Zandipak (2017)

Table 2.5 continued

$Fe_3O_4/SiO_2/TiO_2$ core-shell nanoparticles	Ag(I)	• Concentration of Ag(I): 12.5 ppm	Maximum percentage removal: (1) 97.0%	Kunarti *et al.* (2017)
Fe_3O_4/TiO_2 embedded in CaAlg beads	Pb(II)	• Concentration of Pb(II): 25-200 ppm • pH: 6.2 • Contact time: 240 min	Maximum percentage removal: (1) 100.0% (achieved at 25 ppm)	Jiao *et al.* (2014)
$rGO/TiO_2/Fe_3O_4$	As(III)	• Contact time: 50 – 100 min	Maximum adsorption capacity: (1) 147.05 mg g^{-1}	Benjwal *et al.* (2015)

2.8 Model Pollutants

2.8.1 Dyes

Dyes are substances that can provide colour when applied to a substrate through dyeing process (Chequer *et al.*, 2013). The coloured substances are permanent and cannot be removed by washing with water, soap or *via* exposure to sunlight (Sharma e*t al.*, 2014). This substances are widely used in the pharmaceuticals, textile, food, cosmetics, plastics, and paper industries (Sharma *et al.*, 2014). Among these industries, dyes are mostly used in the textile industry to colour materials such as fibre, yarn, fabric, and garment (Kanawade & Gaikwad, 2011). According to Sadeghi-Kiakhani *et al.* (2013), there are hundreds of thousands of commercially available dyes with annual productions exceeding 7×10^5 tons. There is no exact data that have been reported on the amount of dyes discharged into water streams. However, in the worldwide textile industry, approximately 100 tonnes per year of dyes used during the dyeing process and finishing operations are discharged into water streams (Chequer *et al.*, 2013; Yagub *et al.*, 2014). If left untreated, this will lead to numerous serious environmental problems such as reduced photosynthesis by aquatic plant and high toxicity level in the aquatic ecosystem (Tayeb

& Hussein, 2015). Exposure of dye-contaminated effluents to humans may also cause health related impacts such as severe headache, mental confusion, and profuse sweating (Singh *et al.*, 2011).

Common conventional methods such as adsorption, ion-exchange, ultrafiltration, coagulation, and membranes have been applied to remove dyes from wastewater (Bafana *et al.*, 2011; Kumar, 2017). However, dyes tend to escape from wastewater treatment plants due to their high stability to light, temperature, water, detergents, and other parameters such as bleach and perspiration, making them persist in the environment (Joshi *et al.*, 2004). Advanced wastewater treatment is therefore necessary to deal with highly stable and persistent dyes.

Dyes are classified based on their chemical structures that predominantly determine their colours, properties, and uses. The classes of dyes are shown in Table 2.6.

Table 2.6: Classification of dyes

Nitroso dyes	Indophenol dyes
Nitro dyes	Indigoid dyes
Azo dyes	Lactone dyes
Azoic dyes	Thiazine dyes
Stilbene dyes	Lactone dyes
Carotenoid dyes	Sulfur dyes
Azine dyes	Anthraquinone dyes
Oxazine dyes	Thiazole dyes

Source: Kiernan (2001)

Among different classes of dyes, thiazine dyes especially methylene blue is most widely used in various industries (Postai *et al.*, 2016). Thiazine, however, impart toxicity and mutagenicity (Attallah *et al.*, 2016). Therefore, their removal from effluents are crucial. The aromatic components present in azo dyes make it toxic to human and aquatic life (Wang & Xu, 2012). In the current study, methylene blue has been selected as the model pollutant due to their heavy consumption in many industries compared to other dyes.

2.8.1.1 Methylene Blue

Methylthionine chloride or most commonly known as methylene blue (MB) is a heterocyclic aromatic chemical compound with the molecular formula $C_{16}H_{18}ClN_3S$ (Figure 2.8). MB is synthesized through the oxidation of *N,N*-dimethyl-phenylenediamine with sodium dichromate ($Na_2Cr_2O_7$) in the presence of sodium thiosulfate ($Na_2S_2O_3$), followed by further oxidation in the presence of *N,N*-dimethylaniline (Randvere & Konzelman, 1980).

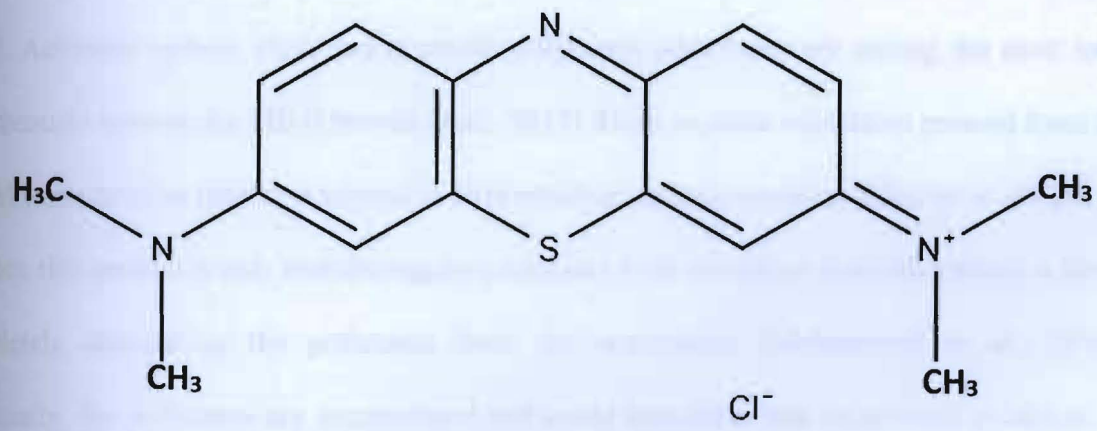

Figure 2.8: Chemical structure of methylene blue

MB is a cationic thiazine dye that exhibits a deep blue colour in the oxidized state and turns colourless when it is reduced to leucomethylene blue (Miclescu & Wiklund, 2010). In industrial applications, MB is used to give colour to textiles such as silk, cotton, and wool (León *et al.*, 2016). MB loaded effluents are highly visible even at low concentrations (Mohammed *et al.*, 2014). Compared to other synthetic dyes, MB is not highly hazardous but the effects of acute exposure to MB may lead to increased heart rate, vomiting, diarrhoea, nausea, and shock (Umoren *et al.*, 2013). Additionally, their discharge into water bodies causes various problems

such as lowered light penetration and photosynthesis and damage to the aesthetic nature of the water surface (Mohammed *et al.*, 2014). Hence, the removal of MB from effluents has significant environmental impact.

Although, there is no data on the permissible exposure limits for MB by the Occupational Safety and Health Administration, MB colour is visible even at low concentration as low as 1 ppm (Nsami *et al.*, 2013). Adsorption method is commonly used as it is the most effective method for MB removal compared to other conventional methods due to their simplicity of design, ease of operation, cost efficiency, and eco-friendly (Keyhanian & Shariati, 2016). Activated carbon, clay, and synthetic polymeric adsorbents are among the most used adsorbents to remove the MB (Umoren *et al.*, 2013). Even so, their separation process from the treated water involve high cost related to its production and regeneration (Charles *et al.*, 2016). Besides, this method is only transferring the pollutants from one phase to another phase without completely eliminating the pollutants from the wastewater (Mohammed *et al.*, 2014). Eventually, the pollutants are accumulated and could transform into more toxic products. In light of these reasons, it is necessary to develop an economical and efficient method to remove the MB from wastewaters to maintain the quality of our water supply from deteriorating.

2.8.2 Heavy Metals

Generally, the term heavy metals refer to trace elements and metalloids that are toxic and very persistent (Bhat & Khan, 2011). List of the most toxic elements present in wastewater are arsenic (As), lead (Pb), mercury (Hg), cadmium (Cd), chromium (Cr), copper (Cu), nickel (Ni), silver (Ag), and zinc (Zn) (Akpor *et al.*, 2014). Examples of metals, semi metals or radionuclides are silver (Ag), aluminium (Al), arsenic (As), gold (Au), cadmium (Cd), chromium (Cr), lead (Pb), copper (Cu), and magnesium (Mg). According to Barakat (2011),

heavy metals are categorized as an inorganic wastewater pollutant with a density of more than 5 g/cm^3. On the other hand, Akpor *et al.* (2014) defined heavy metals as elements with an atomic density greater than 6 g/cm^3. However, classification of heavy metals based on their density, atomic weight, atomic number or chemical properties sounds obsolete in the current context. Thus, it would be more relevant to categorize them with reference to their eco-toxicity (Bhat & Khan, 2011).

The most common toxic heavy metals in wastewaters are As, Pb, Hg, Cd, Cr, Cu, Ni, Ag, and Zn. These heavy metals usually generate from building materials, pigments for glazing ceramics and pipes for transporting water (Järup, 2003). Industries also tend to dump their toxic wastes containing heavy metals directly into water bodies without treatment (Buthiyappan et al., 2016). Industrial effluents usually consist of multi-heavy metals rather than only a single element. The accumulation of these heavy metals in water bodies results in adverse effects to human and aquatic ecosystem, such as low water quality and related diseases (typhoid, hookworm, diarrhea, vomiting and respiratory infections) (Zeitoun & Mehana, 2014). As heavy metals are non-biodegradable, efforts have been made by researchers to remediate and eliminate this toxic substance from our water bodies (Neyaz *et al.*, 2014; Horst *et al.*, 2016).

The removal of heavy metals from the wastewater could be achieved by treatment processes such as chemical precipitation, coagulation and flocculation, complexation, activated carbon adsorption, ion exchange and membrane operation (Gunatilake, 2015). However, these methods are prone to limitations. For instance, the coagulation-flocculation method works the best to remove the heavy metals by continuously enlarging the particles size to discrete particles. This is to ease the filtration process of the heavy metals from the treated wastewater.

But, the formation of sludge and substantial usage of chemicals have been the main drawbacks of this method (Teh *et al.*, 2016).

Another method that is claimed to be one of the best methods is the adsorption. The application of activated carbon for the adsorption of heavy metals has been studied by many researchers (Goel *et al.*, 2005; Jung *et al.*, 2013; Charles *et al.*, 2016;). Activated carbon exhibit large surface area and thus enhances the adsorption process of the heavy metal onto its surface (To *et al.*, 2015). However, the heavy metals will be only transferred from one phase to another and cause an accumulation of these toxic heavy metals (Aguedach *et al.*, 2005). Moreover, the separation and recovery of activated carbon from the treated water is tedious (Charles *et al.*, 2016).

The permissible concentrations for heavy metals in water referred to as the maximum contaminant levels (MCL) have been outlined by the United States Environmental Protection Agency (USEPA) (Table 2.7). The USEPA also identified Cr, Pb, and Cu as the most toxic heavy metals due to their high toxicity levels (Barakat, 2011). The following sections provide detailed information pertaining to the chosen heavy metals, Cu, Pb and Cr.

Table 2.7: The MCL for heavy metals by the USEPA

Heavy metal	Potential health effects from long term exposure above mcl	MCL (ppm)	Sources of contaminant
Arsenic	Skin damage, pose cancer risk and problem with circulatory system	0.050	Erosion of natural deposits; leachate from electronic production waste
Cadmium	Kidney damage, human carcinogen, renal disorder	0.01	Deterioration of galvanized pipes; waste released from metal refineries

Table 2.7 continued

Chromium	Allergic dermatitis, headache, carcinogenic	0.05	Waste released from steel and pulp mills; erosion of natural deposits
Copper	Liver or kidney damage, Wilson disease, insomnia	0.25	Deterioration of household plumbing system; erosion of natural deposits
Lead	For infants and children: slow mental development For adults: high blood pressure, kidney problems	0.015	Deterioration of household plumbing system; erosion of natural deposits
Mercury	Kidney damage, rheumatoid arthritis, and nervous system	0.00003	Deterioration of household plumbing system; erosion of natural deposits

Source: Barakat (2011)

2.8.2.1 Lead

Lead or Pb(II), with the molar mass of 207.2 g/mol, is listed among the heavy metals with a high toxicity even at low exposure levels (less than 0.0015 ppm) (Järup, 2003). It has only two oxidation states, 0 or +2. Human exposure to Pb(II) leads to various illnesses such as kidney damage, increase in blood pressure, and reduced sperm count (Jan *et al.*, 2015). Meanwhile, discharge of Pb(II) into the environment may interfere with the food chains of aquatic organisms as well as mammals due to ingestion. The allowable level of Pb in drinking water was reduced from 0.6 ppm to 0.05 ppm in 2000 (Brooks *et al.*, 2010). Due to the poor environment today, the presence of Pb at any concentrations is considered unsafe (Loredo *et al.*, 2006). Nevertheless, the Indian Standard Institution (ISI) has set the tolerance limit for the Pb discharge into the wastewater at 0.10 ppm (Goel *et al.*, 2005). While, according to World Health Organization (WHO), the presence of Pb in wastewater must be below than 0.05 ppm.

There are numerous sources of Pb(II) from various operations that cannot be controlled and an estimated 300 million tons of Pb(II) has been released into the environment over the past five millennia (Rodriguez, 2015). Both natural sources and industrial effluents are the

major sources that contribute to the pollution of Pb in environment (Arbabi *et al.*, 2015). Volcanic eruption and weathering of rocks are the natural sources of Pb(II) emissions from the earth's crust. Industrial sources of Pb include cement production, fuel additives, waste disposal, battery manufacturing, metal plating (Barakat, 2011). The concentration of Pb in the industrial effluent is dependent on the type of industry with a typical range of 200 to 500 ppm (Arbabi *et al.*, 2015). The Pb level in Pb-contaminated wastewater should be reduced to 0.05-0.10 ppm prior to its discharge into the sewage system (Arbabi *et al.*, 2015).

From the above environmental point of view, Pb can be considered as a highly toxic heavy metal. For Pb removal, treatments such as adsorption, precipitation, electro-dialysis, cementation, and reverse osmosis are mostly applied.

2.8.2.2 Chromium

Chromium (Cr) is regarded as the 17th most abundant element in the Earth's mantle (Bhalerao & Sharma, 2015). It occurs naturally as chromite ($FeCr_2O_4$), crocoite ($PbCrO_4$), bentorite $Ca_6(Cr,Al)_2(SO_4)_3$ and tarapacaite (K_2CrO_4). Cr is mostly found in industries such as plating, alloying, tanning of animal hides, inhibition of water corrosion and textile dyes (Avudainayagam *et al.*, 2003). The anthropogenic application of Cr in various industries have led to an increase in Cr contamination over the years. Cr is known to exist in several oxidation states from 0 to VI, but the most stable states are Cr(0), Cr(III), and Cr(IV) (Oliveira, 2012). The solubility of Cr vary with their oxidation states. For instance, Cr(III) tend to precipitate at natural to basic pH but remain soluble in acidic pH. Cr(III) recommended limit in water is 0.008 ppm. Tannery, textile (printing, dying) and decorative plating are among the industries where Cr(III) are mostly found (Stanin, 2005). For example, in India, about 2000 - 32,000 tons of Cr escaped from the tanning industries to the environment (Nigam *et al.*, 2015). Moreover, the Cr

concentration in these industries are always over the recommended limits 2 to 5 g/L (Bhalerao & Sharma, 2015). Therefore, due to the high concentration of Cr in wastewaters and the stringent environment regulations, their removal has gained importance (Gupta *et al.*, 2009).

2.8.2.3 Copper

According to Okocha & Adedeji (2012), copper (Cu) is one of the important nutrients required in small amounts (5-20 μg/g) by all organisms including human and aquatic life for carbohydrate metabolism. However, when Cu accumulation exceeds 20 μg/g, it becomes toxic (Okocha & Adedeji, 2012). The main sources of Cu are the solid waste from mines, electrolyte from the electro-refining plant, and acid sponge from sulphuric acid plant (Bhatia, 2002). The concentration of Cu in the industrial effluent depends on the industrial activity. For instance, 1550 ppm of Cu was reported present in the mining effluent from the Cu mine "Cerovo" in Serbia (Ochoa-Herrera *et al.*, 2011) while 5 to 100 ppm of Cu was found in the semiconductor effluents (Sierra-Alvarez *et al.*, 2007).

According to Wuana & Okieimen (2011), Cu is the third most used metals in the world. Their applications include seed production, disease resistance, agricultural fertilizers, wood preservatives and regulation of water. Exposure to Cu has been linked to various human diseases such as anaemia, liver damage and kidney failure (Tchounwou *et al.*, 2012). Cu(II), Pb(II) and Ni(II) are proven to retard the metabolic functions of aquatic life by specifically binding to proteins and small metabolites in living cells, leading to various severe health problems (Öztürk & Şahan, 2015). As Cu is persistent in water, it cannot be destroyed biologically but can only be transformed from one state to another state (Jiang *et al.*, 2016).

2.9 Response Surface Methodology (RSM)

In 1951, Box and Wilson developed RSM to study the interactive effect among independent variables with the respect to the response variables (Absalan & Nikazar, 2016). It is defined as a collection of mathematical and statistical techniques based on the fit of a polynomial equation to the experimental data (Bezerra *et al.*, 2008). RSM is an essential tool to illustrate the response surface when it involves more than two independent variables, which is impossible when using conventional method (Morshedi & Akbarian, 2014). Traditional methods using analytical chemistry for optimization are carried out by monitoring one manipulated factor at a time on an experiment response (Thirugnanasambandham & Sivakumar, 2015). The major drawback of this process is that it does not include interactive effects among the variables studied. Other than that, there is a great number of experiments that would lead to an increased consumption of reagents and materials (Bezerra *et al.*, 2008).

According to Bezerra *et al.* (2008), on account of the drawback of the traditional methods, RSM is introduced to optimize multiple independent variables using the multivariate statistic technique, where responses are illustrated in 3D surface and the adequacy of the model can be determined. A remarkable optimization can be achieved by conducting initial experiments with several conditions. This can be used to avoid using the insignificant range in the RSM study and help to focus on important factors and their range to achieve an efficient statistical modelling (Steinberg & Bursztyn, 2010). In the RSM, the independent variables are denoted as $x_1, x_2, \ldots, x_K$ and the response variables is called y (Khidhir *et al.*, 2015).

In order to interpret the data into the 3D surface plots, the first-order and second-order models of the low order of the polynomial are usually used. Their equations are expressed as first-order (Eq. 2.11) and second-order (Eq. 2.12) (Khuri & Mukhopadhyay, 2010):

$$y = \beta_0 + \sum_{i=1}^{k} \beta_i x_i + \varepsilon \quad (2.11)$$

$$y = \beta_0 + \sum_{i=1}^{k} \beta_i x_i + \sum_{i=1}^{k} \beta_{ii} x_1^2 + \sum_{1 \le i \le j}^{k} \beta_{ij} x_i x_j + \varepsilon \quad (2.12)$$

where, k is the number of variables, β_0 is the constant term, β_i represents the coefficients of the linear parameters, x_i represents the variables, β_{ij} represents the coefficients of the interactions parameters, β_{ii} represents the coefficients of the quadratic parameter and ϵ is the residual associated to the experiments.

First order and second order designs are named the designs for first-order model and second-order model, respectively. The most common first order designs are the 2^k factorial (k is the number of control variables), Plackett–Burman and simplex designs. Frequently used second order designs include 3^k factorial, Box-Behnken (BBD) and central composite designs (CCD) (Khuri & Mukhopadhyay, 2010). However, only second order designs are applied in the optimization technique since the first order design is usually used in the preliminary stage of a response surface investigation (Baş & Boyacı, 2007).

Another advantage of using the RSM as a tool for optimization is the lower number of experiments needed compared to the conventional method, thus making it an economical approach to establish a reliable interpretation of data (Morshedi & Akbarian, 2014). Among the designs mentioned above, BBD is the most efficient design to estimate the second order response surface (Robinson, 2007).

2.9.1 Box-Behnken Design (BBD)

Robinson (2007) reported that BBD is based on three-level factorial designs (-1, 0, 1) that are greatly efficient for estimating second-order surface. In a research study, it is necessary and practical to be able to achieve the main objective in the minimum period of time. Hence, having a design that can minimize the number of experiments yet enables an interpretation of

data with a statistically significant model is highly favourable. Emerson & Cavazzuti (2013) stated that BBD can limit the number of experiments that will be conducted as the number of parameters used in the study increases.

Besides, the number of experiments is sufficient for data interpretation using the second order degree of the polynomial. It has also been described by Robinson (2007) that BBD is comparable to CCD in terms of size. Table 2.8 shows the application of this design based on three variables in coded values (x_1, x_2 and x_3) (Ferreira *et al.*, 2007). Each of the variables will be varied at three levels and three replicates are conducted in the center (Yu & He., 2017). The equation is expressed as follows (Eq. 2.13):

$$n = 2k(k-1) + C \tag{2.13}$$

where, n is the number of experiments, k is the number of variables (3 for each Box-Behnken design) and C is the number of replicates at the center.

From Table 2.8, BBD appears to be smaller in size as it only contains $12 + n_c$ runs, while CCD has $14 + n_c$ runs (Robinson, 2007). Hence, smaller number of experiments are resulted by BBD than CCD.

Many researchers have employed BBD to explore the efficiency of TiO_2 based nanocomposites in wastewater treatment. A study by Absalan & Nikazar (2016) utilized the BBD application to optimize the removal of the colour of MB using the core-shell of magnetite/silica dioxide/titanium dioxide composite ($Fe_3O_4/SiO_2/TiO_2$) under solar irradiation. The results showed an efficient colour removal of 91.10% under optimized conditions: calcination temperature = 392 °C, Si/Fe_3O_4 wt% = 17.35% and Ti/Fe_3O_4 wt% =50.17%. Another study that also involved SiO_2 and TiO_2 successfully achieved complete removal of

Ni^{2+} and Cd^{2+} from aqueous solutions under optimized conditions suggested by the BBD application. The optimized conditions were pH = 8, initial concentration of Ni^{2+} and Cd^{2+} =10 ppm and contact time = 24 h.

Table 2.8: Coded factor levels for the BBD of a three-variable system

Experiment	x_1	x_2	x_3
1	-1	-1	0
2	1	-1	0
3	-1	1	0
4	1	1	0
5	-1	0	-1
6	1	0	-1
7	-1	0	1
8	1	0	1
9	0	-1	-1
10	0	1	-1
11	0	-1	1
12	0	1	1
C	0	0	0
C	0	0	0
C	0	0	0

Table 2.9 summarizes other studies that used the BBD application for the optimization of TiO_2 based nanocomposite in the removal of water pollutants. Based on the above reasons, RSM was selected for the current study in the optimization of the parameters (pH, contact time, and initial concentration) on enhancing the photocatalytic degradation of wastewater pollutants using optimized Alg/TiO_2/FeNPs.

Table 2.9: Examples of studies which used BBD to assess the efficiency of TiO_2 based nanocomposite for the removal of pollutants

Type of TiO_2 based nanocomposite	Type of water pollutants	Independent variables	Responses	Results	References
$Fe_3O_4/SiO_2/TiO_2$	Methylene blue (MB)	Calcination temperature, Si/Fe_3O_4 wt% and Ti/Fe_3O_4 wt%	Colour removal	Colour = 91.10%	Absalan & Nikazar (2016)

Table 2.9 continued

Chitosan/TiO_2	Pb^{2+}	Initial metal concentration, pH and temperature	Pb^{2+} removal	Pb^{2+} ions removal = 90.6%	Tao *et al.* (2009)
TiO_2/hydroxyapatite (TiO_2/HAP composite)	Sulfamethoxazole (SMX)	Initial sulfamethoxazole concentration, dose of TiO_2/HAP and UV intensity	SMX and TOX removal	SMX removal = 99.89% TOC removal = 51.01%	Chun *et al.* (2014)
SiO_2/TiO_2	Ni^{2+} and Cd^{2+}	pH, metal ions concentration and shaking time	Ni^{2+} and Cd^{2+} removal	Ni^{2+} and Cd^{2+} removal = 100%	Ismail *et al.* (2008)
Cerium dioxide-modified TiO_2 nanotubes (Ce-TNTs)	Paraquat dichloride (PQ)	CeO_2 ratio, calcination temperature and catalyst loading	PQ removal	PQ removal = 80% TOC removal = 51.10%	Eleburuike *et al.* (2016)
Fe/TiO_2 immobilized GAC	Alachor	Catalyst loading, number of black light and pH	Alachor removal	Alachor removal =69.78%	Wantala *et al.* (2012)
Ti/TiO_2	Acid blue-7	pH, light intensity and bias potential	Decolouriz-ation efficiency	Decolouriz-ation efficiency = 90.44%	Fu *et al.* (2009)
$TiO_2/SnO_2/WO_3$	1,2-dichlorobenzene	Calcination temperature, catalyst loading and pH	Degradatio-n of 1,2-dichlorobenzene	Percentage of degradatio-n = 95.86%	Nadarajan *et al.* (2015)

Table 2.9 continued

TiO_2/RH-SiO_2	Paraquat dichloride	Initial paraquat concentration, pH, TiO_2 content and catalyst loading	Paraquat dichloride removal	Paraquat removal = 90.04%	Tantriratna *et al.* (2011)
Cu/TiO_2	Phenol	Initial phenol concentration, reaction time and Cu/TiO_2 dosage	Phenol removal	Phenol removal = 52.20%	Sohrabi & Akhlaghian (2015)

CHAPTER 3

MATERIALS AND METHODS

3.1 Materials and Reagents

Alginic acid sodium salt (NaAlg), titanium (IV) oxide (TiO_2) (anatase powder, 99.8% trace metal basis), and methylene blue were purchased from Sigma-Aldrich (USA). Lead(II) nitrate ($Pb(NO_3)_2$) and chromium(III) nitrate nonahydrate ($Cr(NO_3)_3.9H_2O$ were both purchased from R&M Chemicals while copper(II) sulfate pentahydrate ($Cu(SO_4)_2.5H_2O$ was acquired from J.T.Baker. Iron (III) hexahydrate ($FeCl_3.6H_2O$), iron (II) chloride tetrahydrate ($FeCl_2.4H_2O$), tri-sodium citrate ($Na_3C_6H_5O_7$), and sodium hydroxide (NaOH) were procured from Merck (Germany). Calcium chloride dehydrate, $CaCl_2.2H_2O$ was purchased from Ajax Finechem Pty. Ltd. (Australia). Sulfuric acid (H_2SO_4) and sodium hydroxide (NaOH) were supplied by Merck (Germany).

3.2 Equipment and Instruments

Equipment and instruments that were used in this study includes mini pump variable flow (Model 3385), field emission scanning electron microscope (FESEM) equipped with an energy dispersive X-ray spectroscopy (EDX) (Model JOEL JSM-6390LA), fourier-transform infrared spectroscopy (FT-IR) (Model Thermo Nicolet iS10), X-ray diffraction (XRD) (Model PaNalytical X'pert Pro XRD), and transmission electron microscopy (TEM) (Model JEM 1230).

3.3 Synthesis of Magnetite Nanoparticles (MNPs)

The method of MNPs synthesis was based on the co-precipitation method adapted from Alizadeh *et al.* (2012) with a slight modification. In the applied protocol, two concentrations of NaOH (2 M and 5 M) were selected (Kanakaraju *et al.*, 2018). $FeCl_2.4H_2O$ (1.00 g, 5 mmol)

and $FeCl_3.6H_2O$ (2.70 g, 10 mmol) were mixed in 130 mL distilled water in the presence of Argon atmosphere (Ar atm) under vigorous stirring. Subsequently, 30 mL of NaOH (either 2 M or 5 M) was added rapidly into the mixture, and formed black precipitates known as MNPs. The mixture was then heated up to 60 °C under rapid stirring for 1 h under Ar atm. A final pH 14.00 of the mixture indicated a complete precipitation. The mixture was left to cool down to room temperature, and the MNPs were separated using an external magnet, followed by washing several times using distilled water and ethanol until neutral pH was achieved.

The MNPs were re-dispersed for 30 min in 200 mL of $Na_3C_6H_5O_7$ solution (0.3 M) before being heated at 80 °C for 1 h. The MNPs were then washed with acetone to remove any remnant of $Na_3C_6H_5O_7$. Finally, the MNPs were re-dispersed in 100 mL of distilled water for 30 min to form a stable ferrofluid. The prepared ferrofluid was stored in the fridge (4 °C) until further use.

3.4 Synthesis of Alg/TiO_2/FeNPs

The process of synthesising Alg/TiO_2/FeNPs was adopted from Hasanpour *et al.* (2012). In this study, however, two different concentrations of NaAlg were chosen to prepare NaAlg solutions, namely 5.0% (w/v) and 3.0% (w/v) (Kanakaraju *et al.*, 2018). NaAlg was dissolved in 100 mL of distilled water overnight. Then, 50 mL of NaAlg solution was added slowly into 50 mL of dispersed ferrofluid and this mixture was sonicated for 30 min. Subsequently, 50 mL of 2 g/L of TiO_2 solution was added into the mixture and sonicated again for 30 min to achieve better dispersion. In this study, commercial TiO_2 was used. The volume ratio of the MNPs-citrate to TiO_2 mixture was kept as 1:1. The final mixture consisting of NaAlg, MNPs-citrate, and TiO_2 photocatalyst was agitated under continuous stirring overnight. Then, the mixture was added drop-by-drop into a beaker filled with 100 mL of 5.0% (w/v) $CaCl_2$ solution, with the

aid of a peristaltic pump, under constant stirring. The falling height of the beads was fixed at 5 cm. The beads were maintained in the $CaCl_2$ solution overnight to complete the gelation process (Kanakaraju *et al.* 2017). The beads were then dried at room temperature for 36 h and later used for model pollutant removal. Alg-5%, TiO_2/Alg, and MNPs/Alg were also prepared as blank beads. Figure 3.1 summarizes the synthesis process of Alg/TiO_2/FeNPs and blank beads, while Figure 3.2 shows the picture of the prepared Alg/TiO_2/FeNPs. The synthesis conditions for the Alg/TiO_2/FeNPs were varied and coded as tabulated in Table 3.1.

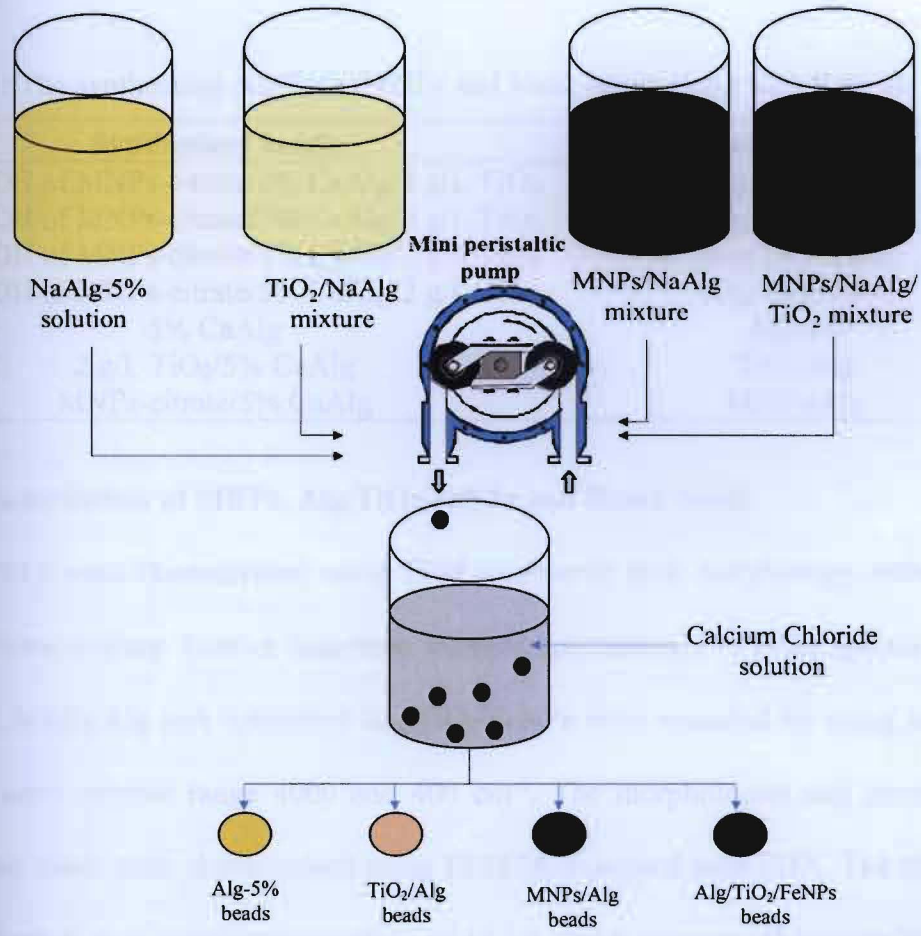

Figure 3.1: Synthesis process of Alg-5%, TiO_2/Alg, MNPs/Alg, and Alg/TiO_2/FeNPs beads

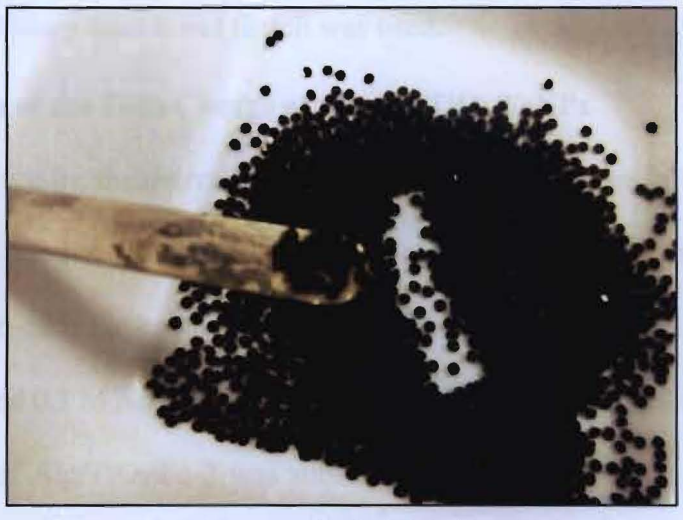

Figure 3.2: Prepared Alg/TiO_2/FeNPs beads

Table 3.1: The synthesized Alg/TiO_2/FeNPs and blank beads along with their assigned codes.

Synthesized beads	Sample code
2 M NaOH of MNPs-citrate/3% CaAlg/2 g/L TiO_2	Alg/TiO_2/Fe-1
2 M NaOH of MNPs-citrate/5% CaAlg/2 g/L TiO_2	Alg/TiO_2/Fe-2
5 M NaOH of MNPs-citrate/3% CaAlg/2 g/L TiO_2	Alg/TiO_2/Fe-3
5 M NaOH of MNPs-citrate/5% CaAlg/2 g/L TiO_2	Alg/TiO_2/Fe-4
5% CaAlg	Alg-5%
2 g/L TiO_2/5% CaAlg	TiO_2/Alg
MNPs-citrate/5% CaAlg	MNPs/Alg

3.5 Characterization of MNPs, Alg/TiO_2/FeNPs and Blank beads

MNPs were characterized using TEM to observe their morphology, before and after citrate surface coating. Fourier transform infrared spectroscopy (FT-IR) spectra of Alg-5%, TiO_2/Alg, MNPs/Alg and optimized Alg/TiO_2/FeNPs were recorded by using standard KBr pellet in wave number range 4000 and 400 cm^{-1}. The morphologies and structures of the synthesized beads were characterized using FESEM, equipped with EDX. The measurements were performed at an accelerating voltage of 10 kV under vacuum. The crystalline structures of the beads were observed using XRD method using Cu Kα radiation (λ = 0.154 nm) in the scanning range of 2θ between 10° and 80°, with a rate of 0.04° per second. The accelerating voltage and applied current were 45 kV and 40 mA, respectively. For phase identification, an

automatic JCPDS library search and match was used.

3.6 Determination of the Zero Charge of the Alg/TiO_2/FeNPs

The procedure for the determination of the point zero charge (pH_{pzc}) was adapted from Putra *et al.* (2009). Firstly, 50 mL of 0.01 M of NaCl was added into six different Erlenmeyer flasks. Then, pH in each flask was adjusted to 2.00, 4.00, 5.00, 6.50, 10.00, 12.00 and 14.00 using 0.1 M HCl and 0.1 M NaOH. The solution pH in each flask represented the initial pH (pH initial). A 0.15 g of Alg/TiO_2/Fe-2 was subsequently added into each flask and the solution mixture was continuously stirred for 24 h. The final pH of solution in each flask was measured after 24 h. The pH_{pzc} of the optimized Alg/TiO_2/Fe-2 is the point where the $pH_{final} = pH_{initial}$.

3.7 Model Pollutants

To investigate the adsorption and photocatalytic efficiency of Alg/TiO_2/FeNPs, two model pollutants were selected, namely, MB and MHM solution consisting of Pb(II), Cr(III), and Cu(II) ions.

3.7.1 Methylene Blue (MB)

Initial MB concentration ranging from 5 ppm to 25 ppm were used in all degradation treatments. The initial MB solution pH was recorded as 7.75 ± 0.01. To investigate the effect of pH on the removal of MB, the desired initial solution pHs of 3.00, 7.00, and 10.00 were obtained using either H_2SO_4 or NaOH solutions.

3.7.2 Mixture of Heavy Metals (MHM)

MHM aqueous solution consisting of Pb(II) ions, Cu(II), and Cr(III) was prepared by dissolving the respective metal salts using deionized water. Metal stock solutions (1000 ppm) were diluted to the desired concentrations using deionized water. Initial concentrations of MHM solution ranging from 20 to 60 ppm were used in all treatments. The initial MHM solution pH

was recorded as 2.10 ± 0.01. For the effect of pH study the desired initial pHs of 4.00, 5.50 and 7.00 were adjusted by the addition of H_2SO_4 or NaOH.

3.8 Photocatalytic Experiment

Figure 3.3 shows the photocatalytic experimental setup for both model pollutants (MB and MHM). The study was carried out in a dark box under UVC lamp (λ=254 nm) (Model OSRAM, 30 W). Prior to the optimization of the photocatalytic conditions using Response surface methodology (RSM), the effect of the synthesized conditions of Alg/TiO_2/FeNPs and their adsorbent dosages were investigated.

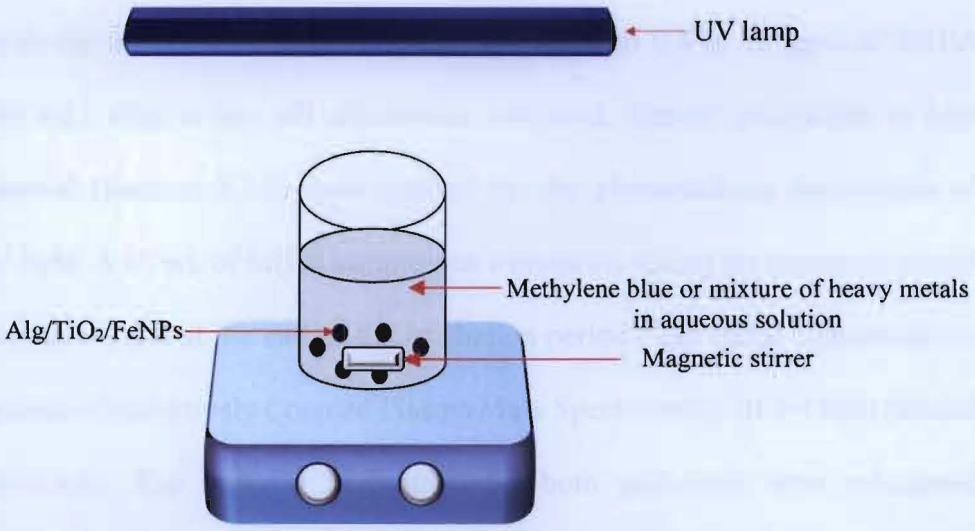

Figure 3.3: Experimental setup of the photocatalytic study

3.8.1 Effect of Synthesis Condition and Adsorbent Dosage on the Pollutant Removal

The optimized Alg/TiO_2/FeNPs was determined in the MB removal and was further studied in the MHM removal. The synthesized Alg/TiO_2/FeNPs, namely, Alg/TiO_2/Fe-1, Alg/TiO_2/Fe-2, Alg/TiO_2/Fe-3 and Alg/TiO_2/Fe-4 with different adsorbent dosage from 0.1 g

to 0.6 g was utilized for the MB removal at low MB concentration (5 ppm) without any pH adjustment. Firstly, the Alg/TiO_2/FeNPs was added into 100 mL of MB solution and stirred with the aid of a magnetic stirrer in the dark for 30 min to establish an equilibrium adsorption of MB molecules onto the adsorbent surface. After that, 10 ml of the sample was taken as t_0. Then, the setup was irradiated by 254 nm UV lamp (OSRAM, 30 W) for 2 h. Samples were withdrawn at fixed intervals (t_{30}, t_{60}, t_{90} and t_{120}) and centrifuged prior to measurement. The absorbance value was measured using a UV-Vis spectrophotometer (Model Lambda 25-PerkinElmer) at a maximum wavelength λ_{max} = 664 nm (MB). A standard calibration of the absorbance against the concentrations was then plotted to determine the concentration of the solution.

The optimized Alg/TiO_2/FeNPs obtained from the MB removal was further applied for MHM removal with the adsorbent dosage ranging from 0.1 g to 0.8 g. 20 ppm of MHM concentration (100 mL) without any pH adjustment was used. Similar procedures in MB photocatalytic removal (Section 3.7.1) were applied for the photocatalytic experiment of MHM under UVC light. A 15 mL of MHM sample was withdrawn during the treatment period at t_0 (initial concentration) and at the end of the irradiation period (t_{120}) (final concentration) and analyzed by means of Inductively Coupled Plasma Mass Spectrometry (ICP-OES) (Model Shidmadzu ICPM-8500). The removal percentage for both pollutants were calculated according to Eq. 3.1:

$$R\,(\%) = \left(\frac{(C_i - C_f)}{C_i}\right) \times 100 \qquad (3.1)$$

where R is MB/MHM removal percentage, C_i is the initial MB/MHM concentration in ppm and C_f is the final concentration of MB/MHM in ppm.

3.8.2 Determining Optimum Condition for MB Removal *via* RSM analysis

From the preliminary study (Section 3.7.1), the optimized Alg/TiO_2/FeNPs and adsorbent dosage was selected and applied in RSM *via* the three-level, three factorial Box-Behnken experimental design as established using Design Expert software (version 7.1.6) for determining the optimum condition of MB removal. This method is appropriate for fitting a quadratic surface and it helps to optimize the effective parameters with a minimum number of experiments, including analyzing the interaction between the parameters (Khosravi & Arabi, 2016). In the optimization study, a series of experiments, known as runs, were employed. Three independent variables were studied, which includes the contact time (ranging between 30 to 120 min), pH value (in the range of 3.00 to 10.00), and initial MB concentration (ranging from 5 to 25 ppm). All experiments recorded were conducted under UVC irradiation ($\lambda = 254$ nm). Samples were withdrawn at a specific contact time as suggested by the RSM design matrix. The factorial levels were coded as -1 (low), 0 (medium), and 1 (high). Table 3.2 summarises the experimental range and levels of independent variables considered in this study.

Table 3.2: Range and levels of the independent variables for MB removal.

		Range and Levels		
Variables	**Coded**	**-1**	**0**	**1**
Contact time (min)	A	30	75	120
pH	B	3.00	6.50	10.00
Initial concentration (ppm)	C	5	15	25

There were a total number of 16 experiments of BBD to be analyzed. Table 3.3 shows the 16 experiments with the ranges and levels in coded units. RSM used regression analysis to analyze the experimental data from BBD.

Table 3.3: RSM for the three independent variables in corresponding natural values and coded units of MB removal.

Run	Independent variables			Coded variables		
	Contact time (min)	pH	Initial concentration (ppm)	A	B	C
1	30	3.0	15	-1	-1	0
2	120	3.0	15	+1	+1	0
3	30	10.0	15	-1	-1	0
4	120	10.0	15	+1	+1	0
5	30	6.5	5	-1	-1	-1
6	120	6.5	5	+1	+1	-1
7	30	6.5	25	-1	-1	+1
8	120	6.5	25	+1	+1	+1
9	75	10.0	5	0	0	-1
10	75	3.0	25	0	0	+1
11	75	10.0	25	0	0	+1
12	75	6.5	15	0	0	0
13	75	6.5	15	0	0	0
14	75	6.5	15	0	0	0
15	75	6.5	15	0	0	0
16	75	6.5	15	0	0	0

The collected data was fitted to a second-order polynomial equation to establish a relationship between the response and the various variables. The equation can be written as in Eq. 3.2 (Liu *et al.* 2010):

$$Y = \beta_0 + \sum \beta_i x_i + \sum \beta_{ii} x_{ii}^2 + \sum \beta_{ij} x_i x_j + \varepsilon \quad (3.2)$$

where,

Y = predicted response, which is the removal percentage of MB by the Alg/TiO_2/FeNPs

β = constant coefficient

β_i = linear coefficient of the input factor xi

β_{ii} = quadratic coefficient of the input factor xi

β_{ij} = different interaction coefficients between the input factors

x_i, x_j, and ε = error of the model

The analysis of variance (ANOVA), which included the lack of fits, the coefficient of regression (R^2), and the Fisher test value (*F*-value), was used to determine the adequacy of the model (Chaibakhsh *et al.*, 2015). The significance of the model and model variables were determined at the 5% probability level ($p < 0.05$). The model is considered as statistically significant and accepted when the significance probability value ($p > F$) is small (<0.05). The significance of the model was further determined by the R^2 value, where higher R^2 indicating a high significance of the model (Javanbakht & Ghoreishi, 2016). This software applied quadratic equation to build the response surfaces.

To find an optimum condition, the response plots such as contour and 3D plot were used. To generate optimal condition, the goal for the response (MB removal) was set to "target", while the independent variables (pH, initial concentration and contact time) were set to be "within the range".

3.8.3 Determining Optimum Condition for MHM Removal *via* RSM Analysis

The optimized Alg/TiO_2/FeNPs and adsorbent dosage obtained from the preliminary study of MHM removal (Section 3.7.1) was utilized for the optimization condition for MHM removal using the BBD (Design Expert software version 7.1.6) likewise the MB removal. The concentration of MHM solution, initial pH of the solution and contact time were set as the independent variables, while the removal percentage was fixed as the dependent variable (response). The independent variables were coded as -1 (low), 0 (centre point) and +1 (high) in the ranges (Table 3.4). There were a total number of 17 experiments of BBD to be analyzed. Table 3.5 shows the 17 experiments with the ranges and levels in coded units. RSM used regression analysis to analyze the experimental data from BBD.

Table 3.4: Range and levels of the independent variables for MHM removal.

Variables	Coded	Range and Levels		
		-1	0	1
Initial concentration (ppm)	A	30	75	120
pH	B	3.00	5.50	7.00
Contact time (min)	C	5	15	25

Table 3.5: RSM for the three independent variables in corresponding natural values and coded unit of MHM removal.

Run	Independent variables			Coded variables		
	Initial concentration (ppm)	pH	Contact time (min)	A	B	C
1	40	4.0	30	0	-1	-1
2	40	4.0	120	0	-1	+1
3	60	4.0	75	+1	-1	0
4	40	5.5	75	0	0	0
5	60	5.5	120	+1	0	+1
6	40	5.5	75	0	0	0
7	40	7.0	120	0	+1	+1
8	40	5.5	75	0	0	0
9	60	7.0	75	+1	+1	0
10	60	5.5	30	+1	0	-1
11	20	5.5	120	-1	0	+1
12	40	5.5	75	0	0	0
13	20	7.0	75	-1	+1	0
14	20	5.5	30	-1	0	-1
15	20	4.0	75	-1	-1	0
16	40	7.0	30	0	+1	-1
17	40	5.5	75	0	0	0

3.9 Efficiency Comparison and Recyclability Study

Photocatalytic experiments of MB and MHM using blank beads, Alg-5%, TiO_2-Alg, and MNPs/Alg under RSM optimized conditions were also conducted to compare their efficiency with the optimized Alg/TiO_2/FeNPs. Additionally, the efficiency of the optimized Alg/TiO_2/FeNPs was investigated in dark condition as well as under direct sunlight on sunny day. The sunlight intensity was recorded using a light meter (Sunche, model HS1010). The

recorded sunlight intensity are ranged between 3,673 ± 1,287 and 37,667 ± 5,750 lux for MB and 14,650 ± 638 and 75,050 ± 2,758 lux for MHM respectively. The sunlight experiments were performed at an open area in the proximity of our laboratory at the Faculty of Resource Science and Technology.

To examine the efficiency of the Alg/TiO_2/FeNPs for repeated use, the optimized Alg/TiO_2/FeNPs was regenerated by washing using deionized water for three times and then, reused for additional three cycles of MB and MHM treatments under the optimized conditions.

3.10 River water for MHM Solution Preparation

The MHM removal was then tested using real river water sample to simulate the discharge of the MHM into the water bodies. River water samples were collected from Sadong Jaya Jetty, Kota Samarahan, Sarawak (02°02'36.1"N, 2°E25'42.4"). Figure 3.4 shows the sample collection point. The water samples were filled into polyethylene bottles and transported to the laboratory. Then, the samples were kept in the refrigerator at 4°C until further analysis.

Figure 3.4: River water collection point

River water samples were tested for turbidity, pH and dissolved oxygen (DO). The characterizations were performed based on the Standard Methods for Water and Wastewater Examination (APHA, 1999). The turbidity of the river water sample was measured using a turbidity meter (Mi 415 model, Martini Instrument). A pH meter (Model H19024 series, HANNA Instrument) previously calibrated using buffer solutions pH 4.00, 7.00, and 10.00 was used to record the pH of river water sample while a DO meter (Milwaukee brand, MW 600 model) was used to measure the DO values. All water quality readings were measured in triplicate. Initial concentrations of Cu(II), Pb(II) and Cr(III) ions were also determined using ICP-OES. Table 3.6 summarizes the water quality and heavy metals of the river water samples.

MHM solution was prepared using the filtered river water. Then, the condition of the river water was adjusted according to the optimized condition as suggested from the RSM analysis for MHM removal (Section 3.7.3). The optimized Alg/TiO_2/FeNPs was then added into the metals loaded-river water and subjected under UVC light, sunlight and in dark (without UVC light) to compare their efficacy in real river water sample. The recorded sunlight intensity for the metals loaded-river water treatment is ranged between 52,800 ± 6,223 and 98,350 ± 2,899 lux. The sunlight experiment was performed similar in section 3.8.

Table 3.6: Parameters of river water samples collected from Samarahan Jetty

Parameters	Value or Concentration
pH	7.3 ± 0.1
DO	4.1 ± 0.1 mg/L
Turbidity	313 ± 5.5 FNU
Cr	nil
Pb	nil
Cu	0.005 ppm

CHAPTER 4

RESULTS AND DISCUSSION

4.1 Characterizations of the Synthesized Beads

Figures 4.1a and b show the TEM images of MNPs and MNPs-citrate, respectively, while the particle size distribution of MNPs and MNPs-citrate can be seen in Figures 4.1c and d, respectively which were prepared by using 2 M of NaOH solution. The image analysis was accomplished upon measurement of about 300 particles per sample (Figure 4.1). The diameter of the MNPs-citrate particle is smaller compared to the MNPs (Figures 4.1c and d). This indicates that the crystal growth of MNPs was hindered by the adsorption of citrate ions on the MNPs surfaces and reduced the aggregation of MNPs (Ruizmoreno *et al.*, 2013). The average particle diameter for MNPs and MNPs-citrate were 1.7 ± 1.4 nm and 0.8 ± 0.4 nm, respectively (Figures 4.1c and d). For the MNPs, the maximum frequency of their particle size was approximately 1.0 nm. Meanwhile, the particle diameter size of approximately 0.4 nm was mostly present in the sample of MNPs-citrate.

Trisodium citrate functionalization is responsible for the formation of monodisperse MNPs (Ruizmoreno *et al.*, 2013). MNPs in Figure 4.1a appeared to be more agglomerated compared to MNPs in Figure 4.1b. The large surface area of MNPs increases the surface energy thus forcing them to aggregate to minimize the surface energy (Mojić *et al.*, 2012). As such, trisodium citrate functionalization reduced the surface energy by introducing the carboxylate functional groups and creates electrostatic repulsion with the hydroxyl groups of the MNPs (Helmi *et al.*, 2014). Moreover, Fe_3O_4-citrate can provide an improvement for the adsorption ability, which enhanced the degradation rate of MB (Li & Wu, 2017).

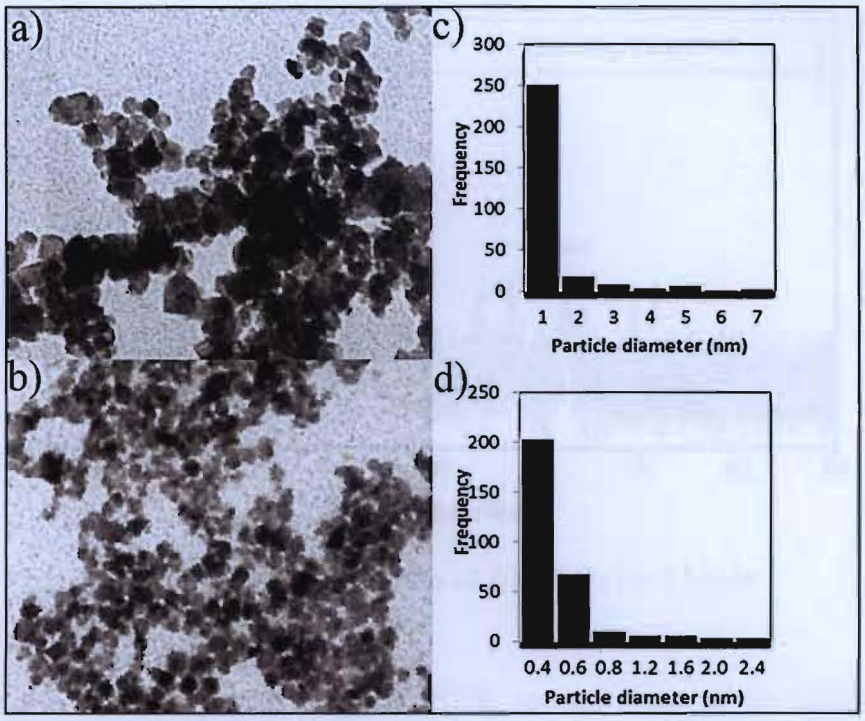

Figure 4.1: TEM micrograph of (a) MNPs, (b) MNPs-citrate and the size distributions of (c) MNPs, and (d) MNPs-citrate

The characterization result for Alg/TiO_2/Fe-2 using XRD is presented in Figure 4.2. Five of the diffraction peaks centred at $2\theta = 30.1°$ (220), 35.3° (311), 43.0° (400), 53.3° (422), and 62.7° (440) were indexed to MNPs (JCPDS 019-0629). Meanwhile, the diffraction peak of anatase TiO_2 was located at $2\theta = 25.3°$ (101), according to JCPDS 21-1272. This data reveals that these nanoparticles have the anatase form of TiO_2 and the single-phase cubic spinel of Fe_3O_4 (Hasanpour *et al.*, 2012). All diffraction peaks appeared to have weak intensities (Figure 4.2). This is due to the Alg coating on the surface of the MNPs, which has a shielding effect that could have substantially led to weakened intensity of the XRD diffraction peaks (Zheng *et al.*, 2016). Hence, the XRD data supported the observation that the synthesis of Alg/TiO_2/Fe-2 was successful.

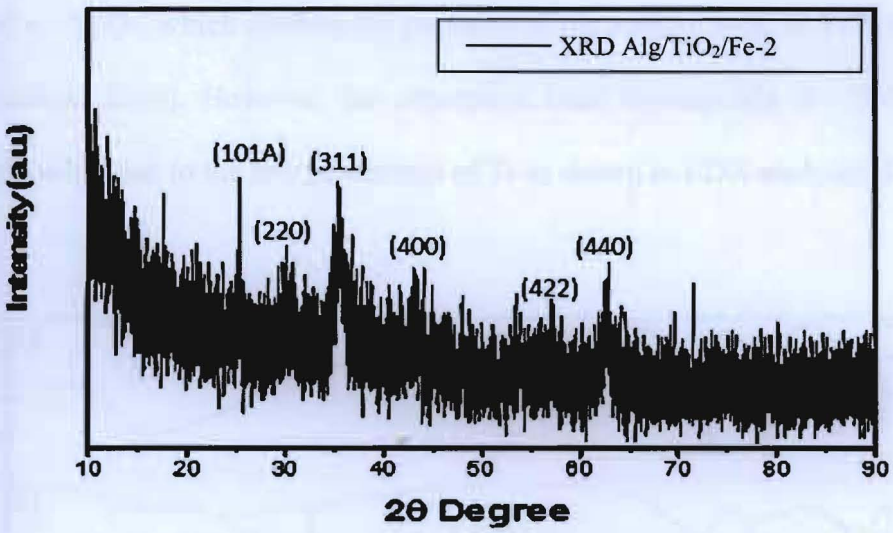

Figure 4.2: XRD pattern of Alg/TiO_2/Fe-2 beads

Figure 4.3 show the comparisons of FTIR spectra range of the different beads for wavelength number 4000 cm^{-1} to 400 cm^{-1}. The wide absorptions band around 3600-3200 cm^{-1} can be attributed to the stretching vibration of -OH from the hydroxyl group (Hammouda *et al.*, 2015). Salamat *et al.* (2017) reported that the -OH originated from the free water molecules and the adsorbed water on the bead surfaces. The absorption bands at 2920 and 2930 cm^{-1}, shown in Figures 4.3b and 4.3d are associated with the -C-H stretching vibrations (Ebenezar *et al.*, 2014). Meanwhile, the absorption bands at 1630, 1590, 1570, and 1420 cm^{-1} in Figures 4.3a to 4.3d correspond to the stretching vibrations of C=O. However, the absorption bands at 1081-1027 cm^{-1} can be associated with the -C-O- stretching band. These absorption bands were the results of the cation exchange between Ca^{2+} and NaAlg, and the stabilizer group of citrate (Mahdavi *et al.*, 2013; Salamat *et al.*, 2017). When comparing Figure 4.3a to Figure 4.3d, it is observed that the absorption band at 400 to 700 cm^{-1} is absent in Figure 4.3a. The absorption bands at 550 and 430 cm^{-1} in Figure 4.3c and 560 cm^{-1} in Figure 4.3d signify the presence of –Fe-O- stretching vibrations (Gopalakannan & Viswanathan, 2016; Salamat *et al.*, 2017). Meanwhile, the absorption bands at 490 cm^{-1} in Figure 4.3b and 470 cm^{-1} in Figure 4.3d

correspond to -Ti-O-, which confirm the presence of the anatase form of TiO_2 (Gopalakannan & Viswanathan, 2016). However, the absorption band corresponds to –Ti-O- is not well resolved plausibly due to the low percentage of Ti as shown in EDX analysis (Table 4.1).

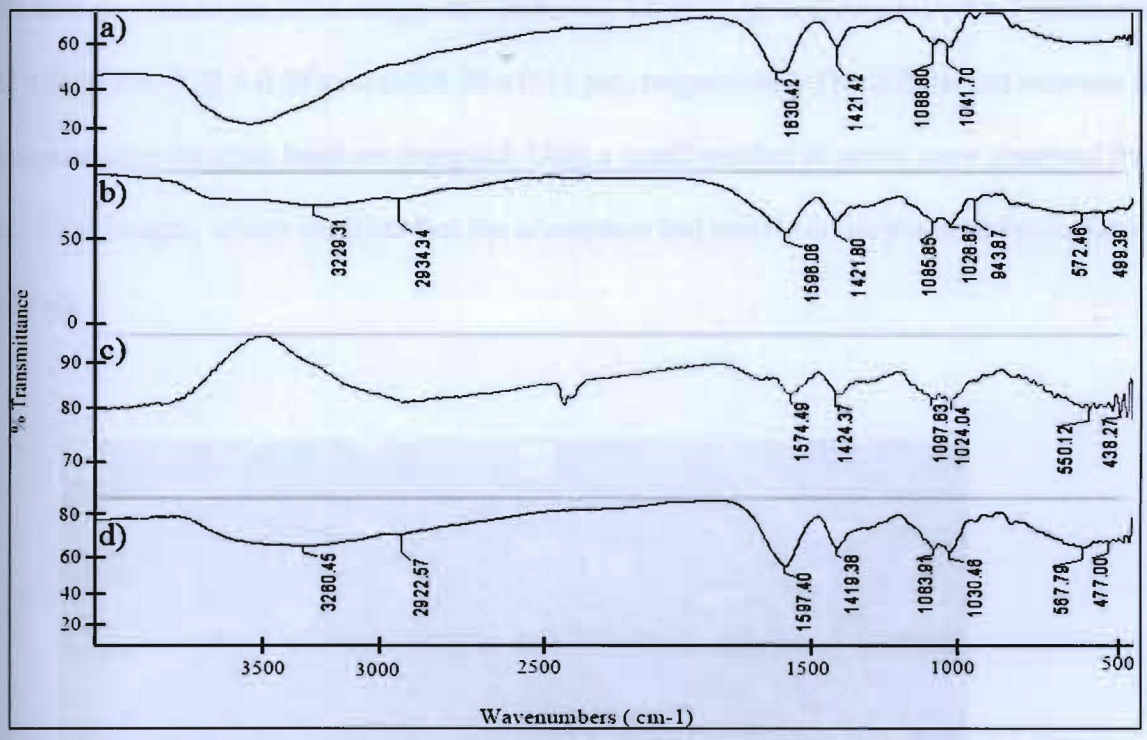

Figure 4.3: FTIR spectra of blank and composite beads (a) Alg-5%, b) TiO_2/Alg, (c) MNPs/Alg, and (d) Alg/TiO_2/Fe-2

Further analysis was done using SEM to compare the surface morphologies of the optimized beads and blank beads (Figure 4.4). The surface of the Alg beads appeared to be smoother compared to the other beads (Figure 4.4a). Meanwhile, the Alg/TiO_2/Fe-2 exhibited rougher surfaces, which made it easier for more pollutants (MB and MHM) to be adsorbed onto its surface (Figure 4.4d). White particles (marked in circles) on the Alg/TiO_2/Fe-2 surface were identified as TiO_2 particles. This finding shows that TiO_2 particles were well dispersed on the Alg/TiO_2/Fe-2 surface compared to those found on the TiO_2/Alg surface (Figure 4.4b). Several

lumps are observed in Figures 4.4c and 4.4d plausibly due to the presence of MNPs as it was not observable in Figures 4.4a and 4.4b. Besides, based on the distinctive dark colour of the MNPs in Figures 4.4c and 4.4d, it can be seen that Alg/TiO_2/Fe-2 had acted as a core, while TiO_2 white particles appeared only to adhere to the surface of Alg/TiO_2/Fe-2. The mean pore sizes measured from the SEM images for TiO_2/Alg, MNPs/Alg, and Alg/TiO_2/Fe-2 beads were 0.22 ± 0.08 μm, 0.22 ± 0.05 μm, and 0.28 ± 0.11 μm, respectively. The differences between the mean pore sizes for each bead are marginal. Only a small number of pores were observed from these SEM images, which suggests that the adsorption had mostly taken place on the surface of the beads.

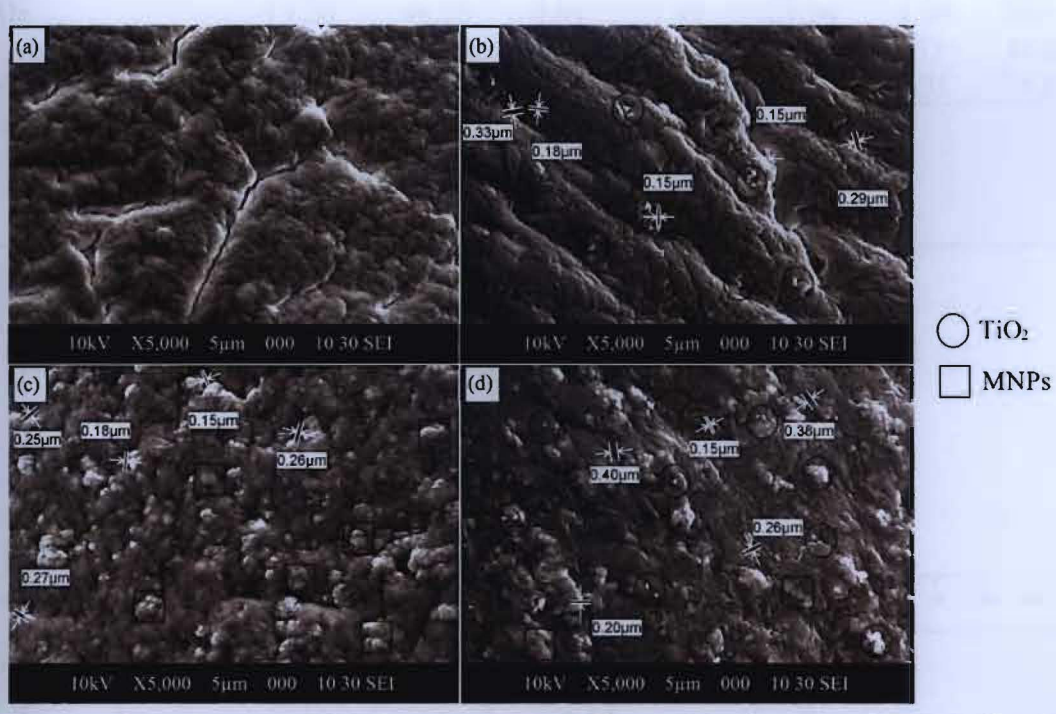

Figure 4.4: SEM images of blank and composite beads (a) Alg-5%. (b) TiO_2/Alg, (c) MNPs/Alg, and (d) Alg/TiO_2/Fe-2 (5000× magnification)

These observations are well supported by the EDX spectrum of the beads, as shown in Figure 4.5. Table 4.2 summarizes the elemental analysis of the beads which comprised of elements C, O, Na, Cl, Ca, Ti, and Fe. The elemental analysis for Alg/TiO_2/Fe-2 demonstrates

that the element with the highest weight percentage in these beads was Ca, followed by O, Fe, Ti, and C. The EDX data show a weight percentage of 6.3% of Ti on the Alg/TiO_2/Fe-2, which was higher than that on the blank TiO_2/Alg beads. In addition, Ca content was the highest in Alg/TiO_2/Fe-2 sample, suggesting that Alg/TiO_2/Fe-2 is the most stable bead compared to TiO_2/Alg and MNPs/Alg. Rocher *et al.* (2008) reported that Ca could be bound to either the carboxylate groups of citrate ions adsorbed on the MNPs, or to the carboxylate groups on the Alg molecules during the gelation process.

Table 4.1: Elemental compositions of the synthesized beads

Type of beads	Weight % of element						
	C	O	Na	Cl	Ca	Ti	Fe
Alg-5%	28.59	41.76	1.17	0.78	27.71	ND	ND
TiO_2/Alg	19.20	46.63	0.01	1.97	27.54	4.66	ND
MNPs/Alg	15.54	17.88	ND	0.32	21.64	ND	44.62
Alg/TiO_2/Fe-2	10.58	21.98	0.48	ND	26.04	6.31	34.61

ND: Not Detected

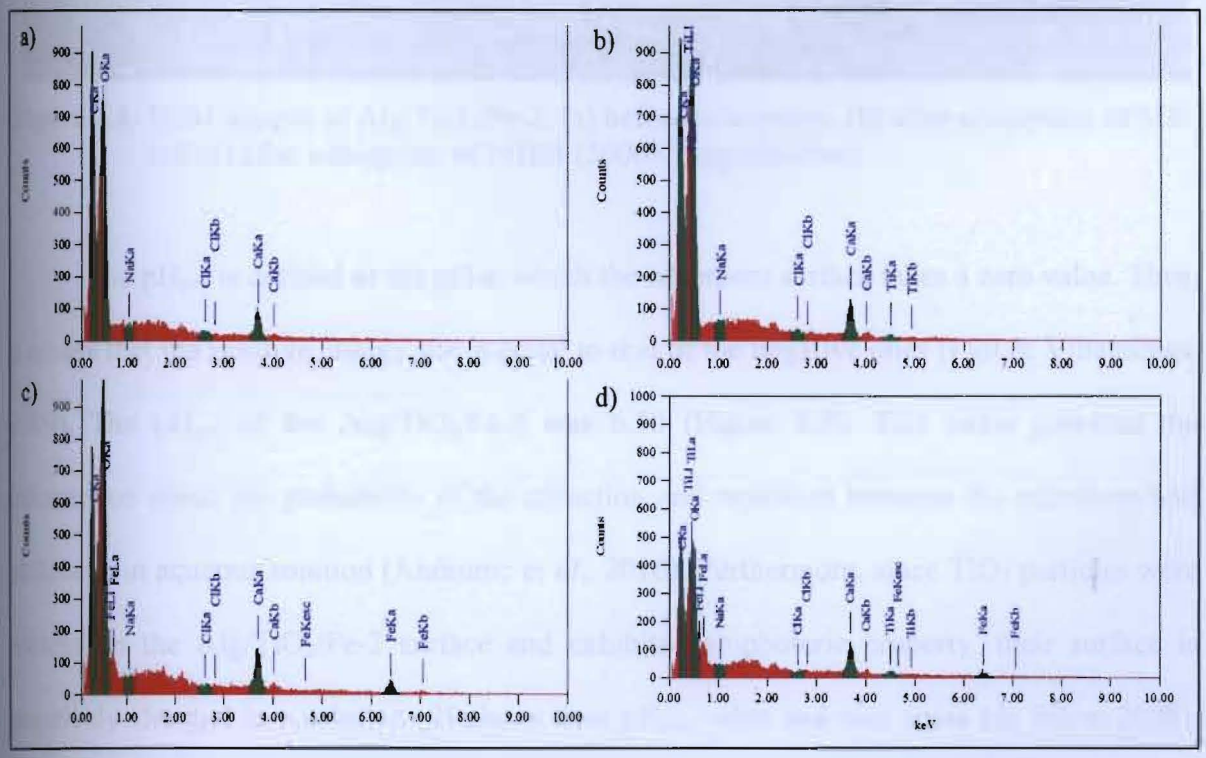

Figure 4.5: EDX data of a) Alg-5%, b) TiO_2/Alg, c) MNPs/Alg, and d) Alg/TiO_2/Fe-2

The SEM images of Alg/TiO_2/Fe-2, before and after MB molecules and MHM ions adsorption were also compared (Figure 4.6). The image of the MB-adsorbed Alg/TiO_2/Fe-2 appeared to be rougher (Figure 4.6a) compared to the image before MB adsorption (Figure 4.6b). On the other hand, MHM-adsorbed Alg/TiO_2/Fe-2 surface (Figure 4.6c) appeared to be smoother compared to the image prior to the MHM adsorption (Figure 4.6a). For both Alg/TiO_2/Fe-2 images after MB and MHM adsorption, fewer TiO_2 nanoparticles were observed, which was likely due to the loss of TiO_2 nanoparticles from the surface as a result of the stirring effect during photocatalytic treatment.

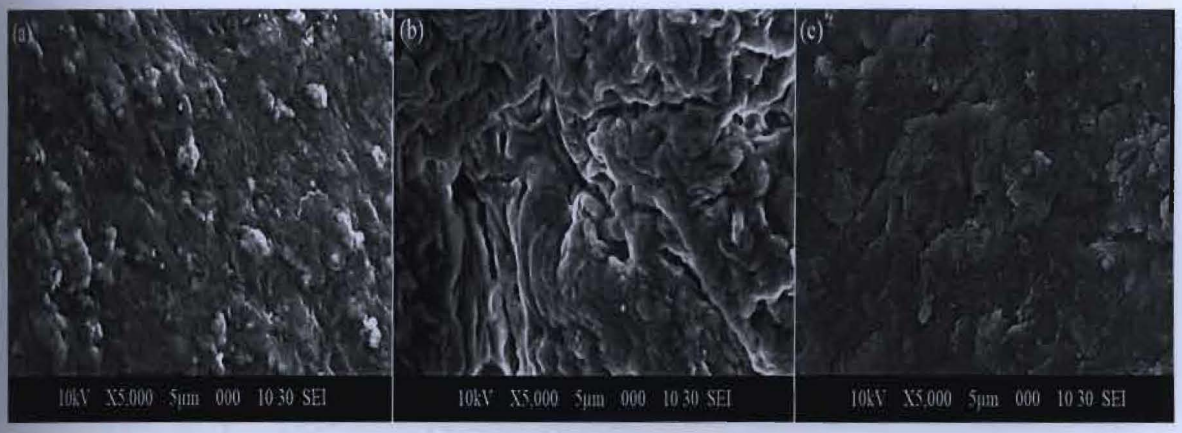

Figure 4.6: SEM images of Alg/TiO_2/Fe-2: (a) before adsorption, (b) after adsorption of MB and (c) after adsorption of MHM (5000× magnification)

The pH_{pzc} is defined as the pH at which the adsorbent surface takes a zero value. Thus, it means that the positive charge site is equal to that of the negative ones (Fiol & Villaescusa, 2009). The pH_{pzc} of the Alg/TiO_2/Fe-2 was 6.50 (Figure 4.7). This value provides the information about the probability of the attraction and repulsion between the adsorbent and pollutants in aqueous solution (Andronic *et al.*, 2016). Furthermore, since TiO_2 particles were present on the Alg/TiO_2/Fe-2 surface and exhibited amphoteric property, their surface is negatively charged in a solution pH above their pH_{pzc} value and vice versa (da Silva, 2008).

This is in agreement with Lo *et al.* (2012) who described that a solution pH above pH_{pzc} causes the adsorbent surface to be negatively charged and might interact with positive species while at pH lower than pH_{pzc}, the adsorbent surface is positively charged and could interact with negative species. Since MB and MHM are positively charged molecules, the adsorption is expected to be more favored at pH solution above the pH_{pzc}. Indeed, the presence of a high number of OH^- groups on the Alg/TiO_2/Fe-2 surface could enhance the adsorption of MB molecules and MHM onto the Alg/TiO_2/Fe-2 surface.

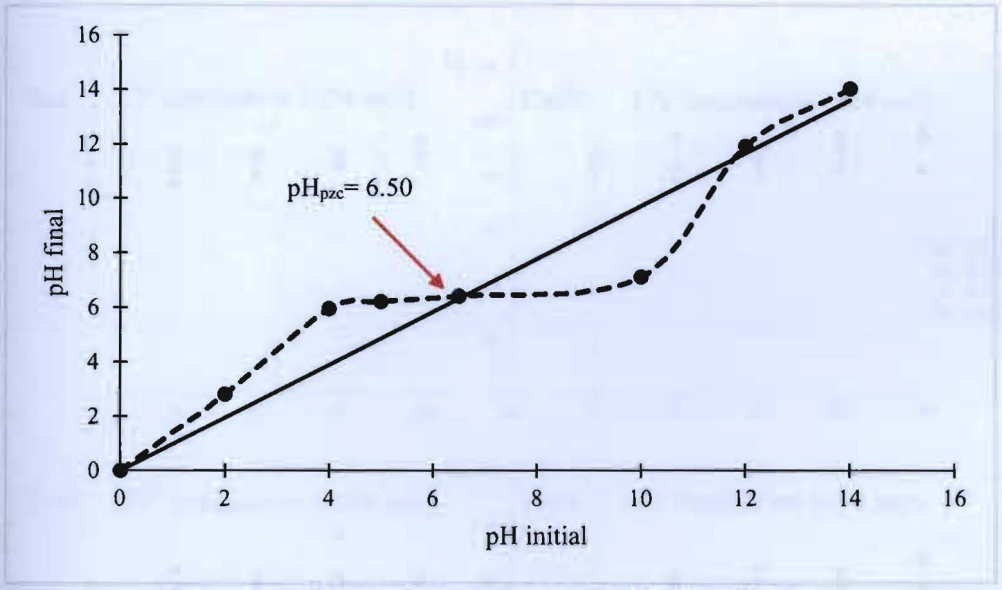

Figure 4.7: Point of zero charge of Alg/TiO_2/Fe-2

4.2 Photocatalytic Removal of MB

4.2.1 Effect of Synthesis Conditions and Adsorbent dosage on the Removal of MB

Figure 4.8 illustrates the effect of varying adsorbent dosage of Alg/TiO_2/FeNPs beads from 0.1 to 0.6 g synthesized under different conditions (Table 3.1) on the removal of MB. In general, Alg/TiO_2/FeNPs demonstrated the ability to remove about 60.0-80.0% of MB in dark condition predominantly by adsorption process (Figure 4.8). Alg bead that is known as a good

adsorbent could have facilitated the MB molecules adsorbed on Alg/TiO_2/FeNPs surface. This finding corroborates with those reported by Zainal *et al.* (2016). The immobilized MNPs in Alg beads demonstrated a great adsorption efficiency of Pb(II) ions. Upon UVC irradiation for 2 h, although MB removal revealed an increasing trend for all four Alg/TiO_2/FeNPs at different dosages, only a small increment ranging from 1.0% to 15.0% was observed (Figure 4.8). Despite the marginal increase in the removal efficiency upon UVC irradiation, decolourisation of MB solution was observed in all cases.

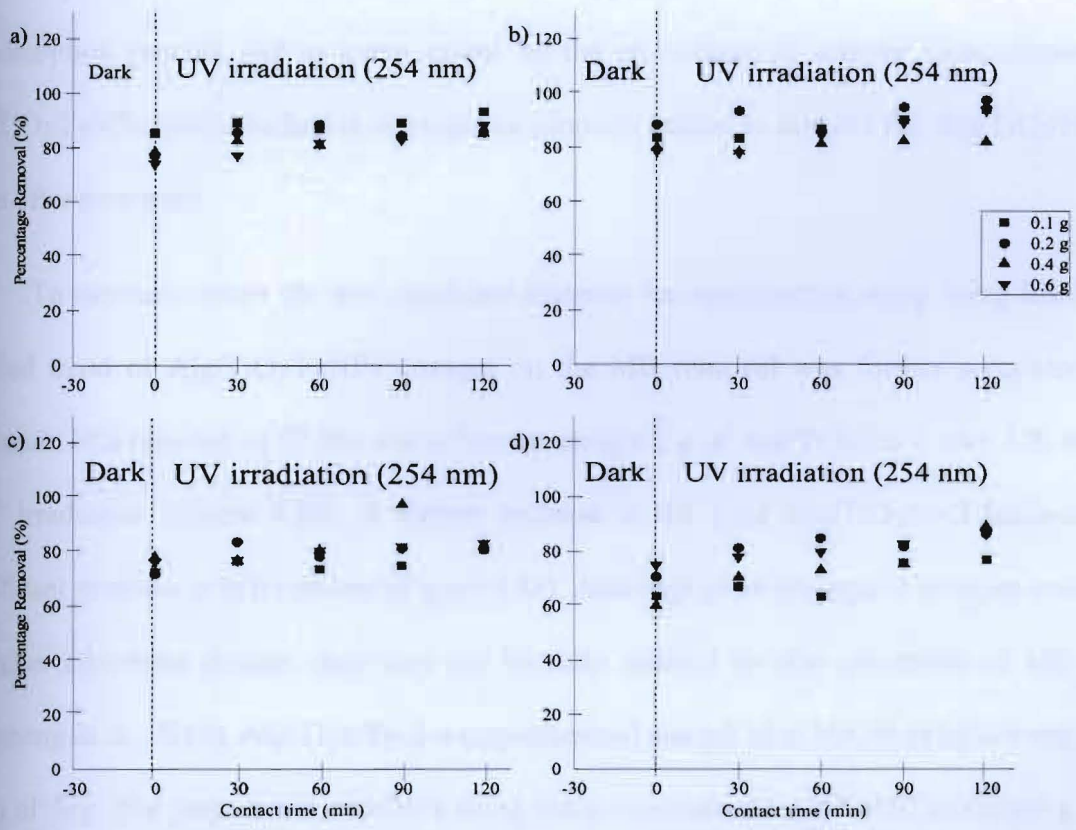

Figure 4.8: Effect of adsorbent dosage of different Alg/TiO_2/FeNPs samples on the removal of MB. a Alg/TiO_2/Fe-1. b Alg/TiO_2/Fe-2. c Alg/TiO_2/Fe-3. d Alg/TiO_2/Fe-4 (MB initial concentration: 5 ppm)

This phenomenon was however, not observed in the dark condition. After dark equilibrium period that has resulted in the adsorption of MB molecules on Alg/TiO_2/FeNPs, the •OH radicals formed during TiO_2 activation by UVC irradiation could have aided the oxidation of MB molecules and also decolourization of MB solution (Ramli *et al.*, 2014).

Alg/TiO_2/Fe-1, Alg/TiO_2/Fe-2, Alg/TiO_2/Fe-3, and Alg/TiO_2/Fe-4 achieved the equilibrium state or plateau at different adsorbent dosages (Figures 4.8a to 4.8d). The results suggest that removal of MB was not greatly enhanced by the increasing dosage of Alg/TiO_2/FeNPs beads and in fact a small amount of Alg/TiO_2/FeNPs beads would be sufficient for MB removal. Therefore, MB removal can be hypothesized to be predominantly favoured by adsorption process and to some extent by the photocatalytic activity demonstrated by Alg/TiO_2/FeNPs beads. Inclusion of magnetic property helped to retrieve the Alg/TiO_2/FeNPs beads after treatment.

To carefully select the best candidate material for optimization study using RSM, the detailed trend of Alg/TiO_2/FeNPs dosages on the MB removal was further scrutinized. A maximum MB removal of 97.6% was achieved using 0.2 g of Alg/TiO_2/Fe-2 after 120 min of UVC irradiation (Figure 4.8b). A further increase to 0.6 g of Alg/TiO_2/Fe-2 displayed no significant increase in MB removal (Figure 4.8b). Although more adsorption sites are available at higher adsorbent dosage, they may not be fully utilized for the adsorption of MB dyes (Qiusheng *et al.*, 2015). Alg/TiO_2/Fe-2 was synthesized using 2 M of NaOH of MNPs and 5.0% (w/v) of Alg. The preparation of MNPs using lower concentration of NaOH exhibited a large surface area and strong magnetic property, thus providing more sites for the immobilization with Alg and TiO_2 (Tajabadi & Khosroshahi, 2012).

Higher concentration of NaOH may induce the formation of non-magnetite layer and weaker magnetic properties. Therefore, it can be assumed that lower NaOH concentration improved the immobilization of MNPs with Alg and TiO_2. Furthermore, an improved mechanical strength of Alg/TiO_2/Fe-2 after the treatment with UVC irradiation was observed when using 5.0% (w/v) of Alg as the beads maintained their shape even after 120 min of photocatalytic treatment (Figure 4.9). This could be due to the increasing intermolecular cross-linking of G-blocks with the $CaCl_2$ to form the hydrogel (Lee & Mooney, 2012). Higher concentration of Alg could have enhanced the dispersion of TiO_2 concentration by reducing the TiO_2 fragment size (Loosli *et al.*, 2015). Based on the abovementioned points, 0.2 g of Alg/TiO_2/Fe-2 was chosen as the fixed variable, with three independent variables (pH, contact time, and initial concentration) to investigate the optimized conditions for MB removal using RSM design.

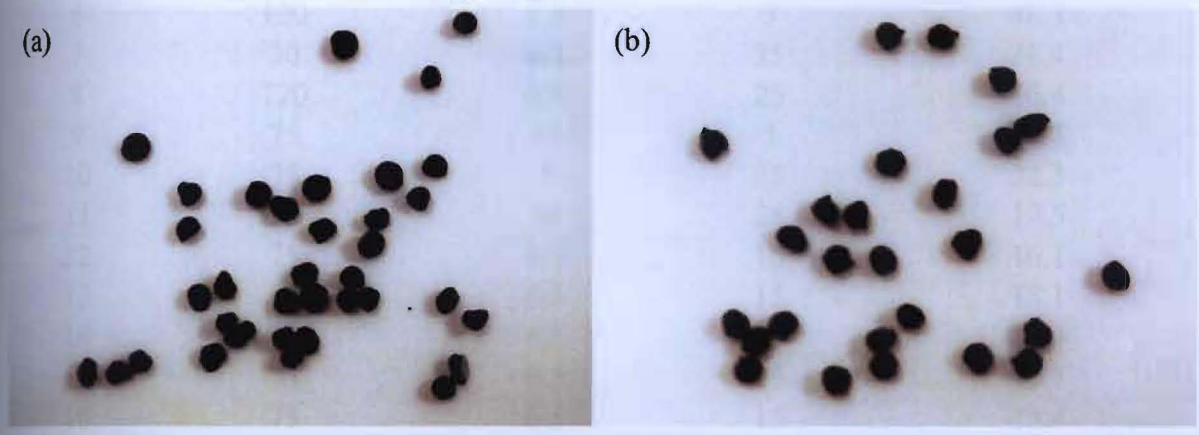

Figure 4.9: Alg/TiO_2/Fe-2 beads (a) before adsorption and (b) after adsorption of MB

4.3 Model Fitting and Statistical Analysis of BBD for MB Removal

Table 4.2 shows the experimental design matrix of BBD with a total number of 16 experiments and the responses for the MB removal. MB removal varied from 15.1% to 92.8%. Based on the experimental results, the data was found to fit the second order polynomial

equation. The equation was generated in terms of the coded values and expressed as shown in Eq. 4.1:

$$Y = 15.54 - 0.46A + 1.15B - 34.00C - 3.77AB - 1.97\,AC - 3.62BC + 3.51\,A^2 + 4.59\,B^2 + 33.81C^2 \quad (4.1)$$

where, Y is the MB removal (percentage), and A, B, and C are the coded values for the contact time, pH, and initial MB concentration, respectively.

Table 4.2: Results for the Design Matrix of RSM study

	Variables			MB removal (%)
Run	**A**	**B**	**C**	
1	30	3	15	19.2
2	120	3	15	25.9
3	30	10	15	28.9
4	120	10	15	20.6
5	30	6.5	5	85.4
6	120	6.5	5	88.3
7	30	6.5	25	21.4
8	120	6.5	25	16.4
9	75	10	5	92.8
10	75	3	25	22.3
11	75	10	25	17.5
12	75	6.5	15	16.1
13	75	6.5	15	15.1
14	75	6.5	15	15.4
15	75	6.5	15	15.7
16	75	6.5	15	15.4

Figure 4.9 illustrates the accuracy of the model by comparing the experimental results against the predicted responses of the model for the MB removal. From the ANOVA (Table 4.3), the R^2 of 0.9999 shows that the experimental results fitted the polynomial model adequately. Thus, it is believed that the model was able to give a good estimate of response in

the studied range due to the high R^2 value (Khosravi & Arabi, 2016). Table 4.3 shows the ANOVA results for the response surface quadratic model for MB removal. The *F*-value of 13067.60, as shown in Table 4.3 implies that the regression model is statistically significant. There were only 0.01% chances that a "Model *F*-Value" could occur due to noise. The value of "*Prob* > *F*" of less than 0.0500 indicates that the model is significant and, in this case, A, B, C, AB, AC, BC, A^2, B^2, and C^2 are the significant model terms.

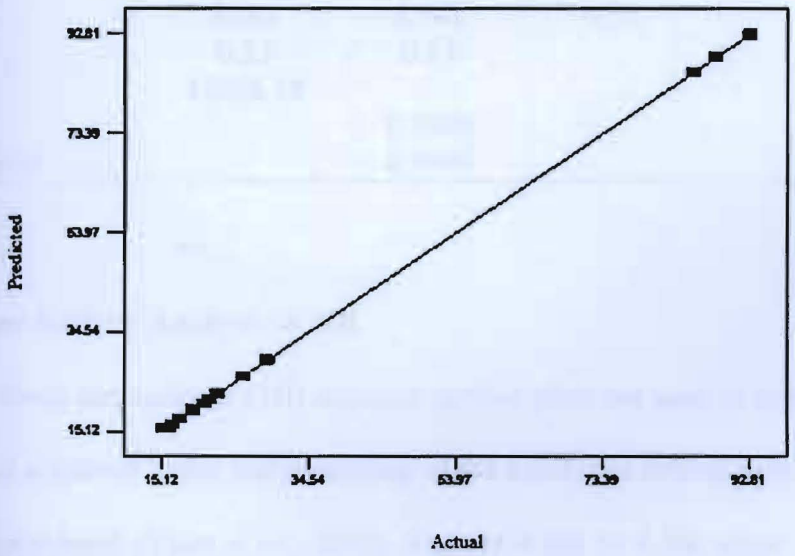

Figure 4.10: The scatter plot of predicted values versus actual values for the Box-Behnken design matrix

If the *F*-value is greater than 0.1, this would indicate that the model terms were insignificant. The "Lack of Fit *F*-value" of 0.31 implies that the "Lack of Fit" is not significant, relative to the pure error. Thus, the model can be concluded to be valid due to the insignificance of the "Lack of Fit *F*-value". There is a 75.3% chance that a "Lack of Fit *F*-value" could occur due to noise.

Table 4.3: Results of ANOVA

Source	Sum of Squares	Mean Square	*F* value	*p*-Value
Model	12067.98	1340.89	13067.60	< 0.0001
A-Contact time	1.71	1.71	16.62	0.0065
B-pH	7.08	7.08	68.96	0.0002
C-Initial Concentration	6167.13	6167.13	60101.71	< 0.0001
AB	56.75	56.75	553.02	< 0.0001
AC	15.48	15.48	150.88	< 0.0001
BC	26.15	26.15	254.80	< 0.0001
A^2	41.16	41.16	401.16	< 0.0001
B^2	70.08	70.08	682.93	< 0.0001
C^2	3810.50	3810.50	37135.20	< 0.0001
Residual	0.62	0.10		
Lack of Fit	0.081	0.041	0.31	0.7528
Pure Error	0.53	0.13		
Cor Total	12068.59			
R-Squared		0.9999		
Adj R-Squared		0.9999		

4.4 Response Surface Analysis of MB

The three-dimensional (3D) response surface plots are used to represent the regression equation and achieved better understanding of the combined effects between variables within the range considered (Vaez *et al.*, 2012). Figures 4.10a to 4.10c show the combined effect between the three independent variables on the response, which are visualised in the 3D response surface plots.

4.4.1 Effect of Initial Concentration and Contact Time

Figure 4.11a depicts the 3D surface of the combined effect of the contact time ranged from 30 to 120 min and initial MB concentrations from 5 to 25 ppm under UVC irradiation, with pH 10.00 as the constant variable. A maximum MB removal of 99.0% was found at 30 min and 5 ppm of MB. MB removal is greatly dependent on the initial concentration of MB. A decrease of about one order of magnitude was observed for the MB removal percentage from

98.0% to 8.0% at the initial 30 min interval, as the initial concentration of MB solution increased from 5 to 25 ppm. At higher MB concentrations, more MB molecules covered and consequently shielded the active sites of Alg/TiO_2/Fe-2 surface and hindered the absorption of UVC, which led to the decrease of •OH radical generation (Yao & Wang, 2010). Thus, this resulted in the 2.5-time decrease of the initial removal percentage. Moreover, repulsive forces between MB molecules due to the excessive numbers of molecules of MB on Alg/TiO_2/Fe-2 surface could have forced MB molecules back to the solution, hence decreasing the MB removal.

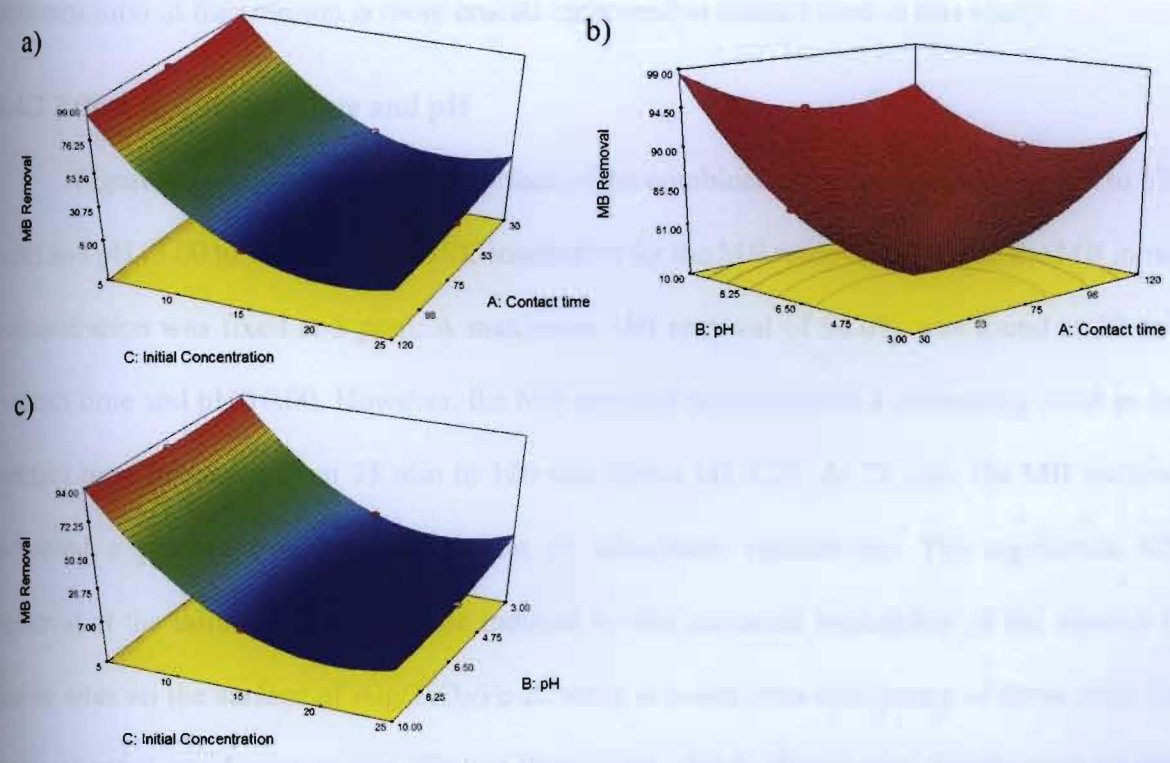

Figure 4.11: A 3D response surface plot that combines the effects of (a) initial concentration and contact time (b) contact time and pH and (c) pH and initial concentration

Meanwhile, more active sites were available at low concentration and thus a significant amount of MB molecules can be adsorbed, resulting in higher MB removal (Albroomi *et al.*,

2015). Similar trends were observed for the adsorption of MB molecules by nano zerovalent iron (NZVI) (Khosravi & Arabi, 2016) and magnetic reusable nanocomposites (Harifi & Montazer, 2014).

As the contact time increased, the MB removal decreased and achieved a plateau at 75 min for each concentration. This behaviour can also be explained by the unoccupied active sites at low contact times compared to that of high contact times. When the treatment was performed at high contact times, the number of MB molecules adsorbed on the active sites of Alg/TiO_2/Fe-2 increased, hence covering the active sites from absorbing UVC irradiation which eventually decreased the photocatalytic activity and MB removal. Thus, it can be concluded that initial concentration of the solution is more crucial compared to contact time in this study.

4.4.2 Effect of Contact Time and pH

Figure 4.11b illustrates the 3D surface of the combined effect of contact time (30 to 120 min) and pH (3.00 to 10.00) under UVC irradiation for the MB removal, in which the MB initial concentration was fixed at 5 ppm. A maximum MB removal of 98.0% was found at 30 min contact time and pH 10.00. However, the MB removal demonstrated a decreasing trend as the contact time increased from 75 min to 120 min above pH 8.25. At 75 min, the MB removal achieved a plateau signifying attainment of adsorption equilibrium. The significant MB removal at the initial 30 min could be induced by the increased availability of the number of active sites on the surface of Alg/TiO_2/Fe-2, while at continuous occupancy of these sites; the removal efficiency becomes less efficient (Bakr *et al.*, 2015). Postai *et al.* (2016) reported that the repulsive forces between the molecules on the adsorbent resulted in low adsorption and decrease the MB removal. In contrast, at lower pH values (3.00–8.25), the MB removal was observed to increase as the contact time increased from 30 to 120 min. This might be due to the

interaction between the MB solution and the Alg/TiO_2/Fe-2 at higher contact times. Continuous stirring could have caused more MB molecules to be exposed to Alg/TiO_2/Fe-2 active sites and thus, gradually increase the MB removal (Hasbullah *et al.*, 2014).

Figure 4.11b also reveals that MB removal increased from pH 3.00 to 10.00. As the Alg/TiO_2//Fe-2 pH_{pzc} was at 6.50, the Alg/TiO_2/FeNPs-2 surface can be assumed to be negatively charged when the solution pH was above the pH_{pzc} value and thus more MB molecules could be adsorbed to their surface (Andronic *et al.*, 2016). The lowest MB removal of 81.0% was found at pH 3.00 and 30 min. At lower pH, MB removal was observed to increase with the increasing contact time. This could be attributed to the availability of more active sites at lower pH compared to that of at higher pH. MB is a cationic dye with a positive charge. Therefore, the adsorption of MB is likely to be more favoured at basic condition (high pH) (Umoren *et al.*, 2013). At low pH, high number of protons (H^+) in MB solution led to the competition between the MB molecules and the protons for the available active sites on Alg/TiO_2/Fe-2 surface (Majidnia *et al.*, 2015). At high pH ($\geq$6.50), as the number of hydroxyl ions (OH^-) increases in the solution, the number of negatively charged sites of Alg/TiO_2/Fe-2 also increases (Albroomi *et al.*, 2015). The observed trends signify the influence of TiO_2 surface on Alg/TiO_2/Fe-2, which exhibits an amphoteric characteristic. Effect of pH can be rather complex as a result of changes to TiO_2 on the Alg/TiO_2/Fe-2 surface and MB substrate. As the pH of the aqueous solution changes at high pH, the surface charge of TiO_2 also changes accordingly (Reza *et al.*, 2017), therefore pH changes will affect the electrostatic interactions between TiO_2 surface and MB ionic forms.

4.4.3 Effect of pH and Initial Concentration

The 3D surface plot describing the interaction between the solution pH (3.00 to 10.00) and initial MB concentration (5 to 25 ppm) when the contact time was kept constant at 120 min is shown in Figure 4.11c. A maximum MB removal of 93.0% was observed at 5 ppm of initial MB concentration and pH 10.00. The MB removal continued to decline as the MB concentration increased from 5 ppm to 25 ppm, but the removal was observed to rise with increasing pH from 3.00 to 10.00 (Figure 4.10c). As the MB initial concentration increased, the formation of degradation products in high concentrations in various pathways during photocatalytic treatment of MB could have caused MB molecules and the degradation products to compete with each other for •OH radicals present on the surface of Alg/TiO_2/Fe-2 (Xu *et al.*, 2014), resulting in lower MB removal at higher MB concentration. Furthermore, it can be also assumed that at higher concentration of MB, the generation of the •OH radicals on the surface of Alg/TiO_2/Fe-2 could be reduced due to the saturation of active sites by MB molecules (Tayeb & Hussein, 2015). Moreover, MB dye is a photosensitizer itself, thus its MB molecules could absorb the UVC irradiation significantly compared to the TiO_2 particles on Alg/TiO_2/Fe-2 surface. As a consequence, the photocatalytic efficiency of Alg/TiO_2/Fe-2 reduces to a lesser number of •OH and $O_2^{\bullet-}$ radicals (Konstantinou & Albanis, 2004).

The effect of pH on MB removal has been previously discussed. Changes in pH exert a large influence in the generation of OH^- ions in MB solution as well as the singlet oxygen and radicals formation. At a pH value of more than pH_{pzc} (6.50), the MB removal greatly increases due to an increase in OH^- ions on the Alg/TiO_2/Fe-2 surface and also the formation of singlet oxygen and radicals (Chen *et al.*, 2011). Conclusively, both initial concentration and pH govern the removal of MB.

4.4.4 Numerical Optimization

Primarily, the RSM study was conducted to determine the optimum operating parameters for maximizing the adsorption of MB on Alg/TiO_2/Fe-2. The optimization process was done by selecting the desired target for each of the variable and response. For the independent variables such as contact time, pH and the initial concentration, "in range" option was selected while a "target" was chosen for the MB removal as our aim was to obtain the maximum MB removal of the treatment. From the analysis, the maximum adsorption capacity, as predicted by the model, was at 5 ppm of MB solution, pH 10.00, and 120 min. The predicted value was calculated by the Design Expert software by using the second order polynomial as shown in Eq. 4.1. These conditions have yielded a better MB removal percentage of 97.2% and this result is in good agreement with the experimental value of 94.0%.

Table 4.4: Optimized conditions given by RSM for MB removal using Alg/TiO_2/Fe-2 beads

Initial concentration (ppm)	Contact time (min)	pH	MB Removal (%)	
			Actual	Predicted
5	120	10.00	97.2	94.0

4.5 Comparison of Efficiency and Recycling Study for MB Removal

The MB removal was also studied using the blank beads and the slurry form of TiO_2 under UVC at optimized condition as suggested by the RSM study (Figure 4.12). The results indicate that the MB removal was the highest when using the slurry form of TiO_2, followed by Alg/TiO_2/Fe-2 under sunlight, Alg/TiO_2/Fe-2 under UVC, MNPs/Alg, TiO_2/Alg, Alg-5%, MB only under UVC and Alg/TiO_2/Fe-2 in the dark. In the absence of TiO_2, MB was photodegraded by 64.9%. As MB is a sensitizer, it can generate singlet oxygen with the presence of UV light

and molecular oxygen (O_2) which might contribute to the degradation of MB alone under UVC light (Nour-Mohhamadi *et al.*, 2005).

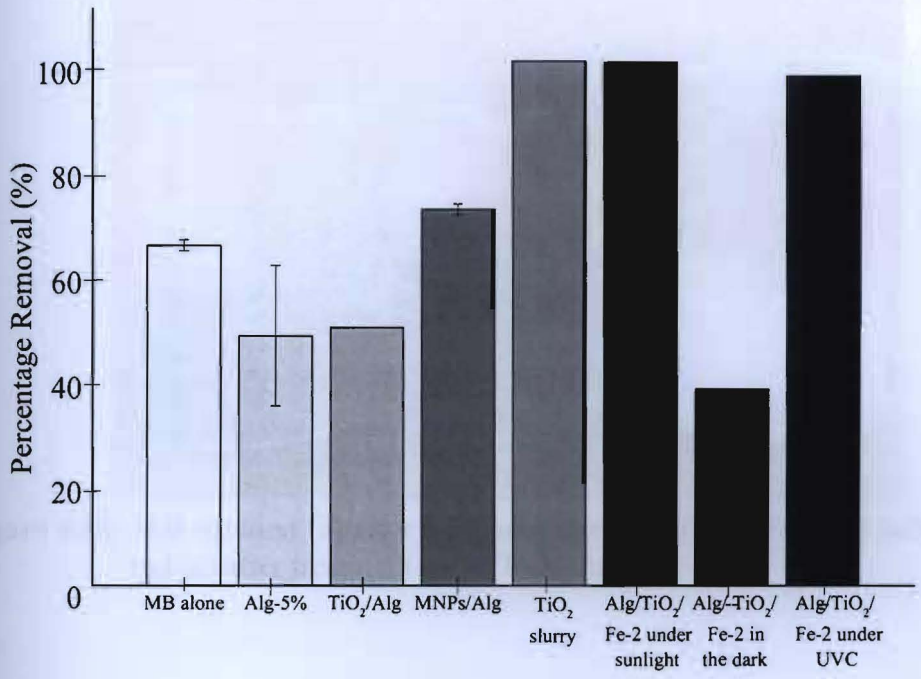

Figure 4.12: Performance comparison between Alg/TiO_2/ Fe-2 under UVC, sunlight and dark condition with TiO_2 slurry, MB only, Alg-5% beads, TiO_2/Alg beads, MNPs/Alg beads in removing MB (initial concentration of MB: 5 ppm; dark equilibration time: 30 min; UVC irradiation time: 2 h; sunlight exposure: 2 h, adsorbent: 0.002 g/mL)

Only partial decolourisation had occurred after the treatment of MB using Alg/TiO_2/Fe-2 under UVC light, which is in contrast to the complete decolourization of MB when using TiO_2 in the powder form (Figure 4.13). Differences in terms of the solution colour were likely due to the different degradation products that were formed during the course of the treatment, owing to the non-selective nature of the •OH radicals. Since the identification of the arising

degradation products is not an objective of this present study, this aspect could be the focus in future studies. Furthermore, the degradation rates would also be likely to differ due to the differences in the physical and chemical characteristics of the photocatalyst materials used.

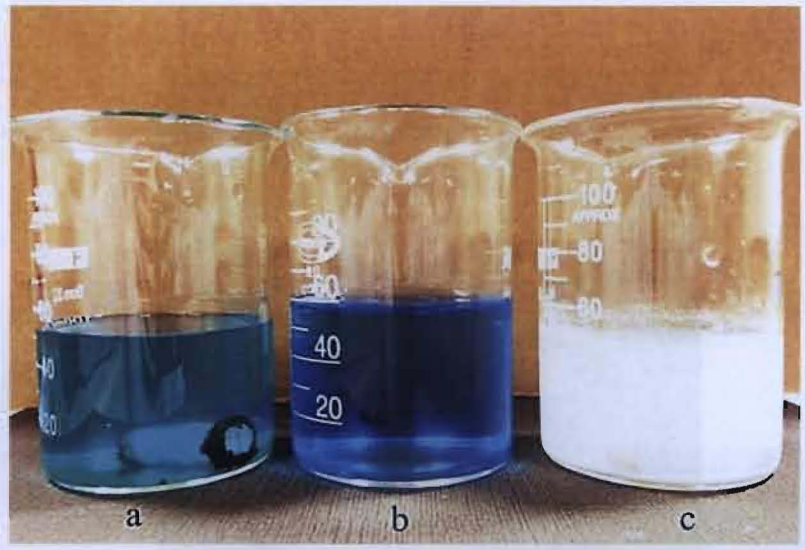

Figure 4.13: MB solution (a) after treatment using Alg/TiO_2/Fe-2 (b) before treatment and (c) after treatment using TiO_2 slurry

As expected, a complete removal of MB was obtained using the slurry form of TiO_2, which signifies its photocatalytic efficiency under UVC. Nonetheless, the TiO_2 photocatalysts could not be completely separated from the MB solution after the treatment.

On the contrary, the Alg/TiO_2/Fe-2 can be easily retrieved using a permanent magnet after the treatment, which would make this nanocomposite material more practical in wastewater remediation (Figure 4.14). In the case of MNPs/Alg, the adsorption capability of the MNPs coupled with Alg had contributed to the 70.7% of MB removal, despite the absence of TiO_2. Both Alg and MNPs are known as good adsorbents. High surface areas and limited internal diffusion resistance had contributed to the adsorption of MNPs (Alqadami *et al.*, 2016).

When comparing between the Alg-5% and TiO_2/Alg beads, the higher removal percentage of MB demonstrated by Alg/TiO_2/Fe-2 can be ascribed to the synergistic effect of the incorporation of MNPs and TiO_2 with the Alg. The dark control experiment revealed that about 38.0% of MB molecules were adsorbed onto Alg/TiO_2/Fe-2 (Figure 4.12).

Figure 4.14: Magnetic susceptibility of Alg/TiO_2/Fe-2 under external magnetic field

In the case of MNPs/Alg, the adsorption capability of the MNPs coupled with Alg had contributed to the 70.7% of MB removal, despite the absence of TiO_2. Both Alg and MNPs are known as good adsorbents. High surface areas and limited internal diffusion resistance had contributed to the adsorption of MNPs (Alqadami *et al.*, 2016). When comparing between the Alg-5% and TiO_2/Alg beads, the higher removal percentage of MB demonstrated by Alg/TiO_2/Fe-2 can be ascribed to the synergistic effect of the incorporation of MNPs and TiO_2 with the Alg. The dark control experiment revealed that about 38.0% of MB molecules were adsorbed onto Alg/TiO_2/Fe-2 (Figure 4.12).

After 120 min of treating MB in dark condition, the poor performance of Alg/TiO_2/Fe-2 was observed. This could be contributed from the desorption of MB molecules back to the solution as TiO_2 can only be activated in the presence of UV irradiation thus resulting in low MB removal (Xu *et al.,* 2014). In this context, both photocatalysis and adsorption work simultaneously to remediate MB-loaded aqueous solution. The MB removal using Alg/TiO_2/Fe-2 beads upon direct sunlight irradiation was comparable to the UV light, which was at 99.8%. This result suggested that Alg/TiO_2/Fe-2 beads could be used either under UV or under the sunlight. However, solar radiation is controlled by geographic latitude, time of the day, cloud cover, and also atmospheric conditions (Kanakaraju *et al.*, 2016) contrary to constant intensity from UV light which might only vary due to its life-time. This result also provides an indication of the potential of using Alg/TiO_2/Fe-2 beads for MB removal under direct sunlight.

Figure 4.15 shows the recyclability of Alg/TiO_2/Fe-2 after being recovered and reused for MB removal study.

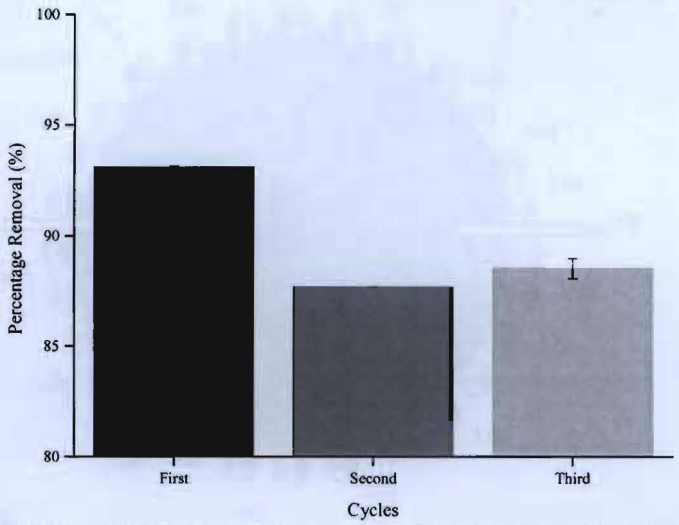

Figure 4.15: Recycling study of optimized Alg/TiO_2/Fe-2 beads

The minor reduction in terms of the removal percentage of approximately 6.0% implied that the stability of the nanocomposites had remained consistent up to three cycles. The minor decrease in the recyclability performance of Alg/TiO_2/Fe-2 after the first cycle could be attributed to the loss of MNPs and TiO_2 during washing and recollection (Harifi & Montazer, 2014).

4.6 Elucidating Methylene Blue Removal by Alg/TiO_2/Fe-2 Beads

Several physical, chemical and photochemical processes can be responsible for MB removal from the aqueous solution under UVC irradiation in the presence of active photocatalysts (Konstantinou & Albanis, 2004). Some of these processes have been studied singularly or as a combination of photolysis and photocatalytic degradation (Tschirch *et al.*, 2008). Therefore, given the hybrid nature of the Alg/TiO_2/Fe-2 (Figure. 4.16), it is useful to describe the series of either synergic or competitive processes involved in MB removal.

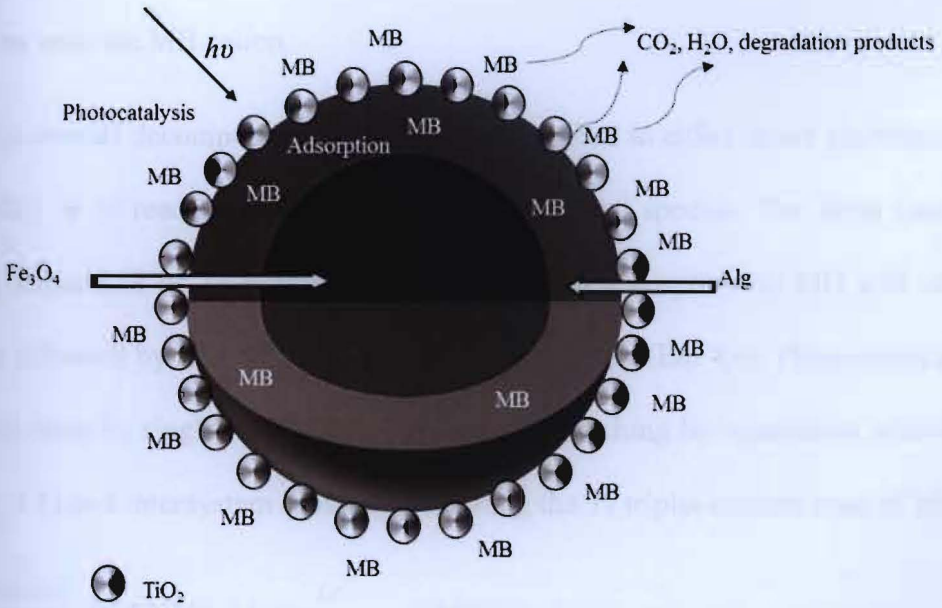

Figure 4.16: A representation of MB removal by Alg/TiO_2/Fe-2

Under the studied conditions, physical removal of MB can easily be interpreted in terms of adsorption by the Alg/TiO_2/Fe-2 beads, either *via* inclusion in their alginate layer (Eq. 4.2) or by ion-dipole interactions with the terminal hydroxy groups (Ti-OH) of titania particles (Eq. 4.3).

$$MB(aq) \leftrightharpoons MB@Alg/TiO_2/Fe-2(Alg) \quad (4.2)$$

$$MB(aq) \leftrightharpoons MB@Alg/TiO_2/Fe-2(TiO_2) \quad (4.3)$$

The former has been postulated as the dominant process in the removal of MB based on the dark experiments performed. An effective adsorption by alginate occurred due to the carboxylate and hydroxyl functional groups of the anionic polysaccharide layer. These functional groups are responsible for capturing MB from aqueous solution *via* electrostatic attraction (Liu *et al.*, 2016). Additionally, the adsorption on titania will be also affected by medium pH. Indeed, basic conditions, with pH above TiO_2 point of zero charge, will produce a negatively charged surface of titania particles on the Alg/TiO_2/Fe-2 beads thus favouring ionic interactions with the MB cation.

The overall decomposition of MB can be ascribed to either direct photolysis (Tschirch *et al.*, 2008) or to reaction with photogenerated reactive species. The latter can be formed involving either MB or TiO_2 as light absorbers. Light absorption by MB will cause $S_0 \rightarrow S_2$ excitation followed by $S_2 \rightarrow S_1$ ultrafast radiation less decay (Eq. 4.4). Photophysical processes originating from S_1 singlet $^1MB^*$ include physical quenching by interaction with the alginate layer (Eq. 4.5) and intersystem crossing generating the T_1 triplet excited state of MB (Eq. 4.6)

$$MB \xrightarrow{h\nu\ (254\ nm)} {}^1[MB]^*(S_2) \xrightarrow{i.c.} {}^1[MB]^*(S_1) \quad (4.4)$$

$$Alg + {}^1[MB]^*(S_1) \longrightarrow Alg + MB \quad (4.5)$$

$$^1[MB]^* \xrightarrow{i.s.c.} {}^3[MB]^* \quad (4.6)$$

Considering the high energy of the incident 254 nm radiation, which is larger than titania band gap energy (3.2 eV), the light absorption by TiO_2 produces charge separation where conduction band electrons (e^-) and valence band positive holes (h^+) will be generated simultaneously (Eq. 4.7) (Zuo *et al.*, 2014).

$$TiO_2 \xrightarrow{hv\ (254\ nm)} TiO_2(e^-_{CB} + h^+_{VB}) \quad (4.7)$$

In secondary photophysical processes triplet $^3MB^*$ could transfer its energy to molecular oxygen thus generating singlet oxygen $^1O_2$ (Eq. 4.8), while titania hole (h^+_{VB}) and electron (e^-_{CB}) can either recombine unproductively (Eq. 4.9) or react with either water, hydroxide anion or molecular oxygen to produce the hydroxide radical (Eqs. 4.10 and 4.11) or the superperoxide radical anion (Eq. 4.12), respectively.

$$^3O_2 + {}^3[MB]^* \longrightarrow {}^1O_2 + MB \quad (4.8)$$

$$TiO_2(e^-_{CB} + h^+_{VB}) \longrightarrow TiO_2 \quad (4.9)$$

$$TiO_2(h^+_{VB}) + H_2O \longrightarrow TiO_2 + H^+ + \cdot OH \quad (4.10)$$

$$TiO_2(h^+_{VB}) + OH^- \longrightarrow TiO_2 + \cdot OH \quad (4.11)$$

$$TiO_2(e^-_{CB}) + O_2 \longrightarrow TiO_2 + O_2^{\cdot -} \quad (4.12)$$

Any of the above produced reactive oxygen species (ROS) could then attack an organic substrate. Indeed, processes involving Alg as light adsorber or photocatalytically degradable substrate (Eq. 4.13) (Burana-osot *et al.*, 2009) are competing with the decomposition of MB.

$$Alg_{(polymer)} \xrightarrow[TiO_2]{hv} Alg_{(oligomer)} \quad (4.13)$$

However, the integrity of the Alg/TiO_2/Fe-2 after repeated cycles demonstrated the stability of Alg/TiO_2/Fe-2 under the studied conditions. The MB oxidation by reaction with titania photogenerated holes h^+ was excluded since MB is cationic. Therefore, considering that MB alone under UVC demonstrated 64.9% removal, the overall MB degradation can be ascribed to either ^{1}MB* direct reactivity or to MB reaction with any of the generated ROS: singlet oxygen, hydroxyl radical, or superoxide radical anion. While from a mechanistic point of view these processes are competing between each other, they will all contribute to MB partial degradation from an initially formed sulphoxide (Houas *et al.*, 2001) or complete mineralization into carbon dioxide, water, nitrate or ammonium and sulphates ions (Tschirch *et al.*, 2008)

Since all the formed reactive species are short lived in solution (Schmitt *et al.*, 2014; Attri *et al.*, 2015), the use of multifunctional Alg/TiO_2/Fe-2 beads has the advantage of placing the substrate at very close distance with the sites where such species are formed allowing for a sort of *catch-and-degrade* photocatalysis. In this context, reaction conditions should be chosen to maximize the synergy between adsorption and photocatalytic degradation. For instance, irradiation under basic conditions, will enhance both the adsorption (see above) and the generation of •OH radicals (Sugimoto & Zhou, 2002; Konstantinou & Albanis, 2004). Additionally, using UVC irradiation reduces the electron-hole recombination (Joseph *et al.*, 2016), thus enhancing the photocatalytic removal of MB. Overall, among the above described processes, MB dependent mechanisms will be particularly contributing during the initial phase of the irradiation (when the MB concentration is higher) and will become less important with increasing MB removal.

4.7 Photocatalytic Removal of MHM

4.7.1 Effect of Adsorbent Dosage on MHM Removal

The efficiency of Alg/TiO_2/Fe-2 beads was further investigated for the removal of MHM (Pb(II), Cu(II) and Cr(II) ions) in aqueous solutions under UVC irradiation (Figure 4.17). The concentration of MHM solution was fixed at 20 ppm while the adsorbent dosage was varied from 0.1 to 1.0 g. It is clear that the removal percentages of all the metal ions increased with the increasing adsorbent dosage from 0.1 to 0.6 g under UVC irradiation (Figure 4.17). Pb(II) ions was removed in the highest percentage of 89.9% followed by Cu(II), 55.8% and Cr(III) ions, 53.4% at an adsorbent dosage of 0.6 g. At higher adsorbent dosage, more active sites were available on the Alg/TiO_2/Fe-2 surface for adsorption to take place, thus resulting in higher MHM removal (Kalantari *et al.*, 2014).

Nevertheless, as the adsorbent dosage was increased further to 1.0 g, the removal percentages of Cr(III) ions and Cu(II) ions declined to 31.6% and 40.2%, respectively in contrast to Pb(II) ions removal which constantly increased over time. This could be linked to the limited number of available active sites as a result of the saturation of the adsorbent surface with the metal ions (Bakr *et al.*, 2015) and also the dependence upon the different degree of hydration of the metal ion precursors ($Pb(NO_3)_2$, $Cu(SO_4)_2.5H_2O$ and $Cr(NO_3)_3.9H_2O$ (Holmberg, 2006). Among the metal ion precursors, $Pb(NO_3)_2$ exhibits the lowest degree of hydration, followed by $Cu(SO_4)_2.5H_2O$ and $Cr(NO_3)_3.9H_2O$ (Bartczak *et al.*, 2015).

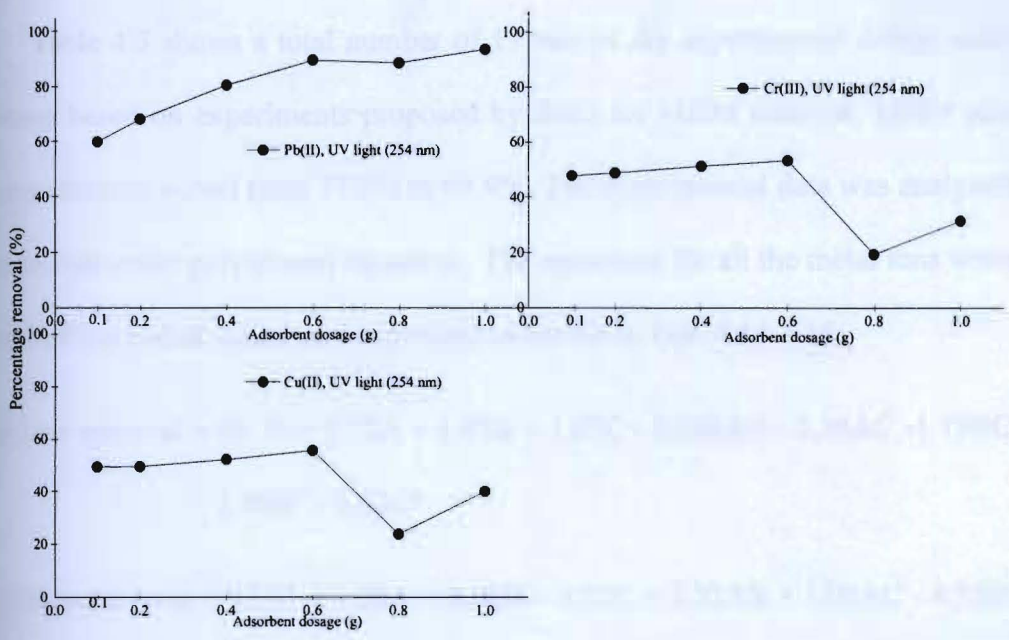

Figure 4.17: Effect of Alg/TiO_2/Fe-2 dosages on the MHM removal under UVC (MHM initial concentration: 20 ppm)

Generally, lower degree of hydration of the metal ions precursor lead to low hydration energy which would cause the metal ions to be easily shed from their hydration shell and results in the stronger electronic attraction (Wang *et al.*, 2016). Thus, the increasing percentage removal of Pb(II) ions could have been contributed by the strong electronic attraction between Pb(II) ions and the active sites of Alg/TiO_2/Fe-2 beads.

Based on the findings, 0.6 g of Alg/TiO_2/Fe-2 was concluded as the optimized adsorbent dosage because further increase to 1.0 g lowered the removal of both Cr(III) and Cu(II) ions. Further investigation was carried out to study the photocatalytic efficiency of Alg/TiO_2/Fe-2 beads by employing BBD, one of the methods of RSM for MHM removal optimization. The effects of three independent variables namely pH, initial concentration and contact time was investigated on the MHM removal percentage, the response.

4.8 Model Fitting and Statistical Analysis of BBD for MHM Removal

Table 4.5 shows a total number of 17 sets of the experimental design matrix and the responses based on experiments proposed by BBD for MHM removal. MHM removal from aqueous solution varied from 77.6% to 99.9%. The experimental data was analyzed and fitted to the second order polynomial equations. The equations for all the metal ions were generated in terms of the coded values and expressed as shown in Eqs. 4.14-4.16:

$$\text{Pb(II) ions removal} = 99.70 + 0.72A + 1.93B + 1.07C - 0.068AB - 0.36AC - 1.73BC - 0.91A^2 - 2.08B^2 - 0.62C^2 \quad (4.14)$$

$$\text{Cr(III) ions removal} = 93.67 + 1.04A + 8.08B + 6.01C + 2.32AB + 1.08AC - 4.53BC - 3.86A^2 - 1.44B^2 - 5.04C^2 \quad (4.15)$$

$$\text{Cu(II) ions removal} = 96.38 - 0.62A + 6.33B + 2.54C + 2.68AB + 4.94AC - 1.16BC - 5.21A^2 - 2.41B^2 - 5.47C^2 \quad (4.16)$$

where, A, B, and C are the coded values for the initial MHM concentration, pH, and contact time, respectively.

Table 4.5: Results for the Design Matrix of RSM study

	Variables			MHM removal (%)		
Run	**A**	**B**	**C**	**Pb(II) ions**	**Cr(III) ions**	**Cu(II) ions**
1	40	4.00	30	92.3	68.6	78.5
2	40	4.00	120	97.8	89.7	85.8
3	60	4.00	75	95.6	79.0	79.2
4	40	5.50	75	99.8	93.8	96.6
5	60	5.50	120	99.6	92.9	92.6
6	40	5.50	75	99.9	93.8	96.3
7	40	7.00	120	98.3	96.8	96.2
8	40	5.50	75	99.7	93.6	96.4
9	60	7.00	75	99.3	99.8	97.1
10	60	5.50	30	98.2	78.8	77.6
11	20	5.50	120	98.9	88.6	84.0
12	40	5.50	75	99.6	93.6	96.3

Table 4.5 continued

13	20	7.00	75	98.0	93.1	93.0
14	20	5.50	30	96.0	78.8	88.7
15	20	4.00	75	94.0	81.6	85.7
16	40	7.00	30	99.6	93.8	93.5
17	40	5.50	75	99.6	93.6	96.4

The accuracy of the model by comparing the experimental results against the predicted responses of the model for MHM removal is presented in Figure 4.18.

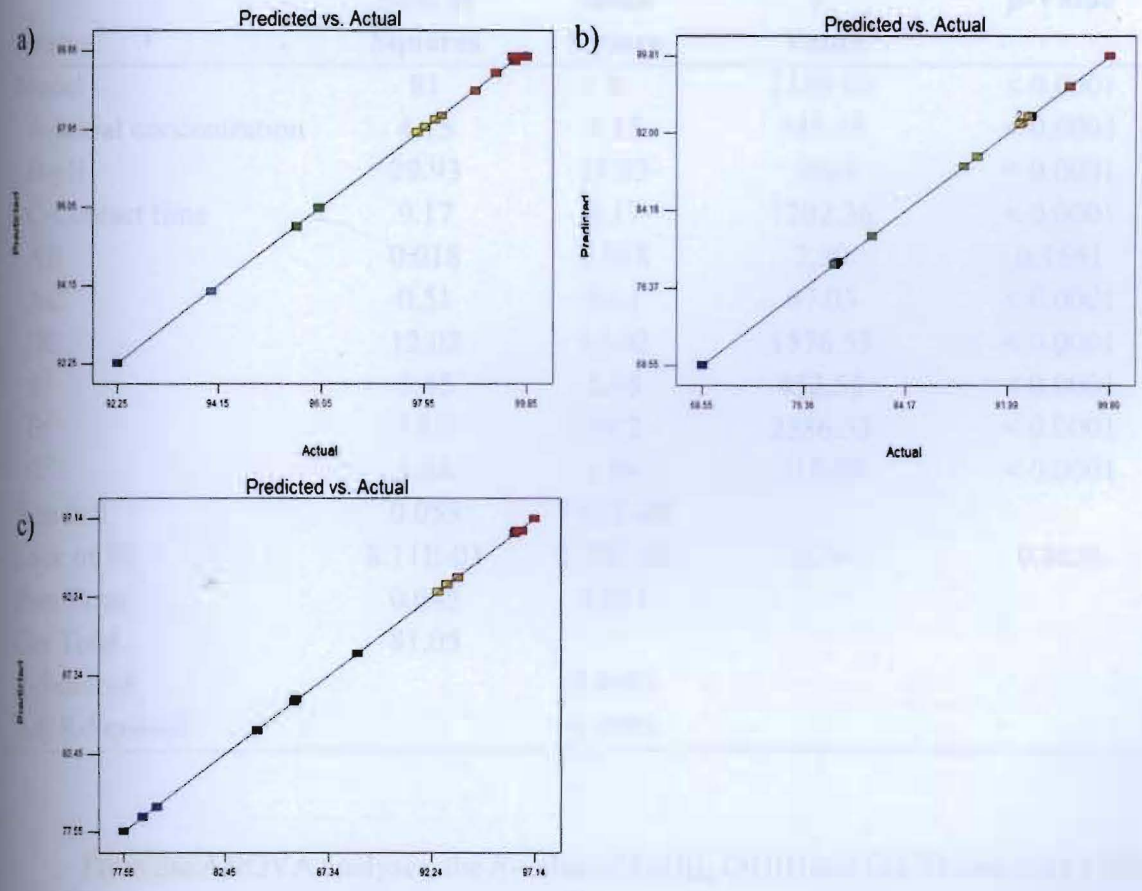

Figure 4.18: The scatter plot of predicted values versus actual values for the Box-Behnken design matrix: a) Pb(II) ions, b) Cr(III) ions, and c) Cu(II) ions

Tables 4.6 to 4.8 show the ANOVA analysis results of the response surface quadratic model for MHM removal. From the ANOVA results, the R^2 of Pb(II) = 0.9993 (Table 4.6), Cr(III) = 1.0000 (Table 4.7), and Cu(II) = 0.9999 (Table 4.8) confirmed that the selected models fitted the data well. The fitted model would be better if the R^2 approaches unity (Salehi *et al.*, 2016). Hence, the high values of the adjusted coefficient, R^2_{adj} of all the metal ions ($\geq$0.9985) show that the models were highly significant.

Table 4.6: ANOVA analysis of Pb(II) ions

Source	Sum of Squares	Mean Square	*F* Value	*p*-Value
Model	81	9	1180.03	< 0.0001
A-Initial concentration	4.15	4.15	543.78	< 0.0001
B-pH	29.93	29.93	3925	< 0.0001
C-Contact time	9.17	9.17	1202.36	< 0.0001
AB	0.018	0.018	2.39	0.1661
AC	0.51	0.51	67.03	< 0.0001
BC	12.02	12.02	1576.53	< 0.0001
A^2	3.45	3.45	452.55	< 0.0001
B^2	18.2	18.2	2386.53	< 0.0001
C^2	1.64	1.64	215.05	< 0.0001
Residual	0.053	7.63E-03		
Lack of Fit	8.11E-03	2.70E-03	0.24	0.8656
Pure Error	0.045	0.011		
Cor Total	81.05			
R-Squared		0.9993		
Adj R-Squared		0.9985		

From the ANOVA analyses, the *F*-value of Pb(II), Cr(III) and Cu(II) ions were 1180.03, 25435.66, and 8062.77, respectively. These values imply that the regression model was statistically significant. There were only 0.01% chances that a "Model *F*-Value" could occur due to noise. The value of "Prob > *F*" of less than 0.0500 indicates that the model was significant

and in this case, A, B, C, AB, AC, BC, A^2, B^2, and C^2 for Pb(II), Cr(III) and Cu(II) ions were significant model terms. If the *F*-values were greater than 0.1000, this would indicate that the model terms were insignificant. The "Lack of Fit *F*-value" of Pb(II) = 0.24, Cr(III) = 0.11, and Cu(II) = 0.38 implies that the "Lack of Fit" was not significant, relative to the pure error. Overall, it shows that all the models for the MHM removal were valid due to the insignificance of the "Lack of Fit *F*-value".

Table 4.7: ANOVA analysis of Cr(III) ions

Source	Sum of Squares	Mean Square	*F* Value	*p*-Value
Model	1122.53	124.73	25435.66	< 0.0001
A-Initial concentration	8.63	8.63	1760.35	< 0.0001
B-pH	522.13	522.13	1.07E+05	< 0.0001
C-Contact time	288.72	288.72	58879.63	< 0.0001
AB	21.62	21.62	4409.54	< 0.0001
AC	4.64	4.64	947.07	< 0.0001
BC	82.17	82.17	16758.04	< 0.0001
A^2	62.65	62.65	12777.2	< 0.0001
B^2	8.76	8.76	1786.72	< 0.0001
C^2	106.95	106.95	21811.47	< 0.0001
Residual	0.034	4.90E-03		
Lack of Fit	2.53E-03	8.42E-04	0.11	0.9523
Pure Error	0.032	7.95E-03		
Cor Total	1122.56			
R-Squared		1.0000		
Adj R-Squared		0.9999		

Table 4.8: ANOVA analysis of Cu(II) ions

Source	Sum of Squares	Mean Square	*F* Value	*p*-Value
Model	798.27	88.7	8062.77	< 0.0001
A-Initial concentration	3.11	3.11	282.94	< 0.0001
B-pH	320.17	320.17	29104.61	< 0.0001
C-Contact time	51.51	51.51	4682.54	< 0.0001
AB	28.73	28.73	2611.61	< 0.0001
AC	97.52	97.52	8864.48	< 0.0001
BC	5.36	5.36	487.17	< 0.0001
A^2	114.44	114.44	10403.38	< 0.0001
B^2	24.53	24.53	2229.51	< 0.0001

Table 4.8 continued

C^2	125.8	125.8	11435.49	< 0.0001
Residual	0.077	0.011		
Lack of Fit	0.017	5.71E-03	0.38	0.7728
Pure Error	0.06	0.015		
Cor Total	798.34			
R-Squared		0.9999		
Adj R-Squared		0.9998		

4.9 Response Surface Analysis of MHM

Figures 4.19 to 4.21 show the combined effects between the three independent variables, contact time, pH and initial concentration on the removal of Pb(II), Cr(III) and Cu(II) *via* 3D response surface plots.

4.9.1 Combined Effect between Contact Time and pH

In a photocatalytic reaction, solution pH is considered as one of the most important parameters that affect the adsorption behaviour of an adsorbate, MHM solution, in this case. Furthermore, the surface charge of the Alg/TiO_2/Fe-2 varies according to the MHM solution pH (Majidnia *et al.*, 2015). Figure 4.19 shows the 3D surface plots of the combined effects between solution pH and contact time on the MHM removal at an initial MHM concentration of 40 ppm. As illustrated in Figures 4.19a to 4.19c, the percentage removal of all metal ions in the solution mixture increased from 30 min to 75 min at the pH range of 4.00 to 6.25. Deprotonation phenomenon at increasing pH leads to an increase in the number of OH^- groups on the active sites of Alg/TiO_2/Fe-2. Adsorption of the metal ions to the active sites of Alg/TiO_2/Fe-2 beads will be enhanced as a result of the electrostatic attraction between the positive metal ions in the aqueous solution and considerable amount of OH^- groups (Baloyi *et al.*, 2014).

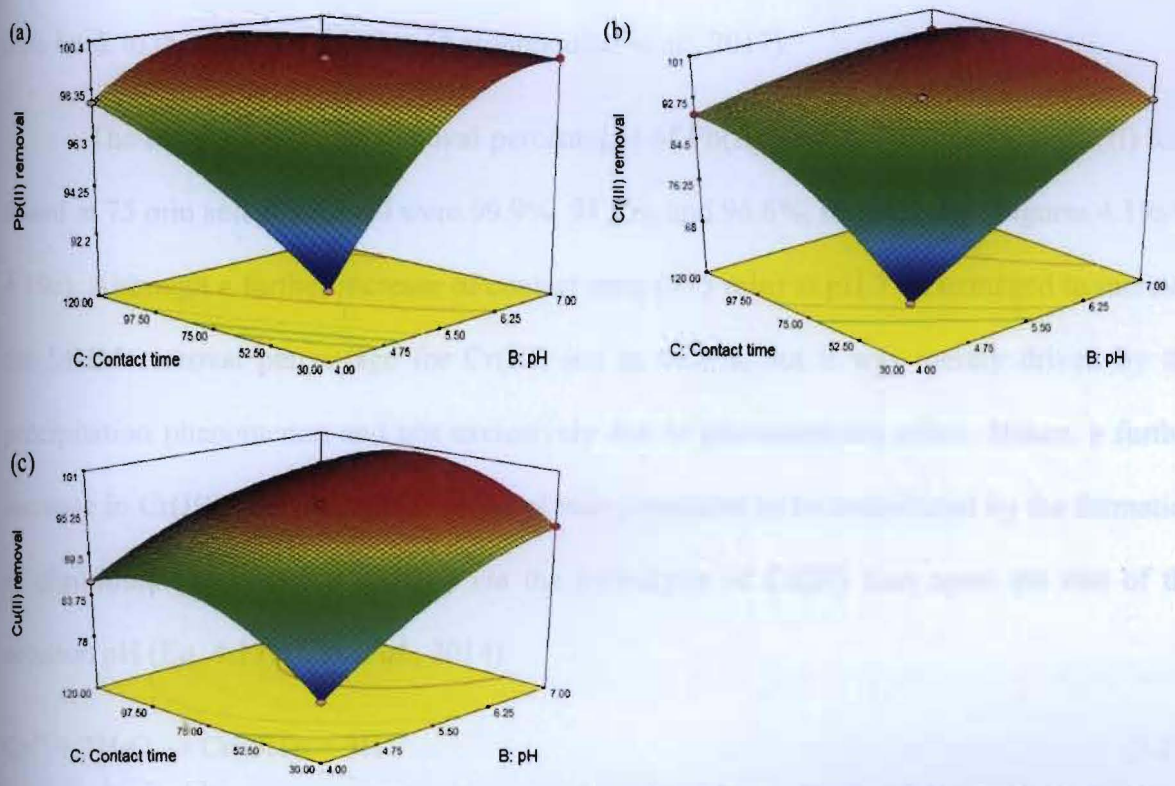

Figure 4.19: 3D response surface plots that show the effects of contact time and pH on the removal of (a) Pb(II), (b) Cr(III), and (c) Cu(II) by Alg/TiO_2/Fe-2 beads

Photogenerated electrons on the TiO_2 surface would eventually reduce Pb(II) ions and Cu(II) ions to their elemental form (Horváth *et al.*, 2001). However, at pH 7.00 and at contact times from 30 to 75 min, percentage removal of metal ions reached a plateau state plausibly due to the availability of fewer active sites or due to unavailable active sites for metal ions adsorption to occur (Singanan, 2011). Moreover, as the contact time increased up to 120 min at pH 7.00, the percentage removal of MHM was noticed to decrease. As the pH of the medium is more than pH_{pzc} of TiO_2, the Alg/TiO_2/Fe-2 surface was assumed to be negatively charged.

This could induce a strong electronic attraction between the cationic metal ions and the active sites on the surface of the Alg/TiO_2/Fe-2 which led to the increase of the adsorption of all the metal ions. As consequences, the Alg/TiO_2/Fe-2 beads became saturated and competition

between the metal ions (electrostatic repulsion) occurred that led to the desorption of the metal ions back to the aqueous solution (Antonopoulou *et al.*, 2017).

The maximum MHM removal percentages of Pb(II) ions, Cr(III) ions and Cu(II) ions found at 75 min and at pH 5.50 were 99.9%, 93.8%, and 96.6%, respectively (Figures 4.19a to 4.19c). Although a further increase of contact time (>75 min) at pH 7.00 managed to increase the MHM removal percentage for Cr(III) ion to 96.8%, but it was merely driven by the precipitation phenomenon and not exclusively due to photocatalysis effect. Hence, a further increase in Cr(III) ions percentage removal was postulated to be contributed by the formation of chromium precipitate ($Cr(OH)_3$) *via* the hydrolysis of Cr(III) ions upon the rise of the solution pH (Eq. 4.17) (Liu *et al.*, 2014).

$$Cr^{3+} + 3H_2O \rightarrow Cr(OH)_3 + 3H^+ \quad (4.17)$$

As such, the increasing removal percentage of Cr(III) ions resulted from the small amount of Cr(III) ions present in the solution mixture. Therefore, pH 7.00 can be considered as inappropriate for photocatalytic reaction due to the undesired precipitation phenomenon. Based on the observation, the potential of Alg/TiO_2/Fe-2 beads to remove metal ions from the aqueous solution was aided by three main processes namely adsorption, photocatalytic reduction and precipitation. Also, as evident in the above discussion, solution pH and contact time significantly affected the MHM removal.

4.9.2 Combined Effect between Contact Time and MHM Initial Concentration

The 3D response surface plots displaying the combined effect between MHM initial concentration and contact time on the MHM removal by Alg/TiO_2/Fe-2 beads under pre-defined condition at pH 5.50 can be seen in Figure 4.20. The MHM removal increased with the contact time from 30 to 75 min and the initial concentration from 20 to 40 ppm before it started

to decline. The increasing trend of MHM removal percentages at low contact time (<75 min) and low initial concentration of MHM (<40 ppm) was favoured by the abundance of unoccupied active sites on the surface of Alg/TiO_2/Fe-2 which led to more adsorption of metal ions onto Alg/TiO_2/Fe-2 surface (Tao *et al.*, 2009).

However, at both higher contact time and initial concentration of MHM, more metal ions would be adsorbed to the active sites on Alg/TiO_2/Fe-2 surface consequently leading to the electrostatic repulsion between the metal ions. As been explained previously, the desorption of metal ions back to the solution results in the decreasing percentage removal (Goel *et al.*, 2005).

At 75 min and an initial MHM concentration of 40 ppm, highest removal percentages were attained for all three metal ions investigated. The removal of Pb(II), Cu(II) and Cr(III) ions were 99.9%, 96.6%, and 93.8%, respectively. It appeared that Cr(III) ions showed slightly lower percentage removal compared to the other two individual ions present in the solution mixture. This behaviour could be related to the different degrees of hydration of the metal ions precursor as explained previously (Section 4.7.1).

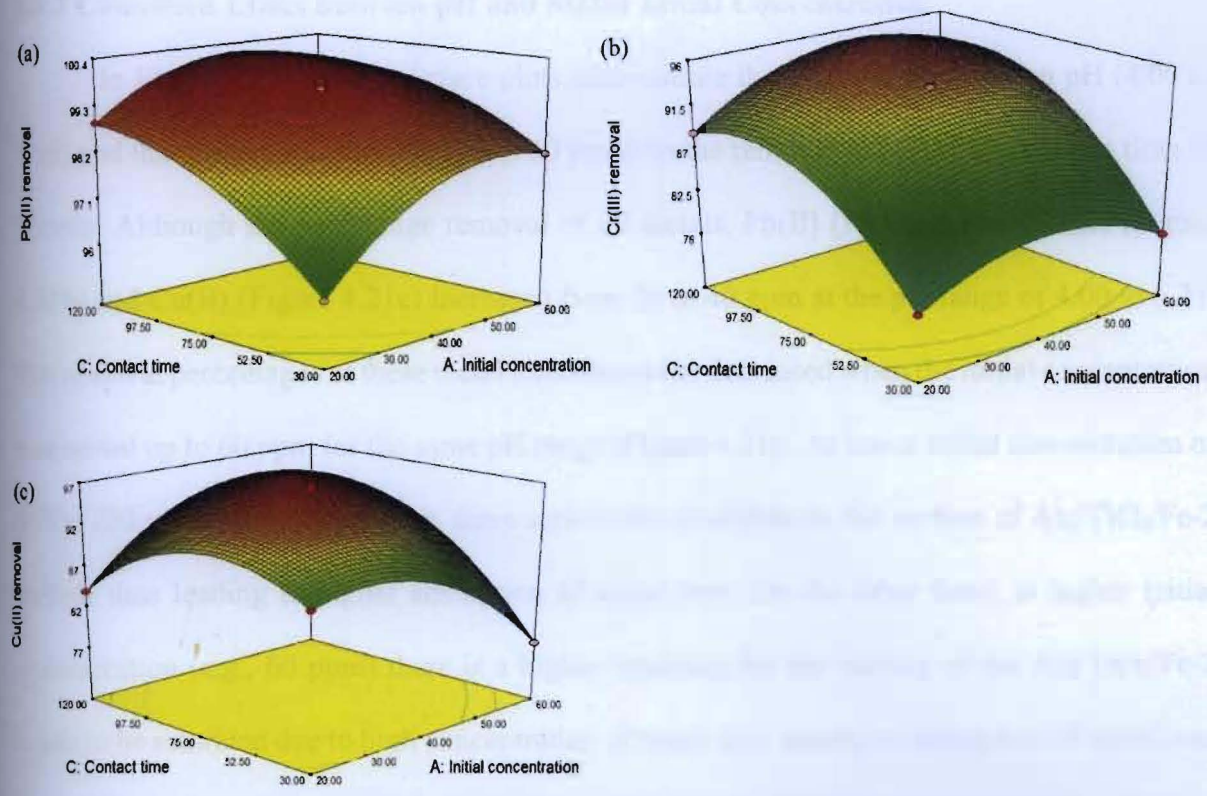

Figure 4.20: 3D response surface plots that show the effects of contact time and initial concentration on the removal of (a) Pb(II), (b) Cr(III), and (c) Cu(II) by Alg/TiO_2/Fe-2 beads

The highest degree of hydration held by Cr(III) ions led to the stronger binding energy than Pb(II) and Cu(II) ions (Rearte *et al.*, 2013). Consequently, it resulted in the poor adsorption efficiency of Cr(III) ions to the active sites of Alg/TiO_2/Fe-2 surface (Wang *et al.*, 2016). It is known that at a lower degree of hydration of the metal ions precursor, it is easier for the cation to detach from the hydration shell. Hence, it would be more favored for adsorption process (Tansel *et al.*, 2006).

Therefore, high percentage removal of metal ions (>68.0%) from aqueous solution can be achieved at a very short contact time (30 to 75 min) and at initial MHM concentrations of 20 to 40 ppm using Alg/TiO_2/Fe-2 beads. These two independent variables, initial concentration and contact time have demonstrated significant effect on the metal ions' removal efficiencies.

4.9.3 Combined Effect between pH and MHM Initial Concentration

In Figure 4.21, the 3D surface plots demonstrate the effect of the solution pH (4.00 to 7.00) and the initial concentration (20 to 60 ppm) on the removal of MHM at a contact time of 75 min. Although the percentage removal of all metals, Pb(II) (Figure 4.21a), Cr(II) (Figure 4.21b) and Cu(II) (Figure 4.21c) increased from 20 to 40 ppm at the pH range of 4.00 to 6.25. The removal percentages of these metal ions somewhat decreased when the initial concentration was raised up to 60 ppm for the same pH range (Figure 4.21). At lower initial concentration of MHM (20 to 40 ppm), there were more active sites available on the surface of Alg/TiO_2/Fe-2 surface thus leading to higher adsorption of metal ions. On the other hand, at higher initial concentration (e.g., 60 ppm) there is a higher tendency for the surface of the Alg/TiO_2/Fe-2 beads to be saturated due to high concentration of metal ions leading to desorption of metal ions from the adsorbents' surface and eventually contributing to the decreasing removal percentage trend.

The highest removal of all the metal ions in the mixture was observed at an initial concentration of 40 ppm and at pH 5.50. The removal of Pb(II), Cu(II), and Cr(III) ions were 99.9%, 96.6%, and 93.8%, respectively. Further increase in the initial concentration from 40 to 60 ppm and pH from 5.50 to 7.00 caused the percentage removal of Pb(II) ions and Cu(II) ions to decrease. But in the case of Cr(III) ions, the removal percentage constantly increased up to 99.8% at pH 7. As mentioned previously, at pH 7.00, the precipitation of the metal ions was most likely to occur. Cr(III) ions may react with OH^- groups to form chromium precipitate, $(Cr(OH)_3$ (Djellabi *et al.*, 2016). Hence, at pH 7.00, it can be assumed that the high percentage removal of Cr(III) ions was not due to the photocatalysis effect but as a result of due Cr(III) ions precipitation.

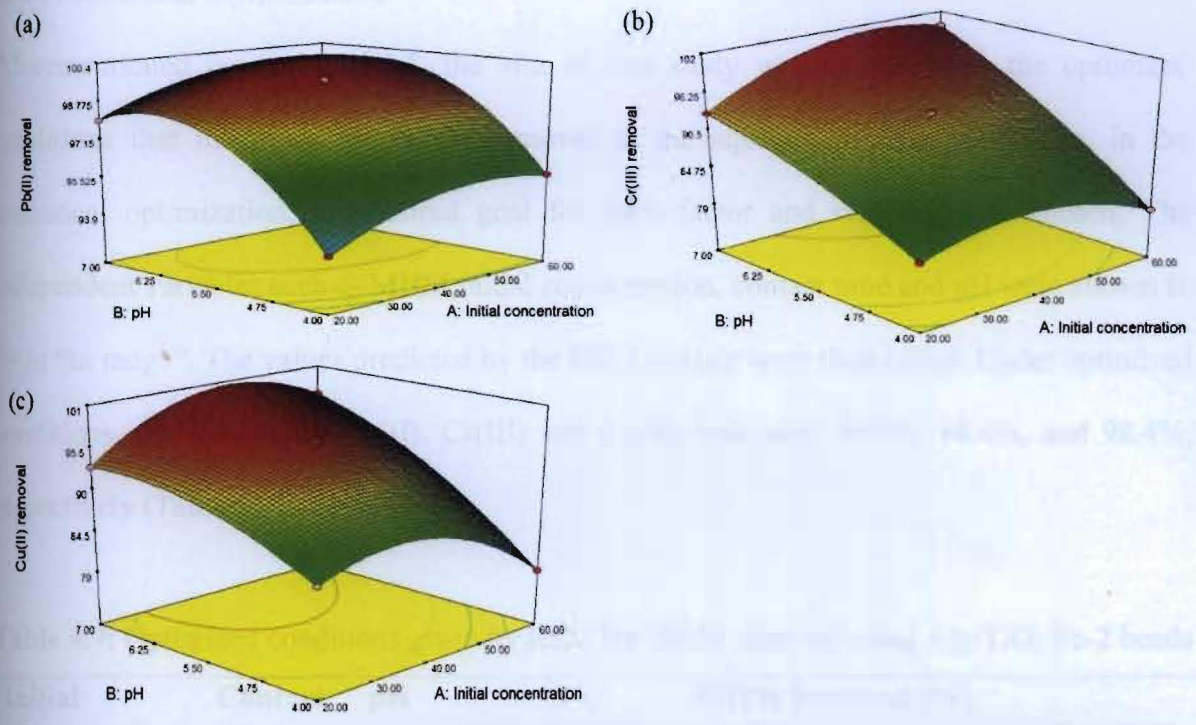

Figure 4.21: 3D response surface plots that show the effects of pH and initial concentration on the removal of (a) Pb(II), (b) Cr(III), and (c) Cu(II) by Alg/TiO_2/Fe-2 beads

As for Pb(II) and Cu(II) ions, the observed decrease in their removal percentages at increasing initial concentration could be attributed to the electrostatic repulsion effect between the metal ions (Antonopoulou *et al.*, 2017). MHM were assumed to have a strong electronic attraction for the adsorption due to the magnetic property of iron oxide in Alg/TiO_2/Fe-2 beads (Kołodyńska *et al.*, 2014). Therefore, even at pH<pH_{pzc} of Alg/TiO_2/Fe-2, high MHM removal percentage (~90.0%) was observed. This condition could lead to the early saturation of Alg/TiO_2/Fe-2 surface and causes the MHM removal percentage to decrease as the pH of the solution was further increased from 5.50 to 7.00. The interaction between the solution pHs and the MHM initial concentrations revealed that both parameters significantly governed the adsorption and the photocatalytic removal of metal ions in aqueous solution.

4.9.4 Numerical Optimization

Aforementioned in section 4.4.4, the aim of this study was to determine the optimized conditions that maximize the MHM removal in the aqueous solution. Therefore, in the numerical optimization, the desired goal for each factor and response was chosen. The independent variables such as MHM initial concentration, contact time and pH were chosen to be in "in range". The values predicted by the RSM models were then tested. Under optimized conditions, the removal of Pb(II), Cr(III) and Cu(II) ions were 99.6%, 98.6%, and 98.4%, respectively (Table 4.9).

Table 4.9: Optimized conditions given by RSM for MHM removal using Alg/TiO_2/Fe-2 beads

Initial concentration (ppm)	Contact time (min)	pH	MHM Removal (%)					
			Actual			Predicted		
			Pb(II)	Cr(III)	Cu(II)	Pb(II)	Cr(III)	Cu(II)
44	72	6.8	99.6	98.6	98.4	100.0	100.0	100.0

4.10 Comparison of Efficiency and Recycling Study for MHM Removal

MHM removal was also studied under different conditions likewise MB. Blank beads and TiO_2 in slurry form was applied for MHM removal under UVC at optimized conditions as suggested by RSM (Table 4.9). The comparison of results obtained for the removal of Pb(II), Cu(II) and Cr(II) ions under all investigated conditions are presented in Figure 4.22. Slurry form of TiO_2 appeared to be superior for MHM removal compared to the other investigated conditions. Application of slurry TiO_2 yielded 99.4% for Cu(II), 99.3% for Cr(III) and 99.9% for Pb(II) removal while Alg/TiO_2/Fe-2 beads yielded 98.4% for Cu(II), 98.6% for Cr(III) and 99.6% for Pb(II). The efficiency of Alg/TiO_2/Fe-2 beads in removing heavy metal ions under UVC was comparable to the slurry TiO_2 as can be seen in Figure 4.22. This is somewhat

expected as TiO_2 slurry is known to demonstrate higher photocatalytic efficiency compared to the immobilized form of TiO_2 (Alg/TiO_2/Fe-2) due to the higher absorption of UV irradiation (Liu *et al.*, 2014).

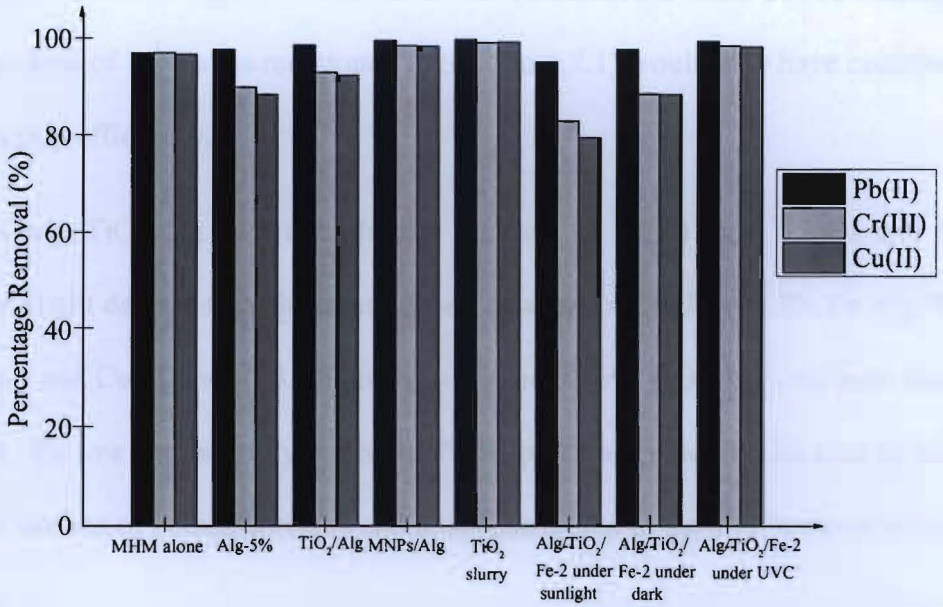

Figure 4.22: Performance comparison between Alg/TiO_2/Fe-2 under UVC, sunlight and dark condition with TiO_2 slurry, MHM only, Alg-5% beads, TiO_2/Alg beads, MNPs/Alg beads in removing MHM (initial concentration of MHM: 44 ppm; dark equilibration time: 30 min; UVC irradiation time: 1 h and 12 min; sunlight exposure: 1 h and 12 min, adsorbent: 0.006 g/mL

As recovery of the fine nanosized TiO_2 is rather tedious owing to its fine particles, Alg/TiO_2/Fe-2 beads, on the other hand, offers a convenient solution by allowing its recovery using an external magnetic field. Despite the absence of Alg/TiO_2/Fe-2 beads, removal percentages of Pb(II), Cr(III) and Cu(II) ions were high with 97.2%, 97.2% and 96.9%, respectively. Due to the fact that pH of the treatment condition was adjusted to the optimized pH 6.8 (Table 4.9), some of the metal ions would have been existed in their precipitate forms and subsequently contributed to the removal of the metal ions *via* precipitation (Li *et al.*, 2013).

The metal ions removal efficiencies by MNPs/Alg beads were 99.8% for Pb(II), 98.7% for Cr(III) and 98.6% for Cu(II) ions. This finding revealed that strong magnetic property of MNP/Alg beads enhanced the adsorption process of MHM in aqueous solution as metal ions can be attracted to the strong magnetic property (Li *et al.*, 2014) in addition to the presence of Alg which is also known as a good natural adsorbent (Kanakaraju *et al.*, 2017). Additionally, the high surface area of MNPs (as mentioned in Section 4.7.1) would also have contributed to the great adsorption efficiency.

Alg-5% and TiO_2/Alg facilitated higher removal of Pb(II) ions, 97.9% and 98.8%, respectively but slight decreased in the removal percentages for Cr(III) (90.2% for Alg-5% and 93.2% TiO_2/Alg) and Cu(II) ions (88.6% for Alg-5% and 92.6% TiO_2/Alg). As been discussed in section 4.9.1, the low degree of hydration of Pb(II) precursor made Pb(II) ions to be easily adsorbed to the surface of both adsorbents and thus contributed to the high removal percentage simultaneously.

When the performance efficiency of Alg/TiO_2/Fe-2 beads was compared between UVC, dark and sunlight, the former appeared to be better than the other two conditions. This could be associated to the high photogenerated electrons by TiO_2 when exposed under UVC irradiation, the shortest wavelength irradiation with 254 nm (Yang *et al.*, 2017; Ali & Kim, 2018). The metal ions will be then reduced to their elemental forms by the photogenerated electron (Lee *et al.*, 2003). In the case of MHM removal by Alg/TiO_2/Fe-2 beads under sunlight, this photon source aided the MHM removal despite a slight discrepancy (less than 20.0%) when compared to its performance under UVC irradiation. It is known that sunlight intensity vary from time and days unlike UV light which only depends on its lifetime (Cho *et al.*, 2007). It is believed that differences in the light intensity and surface area of the reaction medium exposed to both

photon sources would have caused the slight difference observed in the metals removal efficiency. Even though the order of the metal ions removal for both cases were similar, marked decline was however observed for Cr(III) and Cu(II) ions under sunlight (Figure 4.22). This could probably due to different extent of adsorption ability of these ions on the surface of the Alg/TiO_2/Fe-2 beads or due to different interactions that took place between the metals ions in the solution mixture when exposed under direct sunlight mainly due to different light intensity. Based on Figure 4.22, the efficiency of Alg/TiO_2/Fe-2 beads to remove heavy metal ions under dark condition was apparent whereby 97.9%, 88.8% and 88.7% was obtained for Pb(II), Cr(III), and Cu(II) ions, respectively. This finding thus confirmed that adsorption plays an integral part in facilitating the removal of heavy metals from the mixture solution under the investigated conditions.

Catalytic stability of a photocatalyst upon consecutive treatment cycles would indicate its sustainability for an application. Accordingly, Alg/TiO_2/Fe-2 beads which were recovered from the first MHM photocatalytic treatment was washed repeatedly using distilled water before being tested for the same application for two consecutive cycles. Figure 4.23 illustrates the recyclability of Alg/TiO_2/Fe-2 for 3 cycles of MHM removal study. No apparent deterioration in term of the removal percentages was observed between the cycles. Pb(II) displayed a slight increment in the second cycle likely due to higher affinity of Pb(II) for adsorption compared to the other metal ions. Thus, the performance of Alg/TiO_2/Fe-2 beads in removing MHM in aqueous solution remained unaltered up to three cycles indicating its stability when reused continuously.

photon sources would have caused the slight difference observed in the metals removal efficiency. Even though the order of the metal ions removal for both cases were similar, marked decline was however observed for Cr(III) and Cu(II) ions under sunlight (Figure 4.22). This could probably due to different extent of adsorption ability of these ions on the surface of the Alg/TiO_2/Fe-2 beads or due to different interactions that took place between the metals ions in the solution mixture when exposed under direct sunlight mainly due to different light intensity. Based on Figure 4.22, the efficiency of Alg/TiO_2/Fe-2 beads to remove heavy metal ions under dark condition was apparent whereby 97.9%, 88.8% and 88.7% was obtained for Pb(II), Cr(III), and Cu(II) ions, respectively. This finding thus confirmed that adsorption plays an integral part in facilitating the removal of heavy metals from the mixture solution under the investigated conditions.

Catalytic stability of a photocatalyst upon consecutive treatment cycles would indicate its sustainability for an application. Accordingly, Alg/TiO_2/Fe-2 beads which were recovered from the first MHM photocatalytic treatment was washed repeatedly using distilled water before being tested for the same application for two consecutive cycles. Figure 4.23 illustrates the recyclability of Alg/TiO_2/Fe-2 for 3 cycles of MHM removal study. No apparent deterioration in term of the removal percentages was observed between the cycles. Pb(II) displayed a slight increment in the second cycle likely due to higher affinity of Pb(II) for adsorption compared to the other metal ions. Thus, the performance of Alg/TiO_2/Fe-2 beads in removing MHM in aqueous solution remained unaltered up to three cycles indicating its stability when reused continuously.

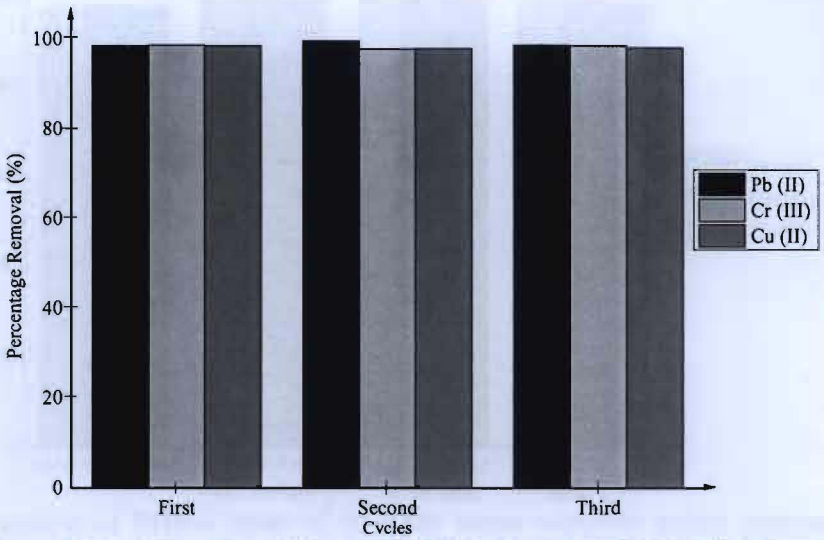

Figure 4.23: Recycling study of optimized Alg/TiO_2/Fe-2 beads for MHM removal

4.11 Application of Alg/TiO_2/Fe-2 Beads to Remove Heavy metals in River Water

In order to determine the ability of Alg/TiO_2/Fe-2 beads to remove heavy metals in real water, river water sample was chosen. MHM solution was prepared using river water and according to the RSM optimized conditions. Prior analysis on the sampled river water showed no presence of Pb(II) and Cr(III) while, Cu(II) was detected in a low concentration, 0.005 ppm (Table 3.6). The efficiency of Alg/TiO_2/Fe-2 beads to remove heavy metal ions in river water under UVC irradiation, sunlight, and dark was compared with the removal of metal ions in river water without the presence of Alg/TiO_2/Fe-2 under UVC (Figure 4.24).

The removal trend was somehow consistent for all investigated conditions with removal percentages above 97.0%. As the river water contained dissolved salts such as Cl^-, it might react with the metal ions such as Pb(II) to form PbCl, a precipitate form of salt thus increasing their removal (Corsi *et al.*, 2010). However, since the optimized pH is 6.80, close to neutral pH, Alg/TiO_2/Fe-2 beads can be potentially applied to remove heavy metals in real in natural aquatic water bodies.

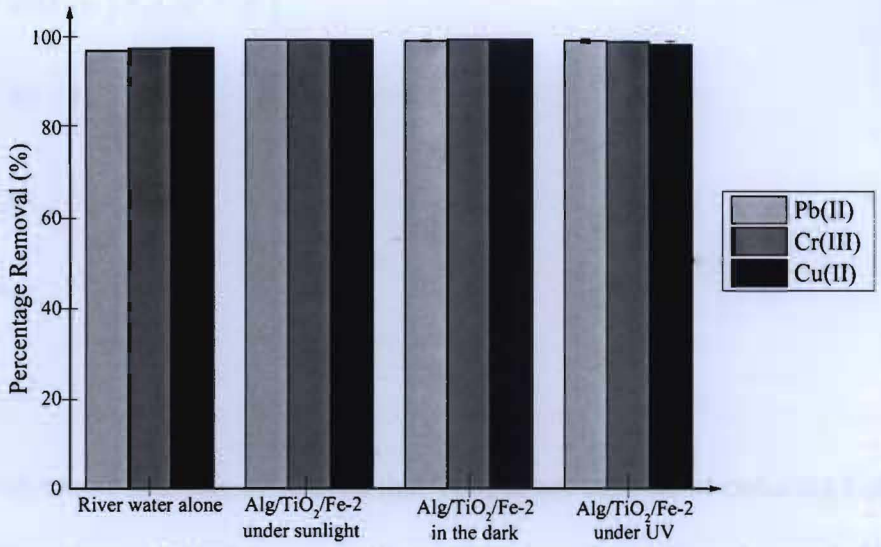

Figure 4.24: Comparison of MHM removal in river water samples under optimized RSM conditions

4.12 Proposed Mechanism of MHM Removal by Alg/TiO_2/Fe-2 Beads

Based on the obtained findings, MHM removal can be postulated to be favoured primarily by three processes namely adsorption, photocatalytic reduction, and precipitation. Likewise MB, the heavy metal ions in the solution mixture were also adsorbed either *via* inclusion in their Alg layer (Eq. 4.18) or by ion-dipole interactions with the terminal hydroxy groups (Ti-OH) of titania particles (Eq. 4.19).

$$MHM(aq) \leftrightharpoons MHM@Alg/TiO_2/Fe-2(Alg) \quad (4.18)$$

$$MHM(aq) \leftrightharpoons MHM@Alg/TiO_2/Fe-2(TiO_2) \quad (4.19)$$

The shortwave UVC light source (254 nm) provide high energy greater than the band gap energy of TiO_2. Hence, upon the UVC light absorption, TiO_2 generates electron-hole pairs which are responsible for the reduction of metal ions in the aqueous solution. The metal ions then underwent photocatalytic reduction as proposed in the following equations (Eqs. 4.20 to 4.24) (Kanakaraju *et al.*, 2017).

$$TiO_2 + h\nu(254\ nm) \rightarrow TiO_2\ (e^- + h^+) \quad (4.20)$$

$$h^+ + H_2O \rightarrow \bullet OH + H^+ \quad (4.21)$$

$$h^+ + OH^- \rightarrow \bullet OH \quad (4.22)$$

$$Pb^{2+} + 2e^- \rightarrow Pb^0 \quad (4.23)$$

$$Cu^{2+} + 2e^- \rightarrow Cu^0 \quad (4.24)$$

Thermodynamic analysis evidenced that TiO_2 is not capable of reducing Cr(III) ions to Cr(0) metal (Wang *et al.*, 2004). As such, the removal of Cr(III) ions was most likely to be attributed to the adsorption as well as precipitation. As the solution pH was increased from 4.00 to 7.00, more OH^- groups were present and thus enhanced the hydrolysis of Cr(III) ions and formation of chromium precipitate, ($Cr(OH)_3$) (Eq. 4.25).

$$Cr^{3+} + 3H_2O \rightarrow Cr(OH)_3 + 3H^+ \quad (4.25)$$

CHAPTER 5

CONCLUSION AND RECOMMENDATIONS

A new adsorbent material with combined adsorption, photocatalytic and magnetic properties has been successfully synthesised. TiO_2 photocatalysts were successfully immobilized on the surface of Alg, while MNPs were incorporated into Alg beads. Therefore, the Alg can act as a potential candidate to prevent the direct contact between TiO_2 and MNPs. The performance of the nanocomposite material in removing MB and MHM from water can be altered or fine-tuned by varying the synthesis conditions because they have a direct effect on the material. Based on the RSM optimization, 97.2% of MB was removed at an initial MB concentration of 5 ppm at pH 10 after 120 min using Alg/TiO_2/Fe-2 beads. For MHM removal, 99.5%, 98.6%, and 98.4% of Pb(II), Cr(III) and Cu(II) ions removal was observed at an initial MHM concentration of 44 ppm and at pH 6.8 after 72 min using Alg/TiO_2/Fe-2 beads.

The ANOVA results revealed that initial MB concentration was the most influential parameter for the removal of MB molecules. While, it was found that solution pH was the most influential parameter for the MHM removal. Based on the recycling study, Alg/TiO_2/Fe-2 beads can be easily separated from the reaction medium and reused up to 3 consecutive cycles indicating its stability and sustainable performance. The MHM removal in the river water demonstrated that Alg/TiO_2/Fe-2 beads are suitable for water loaded with multi-heavy metals.

Alg as a prospective adsorbent in nanocomposite preparation should be pursued and future study should be focused on the arising degradants. Besides, this study should be extended to improve the photocatalytic activity of TiO_2 by varying the ratio of TiO_2 with respect to Alg and Fe_3O_4 or incorporate other semiconductors such as zinc oxide (ZnO) and silicon dioxide (SiO_2) instead of TiO_2 with the Fe_3O_4 and Alg. The treatment of real industrial wastewater

should also be conducted by using the prepared magnetic photocatalyst nanocomposite, in order to confirm its economic viability and efficiency.

REFERENCES

Absalan, F., & Nikazar, M. (2016). Application of response surface methodology for optimization of water treatment by $Fe_3O_4/SiO_2/TiO_2$ core-shell nano-photocatalyst. *Chemical Engineering Communications*, *203*(11), 1523-1531.

Aguedach, A., Brosillon, S., Morvan, J., & Lhadi, E. K. (2005). Photocatalytic degradation of azo-dyes reactive black 5 and reactive yellow 145 in water over a newly deposited titanium dioxide. *Applied Catalysis B: Environmental*, *57*(1), 55–62.

Aghel, S., Bahramifar, N., & Younesi, H. (2016). Kinetics of photocatalytic degradation of reactive black B using core-shell TiO_2-coated magnetic nanoparticle, $Fe_3O_4/SiO_2/TiO_2$. *Journal of Applied Research in Water & Wastewater*, *3*(2), 253-259.

Ai, Q., Yang, D., Zhu, Y., & Jiang, Z. (2013). Fabrication of boehmite/alginate hybrid beads for efficient enzyme immobilization. *Industrial & Engineering Chemistry Research*, *52*(42), 14898-14905.

Ajmal, A., Majeed, I., Malik, R. N., Idriss, H., & Nadeem, M. A. (2014). Principles and mechanisms of photocatalytic dye degradation on TiO_2 based photocatalysts: a comparative overview. *RSC Advances*, *4*(70), 37003-37026.

Akpan, U., & Hameed, B. (2009). Parameters affecting the photocatalytic degradation of dyes using TiO_2-based photocatalysts: A review. *Journal of Hazardous Materials*, *170*(2-3), 520-529.

Akpor, O. B., Ohiobor, G. O., & Olaolu, T. D. (2014). Heavy metal pollutants in wastewater effluents: sources, effects and remediation. *Advances in Bioscience & Bioengineering*, *2*(4), 37-43.

Albarelli, J. Q., Santos, D. T., Murphy, S., & Oelgemöller, M. (2009). Use of Ca–alginate as a novel support for TiO_2 immobilization in methylene blue decolorisation. *Water Science & Technology*, *60*(4), 1081-1087.

Albroomi, H. I., Elsayed, M., Baraka, A., & Abdelmaged, M. A. (2015). Factors affecting the removal of a basic and an azo dye from artificial solutions by adsorption using activated carbon. *Journal of the Turkish Chemical Society, Section A: Chemistry*, *2*(1), 17-33.

Ali, I., & Kim, J. O. (2018). Continuous-flow photocatalytic degradation of organics using modified TiO_2 nanocomposites. *Catalysts*, *8*(2), 1-13.

Alizadeh, A., Khodaei, M.M., Beygzadeh, M., Kordestani, D., & Feyzi, M. (2012). Biguanide-functionalized Fe_3O_4/SiO_2 magnetic nanoparticles: an efficient heterogeneous organosuperbase catalyst for various organic transformations in aqueous media. *Bulletin of the Korean Chemical Society, 33*(8), 2546-2552.

Aljuboury, D. A. D. A., Palaniandy, P., Abdul Aziz, H., & Feroz, S. (2015). Evaluating the TiO_2 as a solar photocatalyst process by response surface methodology to treat the petroleum waste water. *Karbala International Journal of Modern Science, 1*, 78-75.

Alqadami, A.A., Naushad, M., Abdalla, M.A., Khan, M.R. & Alothman, Z.A. (2016). Adsorptive removal of toxic dye using Fe_3O_4–TSC nanocomposite: equilibrium, kinetic, and thermodynamic studies. J*ournal of Chemical & Engineering Data, 61*(11), 3806-3813.

Álvarez, P. M., Jaramillo, J., Lopez-Pinero, F., & Plucinski, P. K. (2010). Preparation and characterization of magnetic TiO_2 nanoparticles and their utilization for the degradation of emerging pollutants in water. *Applied Catalysis B: Environmental*, *100*(1), 338-345.

Aravind, J., Lenin, C., Nancyflavia, C., Rashika, P., & Saravanan, S. (2015). Response surface methodology optimization of nickel(II) removal using pigeon pea pod biosorbent. *International Journal of Environmental Science & Technology*, *12*(1), 105-114.

Arbabi, M., Hemati, S., & Amiri, M. (2015). Removal of lead ions from industrial wastewater: A review of removal methods. *International Journal of Epidemiologic Research*, 2(2), 105-109.

Attri, P., Kim, Y.H., Park, D.H., Park, J.H., Hong, Y.J., Uhm, H.S., Kim, K.N., Fridman, A., & Choi, E.H. (2015). Generation mechanism of hydroxyl radical species and its lifetime prediction during the plasma-initiated ultraviolet (UV) photolysis. *Scientific Reports*, *5*.

Andronic, L., Isac, L., Miralles-Cuevas, S., Visa, M., Oller, I., Duta, A., & Malato, S. (2016). Pilot-plant evaluation of TiO_2 and TiO_2-based hybrid photocatalysts for solar treatment of polluted water. *Journal of Hazardous Materials*, *320*, 469-478.

Antonopoulou, M., Chondrodimou, I., Bairamis, F., Giannakas, A., & Konstantinou, I. (2017). Photocatalytic reduction of Cr(VI) by char/TiO_2 composite photocatalyst: optimization and modeling using the response surface methodology (RSM). *Environmental Science & Pollution Research*, *24*(2), 1063-1072.

Attallah, O. A., Al-Ghobashy, M. A., Nebsen, M., & Salem, M. Y. (2016). Removal of cationic and anionic dyes from aqueous solution with magnetite/pectin and magnetite/silica/pectin hybrid nanocomposites: kinetic, isotherm and mechanism analysis. *RSC Advances*, *6*(14), 11461-11480.

Avudainayagam, S., Megharaj, M., Owens, G., Kookana, R. S., Chittleborough, D., & Naidu, R. (2003). Chemistry of chromium in soils with emphasis on tannery waste sites. In *Reviews of Environmental Contamination & Toxicology* (pp. 53-91). Springer, New York.

Bafana, A., Dutt, S., Kumar, S., & Ahuja, P. S. (2011). Superoxide dismutase: an industrial perspective. *Critical Reviews in Biotechnology*, *31*(1), 65-76.

Bagheri, S., & Julkapli, N. M. (2015). Magnetite hybrid photocatalysis: advance environmental remediation. *Reviews in Inorganic Chemistry*, *36*(3), 135-151.

Bagheri, S., Hir, Z. A. M., Yousefi, A. T., & Hamid, S. B. A. (2015). Progress on mesoporous titanium dioxide: synthesis, modification and applications. *Microporous & Mesoporous Materials*, *218*, 206-222.

Bakr, A. S. A., Moustafa, Y. M., Khalil, M. M., Yehia, M. M., & Motawea, E. A. (2015). Magnetic nanocomposite beads: synthesis and uptake of Cu(II) ions from aqueous solutions. *Canadian Journal of Chemistry*, *93*(3), 289-296.

Baloyi, J., Seadira, T., Moutloali, R., Raphulu, M., & Ochieng, A. (2014). *Kinetic investigation of Hg(II) photoreduction using TiO_2-immobilized on calcium alginate beads: Effect of ferric ion and organic Compound*. Paper presented at Conference on Chemical Engineering and Advanced Computational Technologies, Pretoria, 2014. South Africa (pp. 1-6).

Barakat, M. A. (2011). New trends in removing heavy metals from industrial wastewater. *Arabian Journal of Chemistry*, *4*(4), 361–377.

Baş, D., & Boyacı, İ. H. (2007). Modeling and optimization I: Usability of response surface methodology. *Journal of Food Engineering*, *78*(3), 836-845.

Bedanta, S., Barman, A., Kleemann, W., Petracic, O., & Seki, T. (2013). Magnetic nanoparticles: a subject for both fundamental research and applications. *Journal of Nanomaterials*, *2013*, 1-22.

Behrad, F., Farimani, M. H. R., Shahtahmasebi, N., Roknabadi, M. R., & Karimipour, M. (2015). Synthesis and characterization of Fe_3O_4/TiO_2 magnetic and photocatalyst bifunctional core-shell with superparamagnetic performance. *The European Physical Journal Plus*, *130*(7), 1-9.

Behbahani, M., Babapour, M., Amini, M. M., Sadeghi, O., Bagheri, A., Salarian, M., & Rafiee, B. (2013). Separation/enrichment of copper and silver using titanium dioxide nanoparticles coated with poly-thiophene and their analysis by flame atomic absorption spectrophotometry. *American Journal of Analytical Chemistry*, *4*(2), 90-98.

Behnajady, M. A., Yavari, S., & Modirshahla, N. (2014). Investigation on adsorption capacity of TiO_2-P25 nanoparticles in the removal of a mono-azo dye from aqueous solution: a comprehensive isotherm analysis. *Chemical Industry & Chemical Engineering Quarterly*, *20*(1), 97-107.

Benjwal, P., Kumar, M., Chamoli, P., & Kar, K. K. (2015). Enhanced photocatalytic degradation of methylene blue and adsorption of arsenic(III) by reduced graphene oxide (rGO)–metal oxide (TiO_2/Fe_3O_4) based nanocomposites. *RSC Advances*, *5*(89), 73249-73260.

Bet-Moushoul, E., Mansourpanah, Y., Farhadi, K., & Tabatabaei, M. (2016). TiO_2 nanocomposite based polymeric membranes: a review on performance improvement for various applications in chemical engineering processes. *Chemical Engineering Journal*, *283*, 29-46.

Betigeri, S. S., & Neau, S. H. (2002). Immobilization of lipase using hydrophilic polymers in the form of hydrogel beads. *Biomaterials*, *23*(17), 3627-3636.

Bezerra, M. A., Santelli, R. E., Oliveira, E. P., Villar, L. S., & Escaleira, L. A. (2008). Response surface methodology (RSM) as a tool for optimization in analytical chemistry. *Talanta*, *76*(5), 965-977.

Bhat, U. N., & Khan, A. B. (2011). Heavy metals: An ambiguous category of inorganic contaminants, nutrients and toxins. *Research Journal of Environmental Sciences*, *5*(8), 682-690.

Bhatia, S. C. (2002). *Handbook of industrial pollution and control: air, water, wastes and pollution control in chemical process and allied industries*. CBS Publishers.

Bhalerao, S. A., & Sharma, A. S. (2015). Chromium: As an environmental pollutant. *International Journal of Current Microbiology & Applied Sciences, 4*(4), 732-746.

Bhuiyan, M. H. U., Saidur, R., Amalina, M. A., Mostafizur, R. M., & Islam, A. K. M. S. (2015). Effect of nanoparticles concentration and their sizes on surface tension of nanofluids. *Procedia Engineering*, *105*, 431-437.

Boczkaj, G., & Fernandes, A. (2017). Wastewater treatment by means of advanced oxidation processes at basic pH conditions: A review. *Chemical Engineering Journal*, *320*, 608-633.

Braccini, I., & Pérez, S. (2001). Molecular basis of Ca^{2+}-induced gelation in alginates and pectins: the

egg-box model revisited. *Biomacromolecules*, *2*(4), 1089-1096.

Brooks, R. M., Bahadory, M., Tovia, F., & Rostami, H. (2010). Removal of lead from contaminated water. *International Journal of Soil, Sediment & Water*, *3*(2), 1-14.

Bucak, S., Sezer, A., & Yavuztürk, B. (2012). *Magnetic nanoparticles: synthesis, surface modifications and application in drug delivery* (p. 165). Rijeka, Croatia: INTECH Open Access Publisher.

Burana-osot, J., Hosoyama, S., Nagamoto, Y., Suzuki, S., Linhardt, R. J., & Toida, T. (2009). Photolytic depolymerization of alginate. *Carbohydrate Research*, *344*(15), 2023-2027.

Buthiyappan, A., Aziz, A., Raman, A., Daud, W., & Ashri, W. M. (2016). Recent advances and prospects of catalytic advanced oxidation process in treating textile effluents. *Reviews in Chemical Engineering*, *32*(1), 1-47.

Butter, K., Kassapidou, K., Vroege, G. J., & Philipse, A. P. (2005). Preparation and properties of colloidal iron dispersions. *Journal of Colloid & Interface Science*, *287*(2), 485-495.

Carp, O., Huisman, C. L., & Reller, A. (2004). Photoinduced reactivity of titanium dioxide. *Progress in Solid State Chemistry*, *32*(1), 33-177.

Chaibakhsh, N., Ahmadi, N., & Zanjanchi, M. A. (2016). Optimization of photocatalytic degradation of neutral red dye using TiO_2 nanocatalyst via Box-Behnken design. *Desalination & Water Treatment*, *57*(20), 9296-9306.

Charles, J., Bradu, C., Morin-Crini, N., Sancey, B., Winterton, P., Torri, G., Badot, P.M., & Crini, G. (2016). Pollutant removal from industrial discharge water using individual and combined effects of adsorption and ion-exchange processes: Chemical abatement. *Journal of Saudi Chemical Society*, *20*(2), 185-194.

Chen, Y. F., Lee, C. Y., Yeng, M. Y., & Chiu, H. T. (2003). The effect of calcination temperature on

the crystallinity of TiO_2 nanopowders. *Journal of Crystal Growth, 247*(3-4), 363-370.

Chen, J., Li, G., He, Z., & An, T. (2011). Adsorption and degradation of model volatile organic compounds by a combined titania–montmorillonite–silica photocatalyst. *Journal of Hazardous Material, 190*(1), 416-423.

Cheng, J. P., Ma, R., Li, M., Wu, J. S., Liu, F., & Zhang, X. B. (2012). Anatase nanocrystals coating on silica-coated magnetite: Role of polyacrylic acid treatment and its photocatalytic properties. *Chemical Engineering Journal, 210*, 80-86.

Chequer, F. M. D., de Oliveira, G. A. R., Ferraz, E. R. A., Cardoso, J. C., Zanoni, M. V. B., & de Oliveira, D. P. (2013). Textile dyes: dyeing process and environmental impact. In *Eco-friendly textile dyeing and finishing*. InTech.

Cho, I. H., Lee, N. H., Yang, J. K., & Lee, S. M. (2007). Treatment of wastewater containing Cu(II)-EDTA using immobilized TiO_2/solar light. *Journal of Environmental Science & Health Part A, 42*(2), 165-170.

Chong, M. N., Jin, B., Chow, C. W., & Saint, C. (2010). Recent developments in photocatalytic water treatment technology: a review. *Water Research, 44*(10), 2997-3027.

Chun, S. Y., An, S. W., Lee, S. J., Kim, J. T., & Chang, S. W. (2014). Optimization of sulfamethoxazole degradation by TiO_2/hydroxyapatite composite under ultraviolet irradiation using response surface methodology. *Korean Journal of Chemical Engineering, 31*(6), 994-1001.

Corsi, S. R., Graczyk, D. J., Geis, S. W., Booth, N. L., & Richards, K. D. (2010). A fresh look at road salt: aquatic toxicity and water-quality impacts on local, regional, and national scales. *Environmental Science & Technology, 44*(19), 7376-7382.

Costa, E. da., Zamora, P. P., & Zarbin, A. J. (2012). Novel TiO_2/C nanocomposites: synthesis,

characterization, and application as a photocatalyst for the degradation of organic pollutants. *Journal of Colloid & Interface Science*, *368*(1), 121-127.

Cui, L., Wang, Y., Hu, L., Gao, L., Du, B., & Wei, Q. (2015). Mechanism of Pb(II) and methylene blue adsorption onto magnetic carbonate hydroxyapatite/graphene oxide. *RSC Advances*, *5*(13), 9759-9770.

da Silva, C. S. C. G. (2008). *Synthesis, spectroscopy and characterization of titanium dioxide based photocatalysts for the degradative oxidation of organic pollutants* (Doctoral dissertation, Universidade do Porto, Portugal).

Daemi, H., & Barikani, M. (2012). Synthesis and characterization of calcium alginate nanoparticles, sodium homopolymannuronate salt and its calcium nanoparticles. *Scientia Iranica*, *19*(6), 2023-2028.

Dargo, H., Gabbiye, N., & Ayalew, A. (2014). Removal of methylene blue dye from textile wastewater using activated carbon prepared from rice husk. *International Journal of Innovation & Scientific Research*, *9*(2), 317-325.

Daghrir, R., Drogui, P., & Robert, D. (2013). Modified TiO_2 for environmental photocatalytic applications: a review. *Industrial & Engineering Chemistry Research*, *52*(10), 3581-3599.

Delnavaz, M., Ayati, B., Ganjidoust, H., & Sanjabi, S. (2015). Application of concrete surfaces as novel substrate for immobilization of TiO_2 nano powder in photocatalytic treatment of phenolic water. *Journal of Environmental Health Science & Engineering*, *13*(1), 1-10.

Deng, Y., & Zhao, R. (2015). Advanced oxidation processes (AOPs) in wastewater treatment. *Current Pollution Reports*, *1*(3), 167-176.

Di Valentin, C., & Pacchioni, G. (2013). Trends in non-metal doping of anatase TiO_2: B, C, N and

F. *Catalysis Today*, *206*, 12-18.

Dimitrov, D. T., Milanova, M. M., & Kralshevska, R. P. (2011). Lanthanide oxide doped titania photocatalysts for degradation of organic pollutants under UV and visible light illumination. *Chemical Communication*, *43*(4), 489–501.

Djellabi, R., Ghorab, M. F., Bianchi, C. L., Cerrato, G., & Morandi, S. (2016). Recovery of hexavalent chromium from water using photoactive TiO_2-montmorillonite under sunlight. *Mediterranean Journal of Chemistry*, *5*(3), 442-449.

Dong, H., Zeng, G., Tang, L., Fan, C., Zhang, C., He, X., & He, Y. (2015). An overview on limitations of TiO_2-based particles for photocatalytic degradation of organic pollutants and the corresponding countermeasures. *Water Research*, *79*, 128-146.

Dong, Q., Zhang, K., & An, Y. (2014). A novel synthesis method for TiO_2 particles with magnetic Fe_3O_4 cores. *Water Science & Technology*, *69*(10), 2093-2098.

Dong, X.L., Mou, X.Y., Ma, H.C., Zhang, X.X., Zhang, X.F., Sun, W.J., Ma, C., & Xue, M. (2013). Preparation of CdS–TiO_2/Fe_3O_4 photocatalyst and its photocatalytic properties. *Journal of Sol-Gel Science & Technology*, *66*(2), 231-237.

Dupont, D., Luyten, J., Bloemen, M., Verbiest, T., & Binnemans, K. (2014). Acid-stable magnetic core–shell nanoparticles for the separation of rare earths. *Industrial & Engineering Chemistry Research*, *53*(39), 15222-15229.

Ebenezar, I., Ramalingam, S., Raja, C., & Prabakar, P. (2014). Vibrational spectroscopic [IR and Raman] analysis and computational investigation [NMR, UV-Visible, MEP and Kubo gap] on L-Valinium Picrate. *Journal of Nanotechnology & Advance Materials, 2*(1), 11-25.

Edokpayi, J. N., Odiyo, J. O., Popoola, O. E., & Msagati, T. A. (2016). Assessment of trace metals

contamination of surface water and sediment: A case study of Mvudi River, South Africa. *Sustainability*, *8*(2), 1-13.

Eleburuike, N. A., Bakar, W. A. W. A., Ali, R., & Omar, M. F. (2016). Photocatalytic degradation of paraquat dichloride over CeO_2-modified TiO_2 nanotubes and the optimization of parameters by response surface methodology. *RSC Advances*, *6*(106), 104082-104093.

Elmoubarki, R., Taoufik, M., Moufti, A., Tounsadi, H., Mahjoubi, F.Z., Bouabi, Y., Qourzal, S., Abdennouri, M., & Barka, N. (2017). Box-Behnken experimental design for the optimization of methylene blue adsorption onto Aleppo pine cones. *Journal of Materials & Environmental Science*, *8*(6), 2184–2191.

Emerson, R. W., & Cavazzuti, M. (2013). Design of experiments. *Deterministic optimization. Optimization Methods: From Theory to Design Scientific and Technological Aspects in Mechanics* (pp. 13-42). Berlin, Heidelberg: Springer Berline Heidelberg.

Fagan, R., McCormack, D. E., Hinder, S., & Pillai, S. C. (2016). Improved high temperature stability of anatase TiO_2 photocatalysts by N, F, P co-doping. *Materials & Design*, *96*, 44-53.

Faraji, M., Yamini, Y., & Rezaee, M. (2010). Magnetic nanoparticles: synthesis, stabilization, functionalization, characterization, and applications. *Journal of the Iranian Chemical Society*, *7*(1), 1-37.

Farzana, M., H. & Meenakshi, S. (2015). Photocatalytic aptitude of titanium dioxide impregnated chitosan beads for the reduction of Cr(VI). *International Journal of Biological Macromolecules*, *72*, 1265–1271.

Fauzian, M., Taufik, A., & Saleh, R. (2017). Photocatalytic performance of Fe_3O_4/TiO_2/Ag nanocomposites for photocatalytic activity under visible light irradiation. In *AIP Conference Proceedings* (Vol. 1862, No. 1, p. 030031). AIP Publishing.

Ferreira, S.C., Bruns, R.E., Ferreira, H.S., Matos, G.D., David, J.M., Brandao, G.C., da Silva, E.P., Portugal, L.A., Dos Reis, P.S., Souza, A.S., & Dos Santos, W.N.L. (2007). Box-Behnken design: an alternative for the optimization of analytical methods. *Analytica Chimica Acta*, *597*(2), 179-186.

Fiol, N., & Villaescusa, I. (2009). Determination of sorbent point zero charge: usefulness in sorption studies. *Environmental Chemistry Letters*, *7*(1), 79-84.

Forgacs, E., Cserhati, T., & Oros, G. (2004). Removal of synthetic dyes from wastewaters: a review. *Environment International*, *30*(7), 953-971.

Fox, M. A., & Dulay, M. T. (1993). Heterogeneous photocatalysis. *Chemical Reviews*, *93*(1), 341-357.

Fu, F., & Wang, Q. (2011). Removal of heavy metal ions from wastewaters: a review. *Journal of Environmental Management*, *92*(3), 407-418.

Fu, J. F., Zhao, Y. Q., Xue, X. D., Li, W. C., & Babatunde, A. O. (2009). Multivariate-parameter optimization of acid blue-7 wastewater treatment by Ti/TiO_2 photoelectrocatalysis via the Box–Behnken design. *Desalination*, *243*(1), 42-51.

Fujishima, A., & Zhang, X. (2006). Titanium dioxide photocatalysis: present situation and future approaches. *Comptes Rendus Chimie*, *9*(5), 750-760.

Gaya, U. I., & Abdullah, A. H. (2008). Heterogeneous photocatalytic degradation of organic contaminants over titanium dioxide: a review of fundamentals, progress and problems. *Journal of Photochemistry & Photobiology C: Photochemistry Reviews*, *9*(1), 1-12.

Goel, J., Kadirvelu, K., Rajagopal, C., & Garg, V. K. (2005). Investigation of adsorption of lead, mercury and nickel from aqueous solutions onto carbon aerogel. *Journal of Chemical Technology & Biotechnology*, *80*(4), 469-476.

Gomes, J.F., Leal, I., Bednarczyk, K., Gmurek, M., Stelmachowski, M., Zaleska-Medynska, A., Quinta-

Ferreira, M.E., Costa, R., Quinta-Ferreira, R.M., & Martins, R.C. (2017). Detoxification of parabens using UV-A enhanced by noble metals-TiO_2 supported catalysts. *Journal of Environmental Chemical Engineering*, *5*(4), 3065-3074.

Gómez-Pastora, J., Bringas, E., & Ortiz, I. (2014). Recent progress and future challenges on the use of high performance magnetic nano-adsorbents in environmental applications. *Chemical Engineering Journal*, *256*, 187-204.

Gopalakannan, V., & Viswanathan, N. (2016). One pot synthesis of metal ion anchored alginate–gelatin binary biocomposite for efficient Cr(VI) removal. *International Journal of Biology Macromolecules, 83*, 450-459.

Gunatilake, S. K. (2015). Methods of removing heavy metals from industrial wastewater. *Methods*, *1*(1).

Guillard, C., Lachheb, H., Houas, A., Ksibi, M., Elaloui, E., & Herrmann, J. M. (2003). Influence of chemical structure of dyes, of pH and of inorganic salts on their photocatalytic degradation by TiO_2 comparison of the efficiency of powder and supported TiO_2. *Journal of Photochemistry & Photobiology A: Chemistry*, *158*(1), 27-36.

Gupta, V. K., Carrott, P. J. M., Ribeiro Carrott, M. M. L., & Suhas. (2009). Low-cost adsorbents: growing approach to wastewater treatment-a review. *Critical Reviews in Environmental Science & Technology*, *39*(10), 783-842.

Gupta, S., & Tripathi, M. (2012). A review on the synthesis of TiO_2 nanoparticles by solution route. *Open Chemistry*, *10*(2), 279-294.

Habib, M. A., Shahadat, M. T., Bahadur, N. M., Ismail, I. M., & Mahmood, A. J. (2013). Synthesis and characterization of ZnO-TiO_2 nanocomposites and their application as photocatalysts. *International Nano Letters*, *3*(1), 1-8.

Hammouda, S., Adhoum, N., & Monser, L. (2015). Synthesis of magnetic alginate beads based on Fe_3O_4 nanoparticles for the removal of 3-methylindole from aqueous solution using Fenton process. *Journal of Hazardous Materials, 294*, 128-136.

Harifi, T., & Montazer, M. (2014). A novel magnetic reusable nanocomposite with enhanced photocatalytic activities for dye degradation. *Separation & Purification Technology*, *134*, 210-219.

Harikumar, P., Joseph, L., & Dhanya, A. (2013). Photocatalytic degradation of textile dyes by hydrogel supported titanium dioxide nanoparticles. *Journal of Environmental Engineering & Ecological Science*, *2*(2), 1–9.

Hasbullah, T.T., Selaman, O.S., & Rosli, N.A. (2014). Removal of methylene blue from aqueous solutions using chemical activated carbon prepared from jackfruit (Artocarpus heterophyllus) peel waste. *Journal of Civil Engineering, Science & Technology, 5*(1), 34-38.

Hasanpour, A., Niyaifar, M., Mohammadpour, H., & Amighian, J. (2012). A novel non-thermal process of TiO_2-shell coating on Fe_3O_4-core nanoparticles. *Journal of Physics & Chemistry of Solids*, *73*(9), 1066-1070.

Helmi R. F. M., Shahtahmassebi, N., Rezaee Roknabadi, M., & Ghows, N. (2014). Synthesis and study of structural and magnetic properties of superparamagnetic Fe_3O_4/SiO_2 core/shell nanocomposite for biomedical applications. *Nanomedicine Journal, 1*(2), 71-78.

Hendrix, Y., Lazaro, A., Yu, Q., & Brouwers, J. (2015). Titania-silica composites: a review on the photocatalytic activity and synthesis methods. *World Journal of Nano Science & Engineering*, *5*(4), 161–177.

Herrmann, J. (1999). Heterogeneous photocatalysis: fundamentals and applications to the removal of various types of aqueous pollutants. *Catalysis Today*, *53*(1), 115-129.

Holmberg, J. P. (2006). *Competitive Adsorption and Displacement Behaviour of Heavy Metals on Peat*, Unpublished Master thesis, Chalmers University of Technology, Göteborg, Sweden.

Horst, M. F., Alvarez, M., & Lassalle, V. L. (2016). Removal of heavy metals from wastewater using magnetic nanocomposites: Analysis of the experimental conditions. *Separation Science & Technology*, *51*(3), 550–563.

Horváth, O., & Hegyi, J. (2001). Light-induced reduction of heavy-metal ions on titanium dioxide dispersions. In *Adsorption and Nanostructure* (pp. 211-216). Springer, Berlin, Heidelberg.

Houas, A., Lachheb, H., Ksibi, M., Elaloui, E., Guillard, C., & Herrmann, J. M. (2001). Photocatalytic degradation pathway of methylene blue in water. *Applied Catalysis B: Environmental*, *31*(2), 145-157.

Hu, J., Chen, G., & Lo, I. M. (2005). Removal and recovery of Cr(VI) from wastewater by maghemite nanoparticles. *Water Research*, *39*(18), 4528-4536.

Ibhadon, A., & Fitzpatrick, P. (2013). Heterogeneous photocatalysis: recent advances and applications. *Catalysts*, *3*(1), 189–218.

Islam, S., Nagpure, S., Kim, D., & Rankin, S. (2017). Synthesis and catalytic applications of non-metal doped mesoporous titania. *Inorganics*, *5*(1), 1-43.

Ismail, A. A., El-Midany, A. A., Ibrahim, I. A., & Matsunaga, H. (2008). Heavy metal removal using SiO_2-TiO_2 binary oxide: Experimental design approach. *Adsorption*, *14*(1), 21–29.

Jan, A. T., Azam, M., Siddiqui, K., Ali, A., Choi, I., & Haq, Q. M. R. (2015). Heavy metals and human health: Mechanistic insight into toxicity and counter defense system of antioxidants. *International Journal of Molecular Sciences*, *16*(12), 29592–29630.

Järup, L. (2003). Hazards of heavy metal contamination. *British Medical Bulletin*, *68*, 167–182.

Javanbakht, V., & Ghoreishi, S. M. (2016). Application of response surface methodology for optimization of lead removal from an aqueous solution by a novel superparamagnetic nanocomposite. *Adsorption Science & Technology*, *35*(1-2), 241-260.

Jiang, D., Xu, Y., Hou, B., Wu, D., & Sun, Y. (2007). Synthesis of visible light-activated TiO_2 photocatalyst via surface organic modification. *Journal of Solid State Chemistry*, *180*(5), 1787–1791.

Jiang, J., Wu, X.Y., Zhou, X.Q., Feng, L., Liu, Y., Jiang, W.D., Wu, P., & Zhao, Y. (2016). Glutamate ameliorates copper-induced oxidative injury by regulating antioxidant defences in fish intestine. *British Journal of Nutrition*, *116*(1), 70-79.

Jiao, L., Qi, P. S., Liu, Y. Z., & Wang, B. (2014). Fe_3O_4 and TiO_2 embedded sodium alginate beads of composite adsorbent for Pb(II) removal. *Advanced Materials Research*, *900*, 160–164.

Jobanputra, A. H., Karode, B. A., & Bhaskar, S. (2011). Calcium alginate as supporting material for the immobilization of rifamycin oxidase from Chryseobacterium species immobilization technique. *Biotechnology, Bioinformatics & Bioengineering*, *1*(4), 529–535.

Joseph, C. G., Taufiq-Yap, Y. H., Li Puma, G., Sanmugam, K., & Quek, K. S. (2016). Photocatalytic degradation of cationic dye simulated wastewater using four radiation sources, UVA, UVB, UVC and solar lamp of identical power output. *Desalination & Water Treatment*, *57*(17), 7976–7987.

Joshi, K. M., Patil, B. N., Shirsath, D. S., & Shrivastava, V. S. (2011). Photocatalytic removal of Ni(II) and Cu(II) by using different Semiconducting materials. *Advances in Applied Science Research*, *2*(3), 445-54.

Jung, C., Heo, J., Han, J., Her, N., Lee, S.J., Oh, J., Ryu, J., & Yoon, Y. (2013). Hexavalent chromium removal by various adsorbents: powdered activated carbon, chitosan, and single/multi-walled carbon nanotubes. *Separation & Purification Technology*, *106*, 63-71.

Kabra, K., Chaudhary, R., & Sawhney, R. L. (2007). Effect of pH on solar photocatalytic reduction and deposition of Cu(II), Ni(II), Pb(II) and Zn(II): Speciation modeling and reaction kinetics. *Journal of Hazardous Materials*, *149*(3), 680-685.

Kabra, K., Chaudhary, R., & Sawhney, R. L. (2004). Treatment of hazardous organic and inorganic compounds through aqueous-phase photocatalysis: a review. *Industrial & Engineering Chemistry Research*, *43*(24), 7683-7696.

Kalantari, K., Ahmad, M. B., Masoumi, H. R. F., Shameli, K., Basri, M., & Khandanlou, R. (2014). Rapid adsorption of heavy metals by Fe_3O_4/talc nanocomposite and optimization study using response surface methodology. *International Journal of Molecular Sciences*, *15*(7), 12913-12927.

Kanakaraju, D., Lim, Y. C., & Pace, A. (2018). Magnetic hybrid TiO_2/Alg/FeNPs triads for the efficient removal of methylene blue from water. *Sustainable Chemistry and Pharmacy*, *8*, 50-62.

Kanakaraju, D., Ravichandar, S., & Lim, Y. C. (2017). Combined effects of adsorption and photocatalysis by hybrid TiO_2/ZnO-calcium alginate beads for the removal of copper. *Journal of Environmental Sciences*, *55*, 214-223.

Kanakaraju, D., Motti, C. A., Glass, B. D., & Oelgemöller, M. (2016). Solar photolysis versus TiO_2-mediated solar photocatalysis: a kinetic study of the degradation of naproxen and diclofenac in various water matrices. *Environmental Science and Pollution Research*, *23*(17), 17437-17448.

Kanakaraju, D., Kockler, J., Motti, C. A., Glass, B. D., & Oelgemöller, M. (2015). Titanium dioxide/zeolite integrated photocatalytic adsorbents for the degradation of amoxicillin. *Applied Catalysis B: Environmental*, *166*, 45-55.

Kanawade, S. M., & Gaikwad, R. W. (2011). Removal of zinc ions from industrial effluent by using cork powder as adsorbent. *International Journal of Chemical Engineering & Applications*, *2*(3), 317-319.

Kansal, S. K., Singh, M., & Sud, D. (2007). Studies on photodegradation of two commercial dyes in aqueous phase using different photocatalysts. *Journal of Hazardous Materials*, *141*(3), 581-590.

Keyhanian, F., Shariati, S., Faraji, M., & Hesabi, M. (2016). Magnetite nanoparticles with surface modification for removal of methyl violet from aqueous solutions. *Arabian Journal of Chemistry*, *9*, 48-54.

Khairy, M., & Zakaria, W. (2014). Effect of metal-doping of TiO_2 nanoparticles on their photocatalytic activities toward removal of organic dyes. *Egyptian Journal of Petroleum*, *23*(4), 419-426.

Khidhir, B. A., Al-Oqaiel, W., & Kareem, P. (2015). Prediction Models by Response Surface Methodology for turning operation. *American Journal of Modeling & Optimization*, *3*(1), 1-6.

Khosravi, M., & Arabi, S. (2016). Application of response surface methodology (RSM) for the removal of methylene blue dye from water by nano zero-valent iron (NZVI). *Water Science & Technology*, *74*(2), 343-352.

Khuri, A. I., & Mukhopadhyay, S. (2010). Response surface methodology. *Wiley Interdisciplinary Reviews: Computational Statistics*, *2*(2), 128–149.

Kiernan, J. A. (2001). Classification and naming of dyes, stains and fluorochromes. *Biotechnic & Histochemistry*, *76*(5-6), 261-278.

Kimling, M. C., & Caruso, R. A. (2012). Sol–gel synthesis of hierarchically porous TiO_2 beads using calcium alginate beads as sacrificial templates. *Journal of Materials Chemistry*, *22*(9), 4073-4082.

Kołodyńska, D., Kowalczyk, M., & Hubicki, Z. (2014). Evaluation of iron-based hybrid materials for heavy metal ions removal. *Journal of Materials Science*, *49*(6), 2483-2495.

Konstantinou, I. K., & Albanis, T. A. (2004). TiO_2-assisted photocatalytic degradation of azo dyes in aqueous solution: kinetic and mechanistic investigations: a review. *Applied Catalysis B:*

Environmental, *49*(1), 1-14.

Konwar, A., Gogoi, A., & Chowdhury, D. (2015). Magnetic alginate–Fe_3O_4 hydrogel fiber capable of ciprofloxacin hydrochloride adsorption/separation in aqueous solution. *RSC Advances*, *5*(99), 81573-81582.

Krishnan, S., Rawindran, H., Sinnathambi, C. M., & Lim, J. W. (2017). Comparison of various advanced oxidation processes used in remediation of industrial wastewater laden with recalcitrant pollutants. In *IOP Conference Series: Materials Science & Engineering*, *206*(1), 1-12.

Krzemińska, D., Neczaj, E., & Borowski, G. (2015). Advanced oxidation processes for food industrial wastewater decontamination. *Journal of Ecological Engineering*, *16*(2), 61–71.

Kumar, S.G., & Devi, L.G. 2011. Review on modified TiO_2 photocatalysis under UV/visible light: selected results and related mechanisms on interfacial charge carrier transfer dynamics. *The Journal of Physical Chemistry A*, *115*, 13211–13241.

Kumar, A. (2017). A review on the factors affecting the photocatalytic degradation of hazardous materials. *Material Science & Engineering International Journal*, *1*(3), 1–10.

Kumar, A., Guo, C., Sharma, G., Pathania, D., Naushad, M., Kalia, S., & Dhiman, P. (2016). Magnetically recoverable ZrO_2/Fe_3O_4/chitosan nanomaterials for enhanced sunlight driven photoreduction of carcinogenic Cr(VI) and dechlorination & mineralization of 4-chlorophenol from simulated waste water. *RSC Advances*, *6*(16), 13251-13263.

Kunarti, E. K., Roto, R., Pradipta, A. R., & Budi, I. S. (2017). Fe_3O_4/SiO_2/TiO_2 core-shell nanoparticles as catalyst for photoreduction of Ag(I) Ions. *Oriental Journal of Chemistry, 33*(4), 1933-1940.

Lachheb, H., Puzenat, E., Houas, A., Ksibi, M., Elaloui, E., Guillard, C., & Herrmann, J. M. (2002). Photocatalytic degradation of various types of dyes (Alizarin S, Crocein Orange G, Methyl Red,

Congo Red, Methylene Blue) in water by UV-irradiated titania. *Applied Catalysis B: Environmental, 39*(1), 75–90.

Lakouraj, M. M., Mojerlou, F., & Zare, E. N. (2014). Nanogel and superparamagnetic nanocomposite based on sodium alginate for sorption of heavy metal ions. *Carbohydrate Polymers, 106*, 34-41.

Lam, S. M., Sin, J. C., Abdullah, A. Z., & Mohamed, A. R. (2012). Degradation of wastewaters containing organic dyes photocatalysed by zinc oxide: a review. *Desalination & Water Treatment, 41*(1-3), 131-169.

Lan, Y., Lu, Y., & Ren, Z. (2013). Mini review on photocatalysis of titanium dioxide nanoparticles and their solar applications. *Nano Energy, 2*(5), 1031–1045.

Laurent, S., Forge, D., Port, M., Roch, A., Robic, C., Vander Elst, L., & Muller, R. N. (2008). Magnetic iron oxide nanoparticles: synthesis, stabilization, vectorization, physicochemical characterizations, and biological applications. *Chemical Reviews, 108*(6), 2064-2110.

Lazaridis, N., & Charalambous, C. (2005). Sorptive removal of trivalent and hexavalent chromium from binary aqueous solutions by composite alginate–goethite beads. *Water Research, 39*(18), 4385-4396.

Lee, K. Y., & Mooney, D. J. (2012). Progress in polymer science alginate : Properties and biomedical applications. *Progress in Polymer Science, 37*(1), 106–126.

Lee, S. M., Lee, T. W., Choi, B. J., & Yang, J. K. (2003). Treatment of Cr(VI) and phenol by illuminated TiO_2. *Journal of Environmental Science & Health, Part A, 38*(10), 2219-2228.

León, E. R., Rodríguez, E. L., Beas, C. R., Plascencia-Villa, G., & Palomares, R. A. I. (2016). Study of methylene blue degradation by gold nanoparticles synthesized within natural zeolites. *Journal of Nanomaterials, 2016*, 1-11.

Li, H., Shi, A., Li, M., & Zhang, X. (2013). Effect of pH, temperature, dissolved oxygen, and flow rate

of overlying water on heavy metals release from storm sewer sediments. *Journal of Chemistry, 2013,* 1-11.

Li, C., Lu, J., Li, S., Tong, Y., & Ye, B. (2017). Synthesis of magnetic microspheres with sodium alginate and activated carbon for removal of methylene blue. *Materials*, *10*(1), 1-14.

Li, W., & Wu, H. 2017. Sodium citrate functionalized reusable Fe_3O_4@TiO_2 photocatalyst for water purification. *Chemical Physics Letters, 686*, 178-182.

Li, H., Duan, X., Liu, G., & Li, L. (2008). Synthesis and characterization of copper ions surface-doped titanium dioxide nanotubes. *Materials Research Bulletin*, *43*(8), 1971-1981.

Li, L., Li, X., Duan, H., Wang, X., & Luo, C. (2014). Removal of Congo Red by magnetic mesoporous titanium dioxide–graphene oxide core–shell microspheres for water purification. *Dalton Transactions*, *43*(22), 8431-8438.

Li, X., Liu, D., Song, S., & Zhang, H. (2014). $Fe_3O_4/SiO_2/TiO_2$/Pt Hierarchical Core–Shell Microspheres: Controlled Synthesis, Enhanced Degradation System, and Rapid Magnetic Separation to Recycle. *Crystal Growth & Design*, *14*(11), 5506-5511.

Liu, W., Ni, J., & Yin, X. (2014). Synergy of photocatalysis and adsorption for simultaneous removal of Cr(VI) and Cr(III) with TiO_2 and titanate nanotubes. *Water Research*, *53*, 12-25.

Liu, Y., Zheng, Y. & Wang, A. (2010). Response surface methodology for optimizing adsorption process parameters for methylene blue removal by a hydrogel composite. *Adsorption Science & Technology, 28*(10), 913-922.

Liu, X., Zhang, Q., Yu, B., Wu, R., Mai, J., Wang, R., Chen, L., & Yang, S.T. (2016). Preparation of Fe_3O_4/TiO_2/C nanocomposites and their application in fenton-like catalysis for dye decoloration. *Catalysts*, *6*(9), 1-12.

Ljubas, D., Franzreb, M., Hansen, H. C. B., & Weidler, P. G. (2014). Magnetizing of nano-materials on example of Degussa's P-25 TiO_2 photocatalyst: synthesis of magnetic aggregates, characterization and possible use. *Separation & Purification Technology, 136*, 274-285.

Lo, S. F., Wang, S. Y., Tsai, M. J., & Lin, L. D. (2012). Adsorption capacity and removal efficiency of heavy metal ions by Moso and Ma bamboo activated carbons. *Chemical Engineering Research & Design, 90*(9), 1397-1406.

Long, M., & Cai, W. (2011). Visible light responsive TiO_2 modification with nonmetal elements. *Frontiers of Chemistry in China, 6*(3), 190-199.

Loosli, F., Vitorazi, L., Berret, J.F., & Stoll, S. (2015). Towards a better understanding on agglomeration mechanisms and thermodynamic properties of TiO_2 nanoparticles interacting with natural organic matter. *Water Resources, 80,* 139-148.

López-Quintela, M. A., & Rivas, J. (1993). Chemical reactions in microemulsions: a powerful method to obtain ultrafine particles. *Journal of Colloid & Interface Science, 158*(2), 446-451.

Loredo, J., Ordónez, A., & Alvarez, R. (2006). Environmental impact of toxic metals and metalloids from the Munon Cimero mercury-mining area (Asturias, Spain). *Journal of Hazardous Materials, 136*(3), 455-467.

Lucas, M. S., Tavares, P. B., Peres, J. A., Faria, J. L., Rocha, M., Pereira, C., & Freire, C. (2013). Photocatalytic degradation of Reactive Black 5 with TiO_2-coated magnetic nanoparticles. *Catalysis Today, 209*, 116-121.

Lunge, S. S., Singh, S., & Sinha, A. (2014). Magnetic nanoparticle : synthesis and environmental applications. Paper presented at the International Conference on Chemical, Civil and Environmental Engineering, Singapore.

Ma, P., Jiang, W., Wang, F., Li, F., Shen, P., Chen, M., Wang, Y., Liu, J., & Li, P. (2013). Synthesis and photocatalytic property of Fe_3O_4/TiO_2 core/shell nanoparticles supported by reduced graphene oxide sheets. *Journal of Alloys & Compounds*, *578*, 501–506.

Mahdavi, M., Ahmad, M. Bin, Haron, M. J., Namvar, F., Nadi, B., Ab Rahman, M. Z., & Amin, J. (2013). Synthesis, surface modification and characterisation of biocompatible magnetic iron oxide nanoparticles for biomedical applications. *Molecules*, *18*(7), 7533–7548.

Majidi, S., Zeinali Sehrig, F., Farkhani, S., Soleymani Goloujeh, M., & Akbarzadeh, A. (2014). Current methods for synthesis of magnetic nanoparticles. *Artificial Cells, Nanomedicine, & Biotechnology*, *44*(2), 722-734.

Majidnia, Z., Idris, A., Majid, M. Z. A., Zin, R. M., & Ponraj, M. (2015). Efficiency of barium removal from radioactive waste water using the combination of maghemite and titania nanoparticles in PVA and alginate beads. *Applied Radiation & Isotopes*, *105*, 105–113.

Mamba, G., & Mishra, A. (2016). Advances in Magnetically Separable Photocatalysts: Smart, Recyclable Materials for Water Pollution Mitigation. *Catalysts*, *6*(6), 1-34.

Mascolo, M. C., Pei, Y., & Ring, T. A. (2013). Room temperature co-precipitation synthesis of magnetite nanoparticles in a large pH window with different bases. *Materials*, *6*(12), 5549-5567.

Miclescu, A., & Wiklund, L. (2010). Methylene blue, an old drug with new indications. *Jurnalul Roman de Anestezie Terapie Intaensiva*, *17*(1), 35-41.

Mojić, B., Giannakopoulos, K.P., Cvejić, Ž., & Srdić, V.V. (2012). Silica coated ferrite nanoparticles: influence of citrate functionalization procedure on final particle morphology. *Ceramics International, 38*(8), 6635-6641.

Mogal, S., Mishra, M., Gandhi, V., & Tayade, R. (2013). Metal doped titanium dioxide: synthesis and

effect of metal ions on physico-chemical and photocatalytic properties. *Materials Science Forum*, *734*, 364-378.

Mohammad-beigi, H., Yaghmaei, S., Roostaazad, R., Bardania, H., & Arpanaei, A. (2011). Effect of pH, citrate treatment and silane-coupling agent concentration on the magnetic, structural and surface properties of functionalized silica-coated iron oxide nanocomposite particles. *Physica E: Low-Dimensional Systems & Nanostructures*, *44*(3), 618–627.

Mohammed, M. A, Shitu, A., & Ibrahim, A. (2014). Removal of Methylene Blue Using Low Cost Adsorbent : A Review. *Research Journal of Chemical Sciences*, *4*(1), 91–102.

Mohapatra, D. P., Brar, S. K., Daghrir, R., Tyagi, R. D., Picard, P., Surampalli, R. Y., & Drogui, P. (2014). Photocatalytic degradation of carbamazepine in wastewater by using a new class of whey-stabilized nanocrystalline TiO_2 and ZnO. *Science of the Total Environment*, *485–486*(1), 263–269.

Morshedi, A., & Akbarian, M. (2014). Application of response surface methodology: design of experiments and optimization: a mini review. *Indian Journal of Fundamental & Applied Life Sciences*, *4*(2002), 2434–2439.

Mota, A. L. N., Albuquerque, L. F., Beltrame, L. C., Chiavone-Filho, O., Machulek Jr, A., & Nascimento, C. A. O. (2008). Advanced oxidation processes and their application in the petroleum industry: a review. *Brazilian Journal of Petroleum & Gas*, *2*(3), 122–142.

Munter, R. (2001). Advanced oxidation processes–current status and prospects. *Proceedings of the Estonian Academy Sciences Chemistry*, *50*(2), 59-80.

Nadarajan, R., Bakar, W. A. W. A., Ali, R., & Ismail, R. (2016). Photocatalytic degradation of 1, 2-dichlorobenzene using immobilized $TiO_2/SnO_2/WO_3$ photocatalyst under visible light: Application of response surface methodology. *Arabian Journal of Chemistry*, *11*(1), 1878-5352.

Nalamothu, N., Potluri, A., & Muppalla, M. B. (2014). Review on marine alginates and its applications. *Journal of Pharmaceutical Research*, *4*(10), 4006-4015.

Nasikhudin, Ismaya, E. P., Diantoro, M., Kusumaatmaja, A., & Triyana, K. (2017). Preparation of PVA/TiO_2 Composites Nanofibers by using electrospinning method for photocatalytic degradation. *Materials Science & Engineering*, *202*(1), 1-8.

Nasirian, M., & Mehrvar, M. (2016). Modification of TiO_2 to enhance photocatalytic degradation of organics in aqueous solutions. *Journal of Environmental Chemical Engineering*, *4*(4), 4072–4082.

Nassar, N. N., Marei, N. N., Vitale, G., & Arar, L. A. (2015). Adsorptive removal of dyes from synthetic and real textile wastewater using magnetic iron oxide nanoparticles: Thermodynamic and mechanistic insights. *The Canadian Journal of Chemical Engineering*, *93*(11), 1965-1974.

Narayana, R. L., Matheswaran, M., Aziz, A. A., & Saravanan, P. (2011). Photocatalytic decolourization of basic green dye by pure and Fe, Co doped TiO_2 under daylight illumination. *Desalination*, *269*(1), 249-253.

Nguyen Thi Thu, T., Nguyen Thi, N., Tran Quang, V., Nguyen Hong, K., Nguyen Minh, T., & Le Thi Hoai, N. (2016). Synthesis, characterisation, and effect of pH on degradation of dyes of copper-doped TiO_2. *Journal of Experimental Nanoscience*, *11*(3), 226-238.

Nsami, J., N., & Ketcha Mbadcam, J. (2013). The adsorption efficiency of chemically prepared activated carbon from cola nut shells by on methylene blue. *Journal of Chemistry*, *2013*, 1-4.

Neyaz, N., Siddiqui, W. A., & Nair, K. K. (2014). Application of surface functionalized iron oxide nanomaterials as a nanosorbents in extraction of toxic heavy metals from ground water : A review. *International Journal of Environmental Sciences*, *4*(4), 472–483.

Nigam, H., Das, M., Chauhan, S., Pandey, P., Swati, P., Yadav, M., & Tiwari, A. (2015). Effect of

chromium generated by solid waste of tannery and microbial degradation of chromium to reduce its toxicity: A review. *Advances in Applied Science Research*, *6*, 129-136.

Nour-Mohhamadi, F., Nguyen, S. D., Boschloo, G., Hagfeldt, A., & Lund, T. (2005). Determination of the light-induced degradation rate of the solar cell sensitizer N719 on TiO_2 nanocrystalline particles. *The Journal of Physics & Chemistry B, 109*(47), 22413-22419.

Ochoa-Herrera, V., León, G., Banihani, Q., Field, J. A., & Sierra-Alvarez, R. (2011). Toxicity of copper(II) ions to microorganisms in biological wastewater treatment systems. *Science of The Total Environment*, *412*, 380-385.

Okocha, R., & Adedeji, O. (2012). Overview of copper toxicity to aquatic life. *Report & Opinion*, *4*(8), 57–68.

Oliveira, H. (2012). Chromium as an environmental pollutant: insights on induced plant toxicity. *Journal of Botany*, *2012*, 1–8.

Onundi, Y. B., Mamun, A. A., Al Khatib, M. F., Al Saadi, M. A., & Suleyman, A. M. (2011). Heavy metals removal from synthetic wastewater by a novel nano-size composite adsorbent. *International Journal of Environmental Science & Technology*, *8*(4), 799-806.

Ozel, F., Kockar, H., & Karaagac, O. (2014). Growth of iron oxide nanoparticles by hydrothermal process: effect of reaction parameters on the nanoparticle size. *Journal of Superconductivity & Novel Magnetism*, *28*(3), 823-829.

Öztürk, D., & Şahan, T. (2015). Design and optimization of Cu(II) adsorption conditions from aqueous solutions by low-cost adsorbent pumice with response surface methodology. *Polish Journal of Environmental Studies*, *24*(4), 1749-1756.

Papageorgiou, S.K., Katsaros, F.K., Favvas, E.P., Romanos, G.E., Athanasekou, C.P., Beltsios, K.G.,

Tzialla, O.I., & Falaras, P. (2012). Alginate fibers as photocatalyst immobilizing agents applied in hybrid photocatalytic/ultrafiltration water treatment processes. *Water Research*, *46*(6), 1858–1872.

Paredes Juárez, G. A., Spasojevic, M., Faas, M. M., & de Vos, P. (2014). Immunological and technical considerations in application of alginate-based microencapsulation systems. *Frontiers in Bioengineering & Biotechnology*, *2*, 1-14.

Pawar, S. N., & Edgar, K. J. (2012). Alginate derivatization: A review of chemistry, properties and applications. *Biomaterials*, *33*(11), 3279–3305.

Pekakis, P. A., Xekoukoulotakis, N. P., & Mantzavinos, D. (2006). Treatment of textile dyehouse wastewater by TiO_2 photocatalysis. *Water Research*, *40*(6), 1276-1286.

Pelaez, M., Nolan, N.T., Pillai, S.C., Seery, M.K., Falaras, P., Kontos, A.G., Dunlop, P.S., Hamilton, J.W., Byrne, J.A., O'shea, K., & Entezari, M.H. (2012). A review on the visible light active titanium dioxide photocatalysts for environmental applications. *Applied Catalysis B: Environmental*, *125*, 331-349.

Postai, D. L., Demarchi, C. A., Zanatta, F., Melo, D. C. C., & Rodrigues, C. A. (2016). Adsorption of rhodamine B and methylene blue dyes using waste of seeds of Aleurites Moluccana, a low cost adsorbent. *Alexandria Engineering Journal*, *55*(2), 1713-1723.

Putra, E., Pranowo, R., Sunarso, J., Indraswati, N., & Ismadji, S. (2009). Performance of activated carbon and bentonite for adsorption of amoxicillin from wastewater: Mechanisms, isotherms and kinetics. *Water Research*, *43*(9), 2419-2430.

Qiusheng, Z., Xiaoyan, L., Jin, Q., Jing, W., & Xuegang, L. (2015). Porous zirconium alginate beads adsorbent for fluoride adsorption from aqueous solutions. *The Royal Society of Chemistry, 5*(3), 2100-2112.

Quiroz, M. A., Bandala, E. R., & Martínez-Huitle, C. A. (2011). Advanced oxidation processes (AOPs) for removal of pesticides from aqueous media. In *Pesticides-Formulations, effects, fate*. InTech.

Rafatullah, M., Sulaiman, O., Hashim, R., & Ahmad, A. (2010). Adsorption of methylene blue on low-cost adsorbents: A review. *Journal of Hazardous Materials*, *177*(1–3), 70–80.

Rahman, M. A., Amin, S. R., & Alam, A. S. (2012). Removal of methylene blue from waste water using activated carbon prepared from rice husk. *Dhaka University Journal of Science*, *60*(2), 185-189.

Răileanu, M., Crişan, M., Niţoi, I., Ianculescu, A., Oancea, P., Crişan, D., & Todan, L. (2013). TiO_2-based nanomaterials with photocatalytic properties for the advanced degradation of xenobiotic compounds from water. A literature survey. *Water, Air, & Soil Pollution*, *224*(6), 1-1548.

Ramli, Z. A. C., Asim, N., Isahak, W. N., Emdadi, Z., Ahmad-Ludin, N., Yarmo, M. A., & Sopian, K. (2014). Photocatalytic degradation of methylene blue under UV light irradiation on prepared carbonaceous. *The Scientific World Journal, 2014*, 1-8.

Rearte, T. A., Bozzano, P. B., Andrade, M. L., & Fabrizio de Iorio, A. (2013). Biosorption of Cr(III) and Pb(II) by Schoenoplectus californicus and Insights into the binding mechanism. *ISRN Chemical Engineering*, *2013*, 1-13.

Reza, K. M., Kurny, A., & Gulshan, F. (2017). Parameters affecting the photocatalytic degradation of dyes using TiO_2: a review. *Applied Water Science*, *7*(4), 1569–1578.

Rezende, R., Bártolo, P. J., Mendes, A., & Filho, R. M. (2007). Experimental characterisation of the alginate gelation process for rapid prototyping. In *The Eighth International Conference on Chemical & Process Engineering* (Vol. 11, pp. 509-514).

Robinson, B. T. J. (2007). Box-Behnken Designs. *Encyclopedia of Statistics in Quality & Reliability*, *2014*, 1–7.

Rocher, V., Siaugue, J.-M., Cabuil, V., & Bee, A. (2008). Removal of organic dyes by magnetic alginate beads. *Water Research*, *42*(4–5), 1290–1298.

Rodriguez, A. R. C. (2015). *Removal of cadmium(II), lead(II) and chromium(VI) in water with nanomaterials.* Unpublished PhD thesis, Autonomous University of Barcelona, Barcelona, Spain.

Roussy, J., Chastellan, P., Van Vooren, M., & Guibal, E. (2005). Treatment of ink-containing wastewater by coagulation/flocculation using biopolymers. *Water South African*, *31*(3), 369-376.

Ruizmoreno, R.G., Martinez, A.I., Castro-rodriguez, R., & Bartolo, P. (2013) Synthesis and characterization of citrate coated magnetite nanoparticles. *Journal of Superconductivity & Novel Magnetism, 26*(3), 709-712.

Sadeghi-Kiakhani, M., Arami, M., & Gharanjig, K. (2013). Dye removal from colored-textile wastewater using chitosan-PPI dendrimer hybrid as a biopolymer: Optimization, kinetic, and isotherm studies. *Journal of Applied Polymer Science*, *127*(4), 2607–2619.

Saien, J., Azizi, A., & Soleymani, A. R. (2014). Photocatalytic reduction of Ni(II) ions using low amounts of titania nanoparticles: rsm modelling, kinetic. *Iranian Journal of Toxicology*, *8*(26), 1136–1144.

Salamat, S., Younesi, H., & Bahramifar, N. (2017). Synthesis of magnetic core–shell Fe_3O_4@TiO_2 nanoparticles from electric arc furnace dust for photocatalytic degradation of steel mill wastewater. *The Royal Society of Chemistry, 7(*31), 19391-19405.

Salehi, M., Hashemipour, H., & Mirzaee, M. (2012). Experimental study of influencing factors and kinetics in catalytic removal of methylene blue with TiO_2 nanopowder. *American Journal of Environmental Engineering*, *2*(1), 1-7.

Salehi, S., Noaparast, M., & Shafaei, S. Z. (2016). Response surface methodology (RSM) for

optimization of chalcopyrite concentrate leaching with silver-coated pyrite. *Physicochemical Problems of Mineral Processing*, *52*(2), 1023–1035.

Samadi, S., Khalilian, F., & Tabatabaee, A. (2014). Synthesis, characterization and application of Cu–TiO_2/chitosan nanocomposite thin film for the removal of some heavy metals from aquatic media. *Journal of Nanostructure in Chemistry*, *4*(1), 1-8.

Samadi, S., Mirseyfifard, S. M. H., Assari, M., & Hassannejad, M. (2017). Effect of hydroxypropyl cellulose (HPC), polyvinylpyrrolidone (PVP) and polyethylene glycol (PEG) on Nd-TiO_2/graphene oxide nanocomposite for removal of lead(II) and copper(II) from aquatic media. *Water Science & Technology*, *76*(1), 15–27.

Sanchez-Dominguez, M., Pemartin, K., & Boutonnet, M. (2012). Preparation of inorganic nanoparticles in oil-in-water microemulsions: A soft and versatile approach. *Current Opinion in Colloid & Interface Science*, *17*(5), 297-305.

Schmitt, F.J., Renger, G., Friedrich, T., Kreslavski, V.D., Zharmukhamedov, S.K., Los, D.A., Kuznetsov, V.V., & Allakhverdiev, S.I. (2014). Reactive oxygen species: re-evaluation of generation, monitoring and role in stress-signaling in phototrophic organisms. *Biochimica et Biophysica Acta (BBA)-Bioenergetics*, *1837*(6), 835-848.

Scherer, C., & Figueiredo Neto, A. M. (2005). Ferrofluids: properties and applications. *Brazilian Journal of Physics*, *35*(3A), 718-727.

Sharma, S., Saxena, R., & Gaur, G. (2014). Study of removal techniques for azo dyes by biosorption: a review. *Journal of Applied Chemistry*, *7*(10), 6-21.

Shi, F., Li, Y., Zhang, Q., & Wang, H. (2012). Synthesis of Fe_3O_4/C/TiO_2 magnetic photocatalyst via vapor phase hydrolysis. *International Journal of Photoenergy*, *2012*, 1-8.

Shi, H., Magaye, R., Castranova, V., & Zhao, J. (2013). Titanium dioxide nanoparticles: a review of current toxicological data. *Particle & Fibre Toxicology*, *10*(1), 1-60.

Shrivastava, V. S. (2012). Photocatalytic degradation of methylene blue dye and chromium metal from wastewater using nanocrystalline TiO_2 semiconductor. *Archives of Applied Science Research*, *4*(3), 1244-1254.

Singanan, M. (2011). Removal of lead(II) and cadmium(II) ions from wastewater using activated biocarbon. *ScienceAsia*, *37*(2), 115–119.

Singh, K. P., Gupta, S., Singh, A. K., & Sinha, S. (2011). Optimizing adsorption of crystal violet dye from water by magnetic nanocomposite using response surface modeling approach. *Journal of Hazardous Materials*, *186*, 1462–1473.

Sivalingam, G., Nagaveni, K., Hegde, M. S., & Madras, G. (2003). Photocatalytic degradation of various dyes by combustion synthesized nano anatase TiO_2. *Applied Catalysis B: Environmental*, *45*(1), 23–38.

Sobhanardakani, S., & Zandipak, R. (2017). Synthesis and application of $TiO_2/SiO_2/Fe_3O_4$ nanoparticles as novel adsorbent for removal of Cd(II), Hg(II) and Ni(II) ions from water samples. *Clean Technologies & Environmental Policy*, *19*(7), 1913–1925.

Sohrabi, S., & Akhlaghian, F. (2015). Modeling and Optimization of phenol degradation over copper-doped titanium dioxide photocatalyst using response surface methodology. *Process Safety & Environmental Protection*, *9*, 120–128.

Son, B. C., Park, K., Song, S. H., & Yoo, Y. J. (2004). Selective biosorption of mixed heavy metal ions using polysaccharides. *Korean Journal of Chemical Engineering*, *21*(6), 1168–1172.

Stanin, F. T. (2005). *The transport and fate of chromium(VI) in the environment* (pp. 165-214). CRC

Press, Florida, USA.

Stasinakis, A. S. (2008). Use of selected advanced oxidation processes (AOPs) for wastewater treatment-a mini review. *Global NEST Journal*, *10*(3), 376-385.

Steinberg, D. M., & Bursztyn, D. (2010). Response surface methodology in biotechnology. *Quality Engineering*, *22*(2), 78–87.

Su, J., Zhang, Y., Xu, S., Wang, S., Ding, H., Pan, S., Wang, G., Li, G., & Zhao, H. (2014). Highly efficient and recyclable triple-shelled $Ag/Fe_3O_4/SiO_2/TiO_2$ photocatalysts for degradation of organic pollutants and reduction of hexavalent chromium ions. *Nanoscale*, *6*(10), 5181-5192.

Sugimoto, T., & Zhou, X. (2002). Synthesis of uniform anatase TiO_2 nanoparticles by the Gel–Sol method: 2. adsorption of OH^- ions to $Ti(OH)_4$ gel and TiO_2 particles. *Journal of Colloid & Interface Science*, *252*(2), 347-353.

Sun, X., Zheng, C., Zhang, F., Yang, Y., Wu, G., Yu, A., & Guan, N. (2009). Size-controlled synthesis of magnetite (Fe_3O_4) nanoparticles coated with glucose and gluconic acid from a single Fe(III) precursor by a sucrose bifunctional hydrothermal method. *The Journal of Physical Chemistry C*, *113*(36), 16002-16008.

Szekalska, M., Puciłowska, A., Szymańska, E., Ciosek, P., & Winnicka, K. (2016). Alginate: current use and future perspectives in pharmaceutical and biomedical applications. *International Journal of Polymer Science*, *2016*, 1-17.

Tabatabaee, G., S. M., Aminzadeh, R., & Abarzani, M. (2014). Use of response surface methodology to study the combined effect of various parameters on hexavalent chromium adsorption. *Chemical Engineering Communications*, *201*(2), 191–208.

Tajabadi, M., & Khosroshahi, M.E. (2012). Effect of alkaline media concentration and modification of

temperature on magnetite synthesis method using $FeSO_4/NH_4OH$. *International Journal of Chemical Engineering & Applications, 3*(3), 206-210.

Tan, Y. N., Wong, C. L., & Mohamed, A. R. (2011). An overview on the photocatalytic activity of nano-doped-TiO_2 in the degradation of organic pollutants. *ISRN Materials Science, 2011*, 1–18.

Tang, Y., Zhang, G., Liu, C., Luo, S., Xu, X., Chen, L., & Wang, B. (2013). Magnetic TiO_2-graphene composite as a high-performance and recyclable platform for efficient photocatalytic removal of herbicides from water. *Journal of Hazardous Materials, 252*, 115-122.

Tansel, B., Sager, J., Rector, T., Garland, J., Strayer, R.F., Levine, L., Roberts, M., Hummerick, M., & Bauer, J., 2006. Significance of hydrated radius and hydration shells on ionic permeability during nanofiltration in dead end and cross flow modes. *Separation & Purification Technology, 51*(1), 40-47.

Tantriratna, P., Wirojanagud, W., Neramittagapong, S., Wantala, K., & Grisdanurak, N. (2011). Optimization for UV-photocatalytic degradation of paraquat over titanium dioxide supported on rice husk silica using Box-Behnken design. *Indian Journal of Chemical Technology, 18*(5), 363–371.

Tao, Y., Ye, L., Pan, J., Wang, Y., & Tang, B. (2009). Removal of Pb(II) from aqueous solution on chitosan/TiO_2 hybrid film. *Journal of Hazardous Materials, 161*(2–3), 718–722.

Tayeb, A. M., & Hussein, D. S. (2015). Synthesis of TiO_2 nanoparticles and their photocatalytic activity for methylene blue. *American Journal of Nanomaterials, 3*(2), 57–63.

Tchounwou, P. B., Yedjou, C. G., Patlolla, A. K., & Sutton, D. J. (2012). Heavy metal toxicity and the environment. In *Molecular, Clinical & Environmental Toxicology* (pp. 133-164). Springer, Basel.

Teh, C. Y., Budiman, P. M., Shak, K. P. Y., & Wu, T. Y. (2016). Recent advancement of coagulation–flocculation and its application in wastewater treatment. *Industrial & Engineering Chemistry*

Research, *55*(16), 4363-4389.

Teixeira, A.P.C., Tristão, J.C., Araujo, M.H., Oliveira, L.C., Moura, F.C., Ardisson, J.D., Amorim, C.C., & Lago, R.M. (2012). Iron: A versatile element to produce materials for environmental applications. *Journal of the Brazilian Chemical Society*, *23*(9), 1579–1593.

Teoh, W. T., Saito, N., & Sato, K. (2011). Effect of alginate concentration on alginate-TiO_2 hydrogel for lead ion removal. *IOP Conference Series: Materials Science & Engineering*, *21*(1), 1-5.

Thirugnanasambandham, K., & Sivakumar, V. (2015). Enzymatic catalysis treatment method of meat industry wastewater using lacasse. *Journal of Environmental Health Science & Engineering*, *13*(1), 1-8.

To, J.W., Chen, Z., Yao, H., He, J., Kim, K., Chou, H.H., Pan, L., Wilcox, J., Cui, Y., & Bao, Z. (2015). Ultrahigh surface area three-dimensional porous graphitic carbon from conjugated polymeric molecular framework. *ACS Central Science*, *1*(2), 68-76.

Toemen, S., Bakar, W. A. W. A., & Ali, R. (2014). Investigation of Ru/Mn/Ce/Al_2O_3 catalyst for carbon dioxide methanation: Catalytic optimization, physicochemical studies and RSM. *Journal of the Taiwan Institute of Chemical Engineers*, *45*(5), 2370-2378.

Topkaya, E., Konyar, M., Yatmaz, H. C., & Öztürk, K. (2014). Pure ZnO and composite ZnO/TiO_2 catalyst plates: A comparative study for the degradation of azo dye, pesticide and antibiotic in aqueous solutions. *Journal of Colloid & Interface Science*, *430*, 6–11.

Tresilwised, N., Pithayanukul, P., & Plank, C. (2005). Factors affecting sizes of magnetic particles formed by chemical co-precipitation. *Mahidol University Journal of Pharmaceutical Sciences*, *32*(3-4), 71-76.

Tschirch, J., Dillert, R., Bahnemann, D., Proft, B., Biedermann, A., & Goer, B. (2008).

Photodegradation of methylene blue in water, a standard method to determine the activity of photocatalytic coatings?. *Research on Chemical Intermediates*, *34*(4), 381-392.

Umoren, S.A., Etim, U.J., & Israel, A.U. (2013). Adsorption of methylene blue from industrial effluent using poly (vinyl alcohol). *Journal of Materials & Environmental Science, 4*(1), 75-86.

us Saqib, N., Adnan, R., & Shah, I. (2016). A mini-review on rare earth metal-doped TiO_2 for photocatalytic remediation of wastewater. *Environmental Science & Pollution Research*, *23*(16), 15941-15951.

Uyar, G., Kaygusuz, H., & Erim, F. B. (2016). Methylene blue removal by alginate–clay quasi-cryogel beads. *Reactive & Functional Polymers*, *106*, 1-7.

Vaez, M., Zarringhalam Moghaddam, A., & Alijani, S. (2012). Optimization and modeling of photocatalytic degradation of azo dye using a response surface methodology (RSM) based on the Central Composite Design with immobilized titania nanoparticles. *Industrial & Engineering Chemistry Research*, *51*(11), 4199-4207.

Villa, S., Caratto, V., Locardi, F., Alberti, S., Sturini, M., Speltini, A., Maraschi, F., Canepa, F., & Ferretti, M. (2016). Enhancement of TiO_2 NPs activity by Fe_3O_4 nano-seeds for removal of organic pollutants in water. *Materials*, *9*(9), 1-9.

Vilhunen, S., & Sillanpää, M. (2010). Recent developments in photochemical and chemical AOPs in water treatment: A mini-review. *Reviews in Environmental Science & Biotechnology*, *9*(4), 323–330.

Vinu, R., & Madras, G. (2011). Photocatalytic degradation of water pollutants using nano-TiO_2. In *Energy efficiency and renewable energy through nanotechnology* (pp. 625-677). Springer, London.

Wahi, R., Kanakaraju, D., & Yusuf, N. A. (2010). Preliminary study on zinc removal from aqueous

solution by sago wastes. *Global Journal of Environmental Research*, *4*(2), 127–134.

Wahyuni, E., Aprilita, N., Hatimah, H., Wulandari, A., & Mudasir, M. (2015). Removal of toxic metal ions in water by photocatalytic method. *American Chemical Science Journal*, *5*(2), 194–201.

Wan Ngah, W. S., Teong, L. C., & Hanafiah, M. A. K. M. (2011). Adsorption of dyes and heavy metal ions by chitosan composites: A review. *Carbohydrate Polymers*, *83*(4), 1446–1456.

Wang, J. L., & Xu, L. J. (2012). Advanced oxidation processes for wastewater treatment: formation of hydroxyl radical and application. *Critical Reviews in Environmental Science & Technology*, *42*(3), 251–325.

Wang, N., Xu, X., Li, H., Yuan, L., & Yu, H. (2016). Enhanced selective adsorption of Pb(II) from aqueous solutions byone-pot synthesis of xanthate-modified chitosan sponge: behaviors and mechanisms. *Industrial & Engineering Chemistry Research*, *55*(47), 12222–12231.

Wang, X., Pehkonen, S. O., & Ray, A. K. (2004). Removal of aqueous Cr(VI) by a combination of photocatalytic reduction and coprecipitation. *Industrial & Engineering Chemistry Research*, *43*(7), 1665–1672.

Wantala, K., Neramittagapong, S., Neramittagapong, A., Kasipar, K., Khaownetr, S., & Chuichulcherm, S. (2012). Photocatalytic degradation of alachlor on Fe-TiO-Immobilized on GAC under black light irradiation using Box-Behnken Design. *Materials Science Forum*, *734*, 306–316.

Wei, J. H., Leng, C. J., Zhang, X. Z., Li, W. H., Liu, Z. Y., & Shi, J. (2009). Synthesis and magnetorheological effect of Fe_3O_4-TiO_2 nanocomposite. *Journal of Physics: Conference Series*, *149*(1), 1-4.

Weng, Y. X., Li, L., Liu, Y., Wang, L., & Yang, G. Z. (2003). Surface-binding forms of carboxylic groups on nanoparticulate TiO_2 surface studied by the interface-sensitive transient triplet-state

molecular probe. *Journal of Physical Chemistry B*, *107*(18), 4356–4363.

Wu, W., He, Q., & Jiang, C. (2008). Magnetic iron oxide nanoparticles: Synthesis and surface functionalization strategies. *Nanoscale Research Letters*, *3*(11), 397–415.

Wu, W., Wu, Z., Yu, T., Jiang, C., & Kim, W. S. (2015). Recent progress on magnetic iron oxide nanoparticles: Synthesis, surface functional strategies and biomedical applications. *Science & Technology of Advanced Materials*, *16*(2), 1-43.

Wuana, R. A., & Okieimen, F. E. (2011). Heavy metals in contaminated soils: A Review of sources, chemistry, risks and best availablestrategies for remediation. *ISRN Ecology*, *2011*, 1–20.

Xu, P., Zeng, G.M., Huang, D.L., Feng, C.L., Hu, S., Zhao, M.H., Lai, C., Wei, Z., Huang, C., Xie, G.X. & Liu, Z.F. (2012). Use of iron oxide nanomaterials in wastewater treatment: A review. *Science of The Total Environment*, *424*, 1–10.

Xu, C., Rangaiah, G. P., & Zhao, X. S. (2014). Photocatalytic degradation of methylene blue by titanium dioxide: experimental and modeling study. *Industrial & Engineering Chemistry Research, 53*(38), 14641-14649.

Xu, X., Zhou, X., Zhang, L., Xu, L., Ma, L., Luo, J., Li, M., & Zeng, L. (2015). Photoredox degradation of different water pollutants (MO, RhB, MB, and Cr(VI)) using Fe–N–S-tri-doped TiO_2 nanophotocatalyst prepared by novel chemical method. *Materials Research Bulletin*, *70*, 106-113.

Yagub, M. T., Sen, T. K., Afroze, S., & Ang, H. M. (2014). Dye and its removal from aqueous solution by adsorption: a review. *Advances in Colloid & Interface Science*, *209*, 172-184.

Yang, X., Chen, W., Huang, J., Zhou, Y., Zhu, Y., & Li, C. (2015). Rapid degradation of methylene blue in a novel heterogeneous Fe_3O_4/rGO/TiO_2-catalyzed photo-Fenton system. *Scientific Reports*, *5*, 1-10.

Yang, Y., Javed, H., Zhang, D., Li, D., Kamath, R., McVey, K., Sra, K., & Alvarez, P.J. (2017). Merits and limitations of TiO_2-based photocatalytic pretreatment of soils impacted by crude oil for expediting bioremediation. *Frontiers of Chemical Science & Engineering*, *11*(3), 387-394.

Yao, H., Fan, M., & Wang, Y. (2015). Magnetic titanium dioxide based nanomaterials : synthesis, characteristics, and photocatalytic application in pollutant degradation. *Journal of Materials Chemistry A: Materials for Energy & Sustainability*, *3*, 17511–17524.

Yao, J., & Wang, C. (2010). Decolorization of methylene blue with sol via UV irradiation photocatalytic degradation. *International Journal of Photoenergy*, *2010*, 1-6.

Yasmina, M., Mourad, K., Mohammed, S. H., & Khaoula, C. (2014). Treatment heterogeneous photocatalysis; Factors influencing the photocatalytic degradation by TiO_2. *Energy Procedia*, *50*, 559–566.

Yonar, T. (2011). Decolourisation of textile dyeing effluents using advanced oxidation processes. In *Advances in treating textile effluent* (pp. 1–26). Bursa, Turkey: InTech.

Yu, X. L., & He, Y. (2017). Application of Box-Behnken designs in parameters optimization of differential pulse anodic stripping voltammetry for lead(II) determination in two electrolytes. *Scientific Reports*, *7*(1), 1-8.

Zainal, N.I., Marsin, F.M., & Ibrahim, W.A.W. (2016). Application of magnetite-calcium alginate sorbent with flame atomic absorption spectrometry for lead(II) ions analysis from water samples. *eProceedings Chemistry*, *1*(1), 36-41.

Zaleska, A. (2008). Doped-TiO_2: a review. *Recent Patents on Engineering*, *2*(3), 157-164.

Zeitoun, M. M., & Mehana, E. E. (2014). Impact of water pollution with heavy metals on fish health: overview and updates. *Global Veterinaria*, *12*(2), 219-231.

Zhang, K., Xu, W., Li, X., Zheng, S., & Xu, G. (2006). Effect of dopant concentration on photocatalytic activity of TiO_2 film doped by Mn non-uniformly. *Open Chemistry*, *4*(2), 234-245.

Zhang, J., Tse, K., Wong, M., Zhang, Y., & Zhu, J. (2016). A brief review of co-doping. *Frontiers of Physics*, *11*(6), 1-21.

Zheng, C., Zhao, L., Zhou, X., Fu, Z., & Li, A. (2013). Treatment technologies for organic wastewater. In *Water Treatment*. InTech.

Zheng, J., Wu, Y., Zhang, Q., Li, Y., Wang, C., & Zhou, Y. (2016). Direct liquid phase deposition fabrication of waxberry-like magnetic Fe_3O_4/TiO_2 core-shell microspheres. *Materials Chemistry & Physics*, *181*, 391-396.

Zuo, R., Du, G., Zhang, W., Liu, L., Liu, Y., Mei, L., & Li, Z. (2014). Photocatalytic degradation of methylene blue using TiO_2 impregnated diatomite. *Advances in Materials Science & Engineering, 2014*, 1-7.

APPENDICES

Appendix 1: SEM micrograph of other synthesized beads (a) Alg/TiO_2/Fe-1, (b) Alg/TiO_2/Fe-3, and (c) Alg/TiO_2/Fe-4 (5000× magnification)

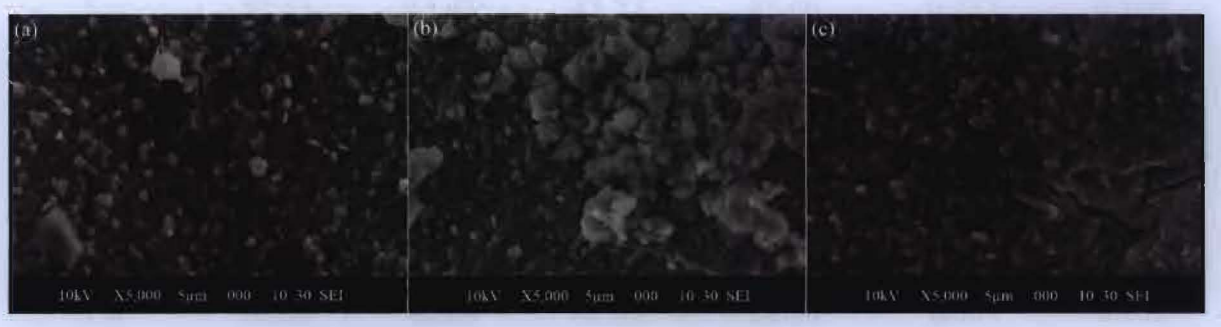

Appendix 2: Calibration curve of standard MB

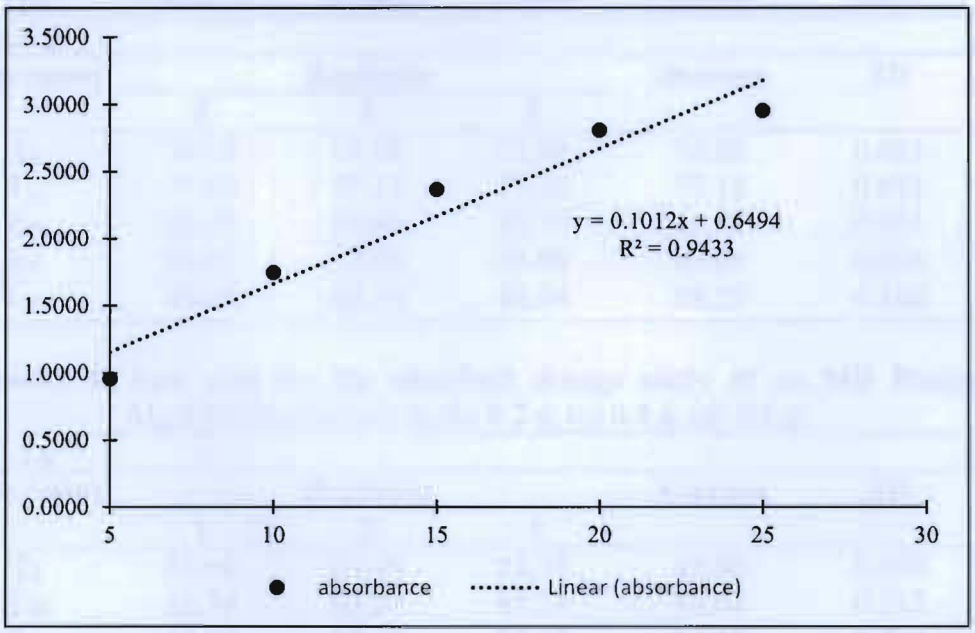

Appendix 3: Raw data for the adsorbent dosage study of on MB Removal by using Alg/TiO_2/Fe-1 (a) 0.1 g, (b) 0.2 g, (c) 0.4 g, (d) 0.6 g

(a) 0.1 g

Time (min)	Replicate			Average	SD	SE
	1	2	3			
T_0	85.52	85.48	85.59	85.53	0.058	0.033
T_{30}	89.32	89.35	89.39	89.35	0.033	0.019
T_{60}	87.21	87.04	87.04	87.10	0.094	0.054
T_{90}	89.35	89.30	89.24	89.30	0.053	0.031
T_{120}	93.18	93.40	93.64	93.41	0.227	0.131

(b) 0.2 g						
Time (min)	**Replicate**			**Average**	**SD**	**SE**
	1	**2**	**3**			
T_0	77.26	77.22	77.21	77.23	0.024	0.014
T_{30}	85.98	85.43	85.57	85.66	0.287	0.166
T_{60}	90.60	90.60	84.66	88.62	3.434	1.983
T_{90}	84.51	84.59	84.63	84.58	0.060	0.035
T_{120}	85.93	85.93	85.61	85.82	0.182	0.105
(c) 0.4 g						
Time (min)	**Replicate**			**Average**	**SD**	**SE**
	1	**2**	**3**			
T_0	78.52	78.47	78.44	78.48	0.037	0.021
T_{30}	82.68	82.68	82.68	82.68	0.004	0.002
T_{60}	81.12	81.11	81.08	81.10	0.022	0.013
T_{90}	84.18	84.10	84.13	84.14	0.042	0.024
T_{120}	85.20	85.20	85.22	85.20	0.011	0.007
(d) 0.6 g						
Time (min)	**Replicate**			**Average**	**SD**	**SE**
	1	**2**	**3**			
T_0	74.15	74.02	73.99	74.05	0.081	0.047
T_{30}	77.08	77.13	77.18	77.13	0.051	0.030
T_{60}	81.78	81.89	81.79	81.82	0.061	0.035
T_{90}	83.07	83.12	83.09	83.09	0.026	0.015
T_{120}	88.40	88.30	88.04	88.25	0.186	0.107

Appendix 4: Raw data for the adsorbent dosage study of on MB Removal by using Alg/TiO_2/Fe-2 (a) 0.1 g, (b) 0.2 g, (c) 0.4 g, (d) 0.6 g

(a) 0.1 g						
Time (min)	**Replicate**			**Average**	**SD**	**SE**
	1	**2**	**3**			
T_0	83.69	83.45	84.57	83.90	0.590	0.341
T_{30}	83.74	83.37	83.74	83.61	0.212	0.122
T_{60}	87.03	87.43	87.03	87.16	0.230	0.133
T_{90}	90.54	90.18	90.54	90.42	0.206	0.119
T_{120}	95.02	94.29	93.02	94.11	1.015	0.586
(b) 0.2 g						
Time (min)	**Replicate**			**Average**	**SD**	**SE**
	1	**2**	**3**			
T_0	88.72	89.02	88.49	88.75	0.268	0.155
T_{30}	93.92	92.89	93.92	93.57	0.594	0.343
T_{60}	81.93	81.93	94.70	86.19	7.373	4.257
T_{90}	94.96	94.96	94.99	94.97	0.018	0.010
T_{120}	97.61	97.53	97.61	97.59	0.050	0.029
(c) 0.4 g						
Time (min)	**Replicate**			**Average**	**SD**	**SE**
	1	**2**	**3**			

T_0	73.19	84.20	83.45	80.28	6.154	3.553
T_{30}	78.70	78.26	78.70	78.55	0.255	0.147
T_{60}	81.74	81.48	81.74	81.65	0.146	0.084
T_{90}	82.73	82.34	82.73	82.60	0.223	0.129
T_{120}	82.22	82.28	82.26	82.25	0.031	0.018
(d) 0.6 g						
Time (min)	**Replicate**			**Average**	**SD**	**SE**
	1	**2**	**3**			
T_0	78.61	78.62	78.93	78.72	0.182	0.105
T_{30}	78.19	78.14	78.29	78.21	0.075	0.043
T_{60}	84.82	84.95	84.82	84.87	0.075	0.043
T_{90}	89.39	89.39	89.37	89.38	0.015	0.009
T_{120}	93.77	93.77	93.75	93.76	0.007	0.004

Appendix 5: Raw data for the adsorbent dosage study of on MB Removal by using Alg/TiO_2/Fe-3 (a) 0.1 g, (b) 0.2 g, (c) 0.4 g, (d) 0.6 g

(a) 0.1 g						
Time (min)	**Replicate**			**Average**	**SD**	**SE**
	1	**2**	**3**			
T_0	72.50	72.97	71.68	72.38	0.658	0.380
T_{30}	77.27	75.99	76.04	76.43	0.724	0.418
T_{60}	75.64	72.58	72.69	73.64	1.735	1.002
T_{90}	76.21	74.30	74.15	74.89	1.148	0.663
T_{120}	82.83	79.76	79.90	80.83	1.731	0.999
(b) 0.2 g						
Time (min)	**Replicate**			**Average**	**SD**	**SE**
	1	**2**	**3**			
T_0	72.18	71.81	71.68	71.89	0.259	0.150
T_{30}	83.69	83.40	83.58	83.55	0.150	0.086
T_{60}	78.93	78.80	76.92	78.21	1.126	0.650
T_{90}	81.33	81.33	81.26	81.31	0.040	0.023
T_{120}	80.86	81.10	80.90	80.95	0.131	0.075
(c) 0.4 g						
Time (min)	**Replicate**			**Average**	**SD**	**SE**
	1	**2**	**3**			
T_0	82.12	76.07	75.63	77.94	3.622	2.091
T_{30}	76.61	76.87	76.61	76.70	0.149	0.086
T_{60}	80.72	80.46	80.46	80.55	0.149	0.086
T_{90}	97.40	97.40	97.37	97.39	0.016	0.009
T_{120}	82.43	82.34	81.57	82.11	0.474	0.274
(d) 0.6 g						
Time (min)	**Replicate**			**Average**	**SD**	**SE**
	1	**2**	**3**			

T_0	76.45	76.33	75.51	76.10	0.510	0.294
T_{30}	76.93	76.21	77.69	76.94	0.744	0.430
T_{60}	80.26	80.22	80.22	80.23	0.023	0.014
T_{90}	81.87	81.85	81.87	81.86	0.014	0.008
T_{120}	83.19	83.26	83.04	83.16	0.112	0.065

Appendix 6: Raw data for the adsorbent dosage study of on MB Removal by using Alg/TiO_2/Fe-4 (a) 0.1 g, (b) 0.2 g, (c) 0.4 g, (d) 0.6 g

(a) 0.1 g						
Time (min)	**Replicate**			**Average**	**SD**	**SE**
	1	**2**	**3**			
T_0	63.97	64.08	63.05	63.70	0.566	0.327
T_{30}	67.23	67.23	67.08	67.18	0.085	0.049
T_{60}	63.57	62.83	64.16	63.52	0.669	0.386
T_{90}	75.94	75.94	75.88	75.92	0.036	0.021
T_{120}	77.20	77.58	76.38	77.05	0.614	0.354
(b) 0.2 g						
Time (min)	**Replicate**			**Average**	**SD**	**SE**
	1	**2**	**3**			
T_0	69.09	74.12	69.09	70.77	2.905	1.677
T_{30}	81.38	81.36	81.28	81.34	0.051	0.030
T_{60}	85.49	85.00	84.49	84.99	0.504	0.291
T_{90}	82.00	81.44	82.17	81.87	0.384	0.222
T_{120}	87.01	86.34	86.35	86.57	0.387	0.224
(c) 0.4 g						
Time (min)	**Replicate**			**Average**	**SD**	**SE**
	1	**2**	**3**			
T_0	60.59	60.16	60.11	60.29	0.266	0.154
T_{30}	70.73	70.94	70.34	70.67	0.305	0.176
T_{60}	73.50	73.41	73.11	73.34	0.204	0.118
T_{90}	75.58	74.91	75.57	75.35	0.387	0.223
T_{120}	89.26	89.61	88.93	89.27	0.340	0.196
(d) 0.6 g						
Time (min)	**Replicate**			**Average**	**SD**	**SE**
	1	**2**	**3**			
T_0	76.36	76.03	72.78	75.06	1.980	1.143
T_{30}	78.21	78.15	77.57	77.97	0.355	0.205
T_{60}	80.00	79.98	79.55	79.84	0.254	0.147
T_{90}	82.80	83.04	82.27	82.70	0.395	0.228
T_{120}	86.42	86.55	86.55	86.50	0.075	0.043

Appendix 7: UV Profile of MB photodegradation by using Alg/TiO_2/Fe-2

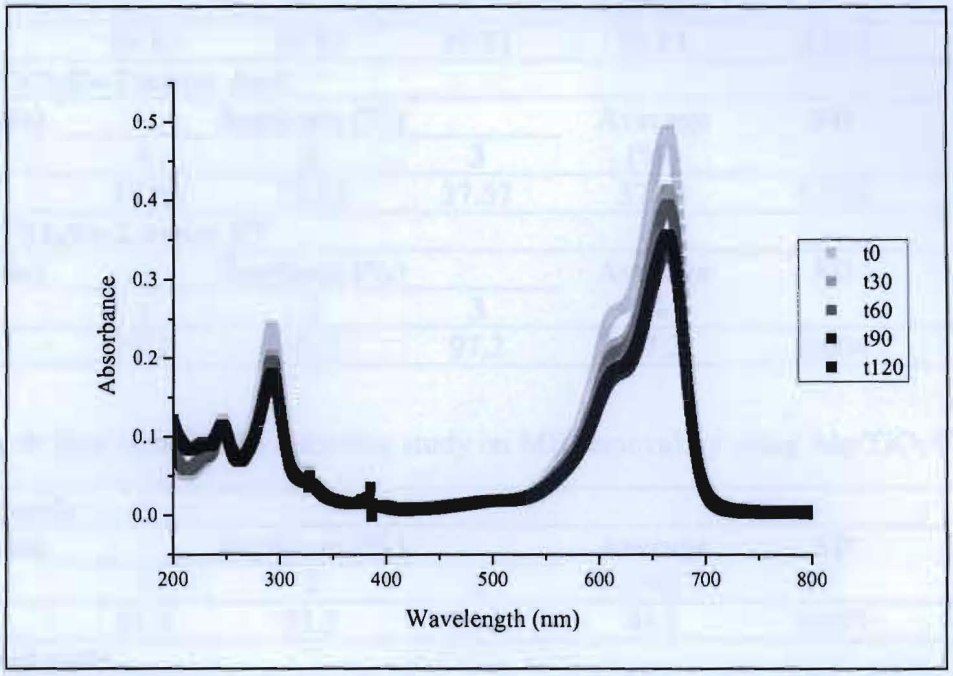

Appendix 8: Raw data for MB removal by using Alg/TiO_2/Fe-2 in aqueous solution under different conditions

(a) MB alone						
Time (min)	**Replicate (%)**			**Average (%)**	**SD**	**SE**
	1	2	3			
T_{120}	65.92	62.72	65.92	64.85	1.8499	1.0680
(b) Alg-5%						
Time (min)	**Replicate (%)**			**Average (%)**	**SD**	**SE**
	1	2	3			
T_{120}	31.53	37.26	74.09	47.63	23.099	13.336
(c) TiO_2/Alg						
Time (min)	**Replicate (%)**			**Average (%)**	**SD**	**SE**
	1	**2**	**3**			
T_{120}	49.22	49.22	49.11	49.18	0.068	0.039
(d) MNPs/Alg						
Time (min)	**Replicate (%)**			**Average (%)**	**SD**	**SE**
	1	**2**	**3**			
T_{120}	70.66	70.66	73.83	71.71	1.830	1.057
(e) TiO_2 slurry						
Time (min)	**Replicate (%)**			**Average (%)**	**SD**	**SE**
	1	**2**	**3**			
T_{120}	100.00	100.00	100.00	100.00	0.000	0.000
(f) Alg/TiO_2/Fe-2 under sunlight						
Time (min)	**Replicate (%)**				**SD**	**SE**

	1	2	3	Average (%)		
T_{120}	99.85	99.83	99.83	99.84	0.010	0.006
(g) Alg/TiO_2/Fe-2 under dark						
Time (min)	**Replicate (%)**			**Average**	**SD**	**SE**
	1	**2**	**3**	**(%)**		
T_{120}	37.54	37.52	37.57	37.54	0.026	0.015
(h) Alg/TiO_2/Fe-2 under UV						
Time (min)	**Replicate (%)**			**Average**	**SD**	**SE**
	1	**2**	**3**	**(%)**		
T_{120}	97.2	97.2	97.2	97.2	0.004	0.003

Appendix 9: Raw data for the recycling study on MB removal by using Alg/TiO_2/Fe-2

(a) First cycle						
Time (min)	**Replicate (%)**			**Average**	**SD**	**SE**
	1	**2**	**3**	**(%)**		
T_{120}	93.0	93.2	93.2	93.1	0.097	0.056
(b) Second cycle						
Time (min)	**Replicate (%)**			**Average**	**SD**	**SE**
	1	2	3	(%)		
T_{120}	87.7	87.7	87.7	87.7	0.007	0.004
(c) Third cycle						
Time (min)	**Replicate (%)**			**Average**	**SD**	**SE**
	1	**2**	**3**	**(%)**		
T_{120}	87.7	89.2	88.6	88.5	0.776	0.448

Appendix 10: Raw data for the adsorbent dosage study of Pb(II) ions removal by using Alg/TiO_2/Fe-2

(a) 0.1 g						
Time (min)	**Replicate (%)**			**Average**	**SD**	**SE**
	1	**2**	**3**	**(%)**		
T_0	54.7	53.9	54.8	54.5	0.52479	0.30299
T_{120}	59.6	61.0	59.6	60.1	0.81858	0.47261
(b) 0.2 g						
Time (min)	**Replicate (%)**			**Average**	**SD**	**SE**
	1	**2**	**3**	**(%)**		
T_0	58.2	58.8	58.0	58.3	0.433	0.250
T_{120}	68.3	68.6	68.3	68.4	0.188	0.109
(c) 0.4 g						
Time (min)	**Replicate (%)**			**Average**	**SD**	**SE**
	1	**2**	**3**	**(%)**		
T_0	65.1	65.8	65.1	65.3	0.40418	0.23335
T_{120}	80.9	80.8	80.7	80.8	0.12816	0.07399
(d) 0.6 g						

Time (min)	Replicate (%)			Average (%)	SD	SE
	1	2	3			
T_0	75.0	75.2	75.8	75.3	0.400	0.231
T_{120}	90.0	89.7	90.0	89.9	0.152	0.088
(e) 0.8 g						
Time (min)	**Replicate (%)**			**Average (%)**	**SD**	**SE**
	1	**2**	**3**			
T_0	66.8	66.2	66.8	66.6	0.383	0.221
T_{120}	88.9	88.9	88.9	88.9	0.018	0.010
(f) 1.0 g						
Time (min)	**Replicate (%)**			**Average (%)**	**SD**	**SE**
	1	**2**	**3**			
T_0	74.1	73.6	73.9	73.8	0.24111	0.1392
T_{120}	93.8	93.8	93.8	93.8	0.01893	0.01093

Appendix 11: Raw data for the adsorbent dosage study of Cr(III) ions removal by using Alg/TiO_2/Fe-2

(a) 0.1 g						
Time (min)	**Replicate (%)**			**Average (%)**	**SD**	**SE**
	1	**2**	**3**			
T_0	48.0	47.4	47.8	47.7	0.278	0.161
T_{120}	48.0	48.3	47.5	47.9	0.404	0.233
(b) 0.2 g						
Time (min)	**Replicate (%)**			**Average (%)**	**SD**	**SE**
	1	**2**	**3**			
T_0	48.3	48.2	47.8	48.1	0.25658	0.14814
T_{120}	48.9	48.5	49.3	48.9	0.40104	0.23154
(c) 0.4 g						
Time (min)	**Replicate (%)**			**Average (%)**	**SD**	**SE**
	1	**2**	**3**			
T_0	49.7	49.7	49.6	49.6	0.07638	0.0441
T_{120}	51.1	51.3	51.5	51.3	0.23785	0.13733
(d) 0.6 g						
Time (min)	**Replicate (%)**			**Average (%)**	**SD**	**SE**
	1	**2**	**3**			
T_0	50.1	50.2	50.2	50.2	0.03055	0.01764
T_{120}	53.7	53.3	53.2	53.4	0.22322	0.12887
(e) 0.8 g						
Time (min)	**Replicate (%)**			**Average (%)**	**SD**	**SE**
	1	**2**	**3**			
T_0	10.3	9.5	11.4	10.4	0.95175	0.54949
T_{120}	20.1	18.4	19.7	19.4	0.89768	0.51828
(f) 1.0 g						
Time (min)	**Replicate (%)**				**SD**	**SE**

	1	2	3	Average (%)		
T_0	12.3	10.7	12.3	11.8	0.910	0.525
T_{120}	31.0	32.1	31.7	31.6	0.535	0.309

Appendix 12: Raw data for the adsorbent dosage study of Cu(II) ions removal by using Alg/TiO_2/Fe-2

(a) 0.1 g						
Time (min)	**Replicate (%)**			**Average**	**SD**	**SE**
	1	**2**	**3**	**(%)**		
T_0	50.41	49.5	50.485	50.1317	0.548	0.317
T_{120}	49.5	49.75	49	49.4167	0.382	0.220
(b) 0.2 g						
Time (min)	**Replicate (%)**			**Average**	**SD**	**SE**
	1	**2**	**3**	**(%)**		
T_0	49.3	49.4	49.3	49.33333	0.058	0.033
T_{120}	49.3	49.55	49.8	49.55	0.250	0.144
(c) 0.4 g						
Time (min)	**Replicate (%)**			**Average**	**SD**	**SE**
	1	**2**	**3**	**(%)**		
T_0	50.01	50.22	50	50.0767	0.124	0.072
T_{120}	52.5	52.26	52.17	52.31	0.171	0.098
(d) 0.6 g						
Time (min)	**Replicate (%)**			**Average**	**SD**	**SE**
	1	**2**	**3**	**(%)**		
T_0	52.1	51.8	52.5	52.1	0.355	0.205
T_{120}	55.6	56.1	55.7	55.8	0.245	0.141
(e) 0.8 g						
Time (min)	**Replicate (%)**			**Average**	**SD**	**SE**
	1	**2**	**3**	**(%)**		
T_0	10.5	9.1	10.5	10.0	0.751	0.433
T_{120}	24.1	23.7	24.1	24.0	0.218	0.126
(f) 1.0 g						
Time (min)	**Replicate**			**Replicate**	**Average**	**SE**
	1	**2**	**3**	**(%)**	**(%)**	
T_0	14.0	12.9	14.4	13.7	0.785	0.453
T_{120}	40.2	40.7	39.9	40.2	0.382	0.220

Appendix 13: Pb(II) ions removal by using Alg/TiO_2/Fe-2 in aqueous solution under different conditions

(a) MHM alone						
Time (min)	**Replicate (%)**			**Average**	**SD**	**SE**
	1	**2**	**3**	**(%)**		
T_{72}	97.2	97.2	97.2	97.2	0.038	0.022

(b) Alg-5%						
Time (min)	**Replicate (%)**			**Average (%)**	**SD**	**SE**
	1	**2**	**3**			
T_{72}	97.9	97.9	97.9	97.9	0.018	0.011
(c) TiO_2/Alg						
Time (min)	**Replicate (%)**			**Average (%)**	**SD**	**SE**
	1	**2**	**3**			
T_{72}	98.8	98.8	98.8	98.8	0.005	0.003
(d) MNPs/Alg						
Time (min)	**Replicate (%)**			**Average (%)**	**SD**	**SE**
	1	**2**	**3**			
T_{72}	99.8	99.8	99.8	99.8	0.001	0.001
(e) TiO_2 slurry						
Time (min)	**Replicate (%)**			**Average (%)**	**SD**	**SE**
	1	**2**	**3**			
T_{72}	99.9	99.9	99.9	99.9	0.004	0.002
(f) Alg/TiO_2/Fe-2 under sunlight						
Time (min)	**Replicate (%)**			**Average (%)**	**SD**	**SE**
	1	**2**	**3**			
T_{72}	95.2	95.3	95.4	95.3	0.084	0.049
(g) Alg/TiO_2/Fe-2 under dark						
Time (min)	**Replicate (%)**			**Average (%)**	**SD**	**SE**
	1	**2**	**3**			
T_{72}	97.9	97.9	97.9	97.9	0.010	0.006
(h) Alg/TiO_2/Fe-2 under UV						
Time (min)	**Replicate (%)**			**Average (%)**	**SD**	**SE**
	1	**2**	**3**			
T_{72}	99.6	99.6	99.6	99.6	0.003	0.002

Appendix 14: Cr(III) ions removal by using Alg/TiO_2/Fe-2 in aqueous solution under different conditions

(a) MHM alone						
Time (min)	**Replicate (%)**			**Average (%)**	**SD**	**SE**
	1	**2**	**3**			
T_{72}	97.2	97.1	97.3	97.2	0.114	0.066
(b) Alg-5%						
Time (min)	**Replicate (%)**			**Average (%)**	**SD**	**SE**
	1	**2**	**3**			
T_{72}	90.3	90.0	90.2	90.2	0.171	0.099
(c) TiO_2/Alg						
Time (min)	**Replicate (%)**			**Average (%)**	**SD**	**SE**
	1	**2**	**3**			
T_{72}	93.1	93.0	93.4	93.2	0.196	0.113
(d) MNPs/Alg						
Time (min)	**Replicate (%)**				**SD**	**SE**

	1	2	3	Average (%)		
T_{72}	79.9	79.6	79.8	79.8	0.155	0.090
(g) Alg/TiO_2/Fe-2 under dark						
Time (min)	**Replicate (%)**			**Average**	**SD**	**SE**
	1	**2**	**3**	**(%)**		
T_{72}	88.6	88.8	88.6	88.7	0.082	0.047
(h) Alg/TiO_2/Fe-2 under UV						
Time (min)	**Replicate (%)**			**Average**	**SD**	**SE**
	1	**2**	**3**	**(%)**		
T_{72}	98.4	98.4	98.4	98.4	0.014	0.008

Appendix 16: Raw data for the recycling study on Pb(II) ions removal by using Alg/TiO_2/Fe-2

(a) First cycle						
Time (min)	**Replicate (%)**			**Average**	**SD**	**SE**
	1	**2**	**3**	**(%)**		
T_{72}	98.5	98.6	98.7	98.6	0.107	0.062
(b) Second cycle						
Time (min)	**Replicate (%)**			**Average**	**SD**	**SE**
	1	**2**	**3**	**(%)**		
T_{72}	99.7	99.7	99.6	99.6	0.004	0.002
(c) Third cycle						
Time (min)	**Replicate**			**Average**	**SD**	**SE**
	1	**2**	**3**			
T_{72}	98.7	98.8	98.8	98.8	0.036	0.021

Appendix 17: Raw data for the recycling study on Cr(III) ions removal by using Alg/TiO_2/Fe-2

(a) First cycle						
Time (min)	**Replicate (%)**			**Average**	**SD**	**SE**
	1	**2**	**3**	**(%)**		
T_{72}	98.7	98.8	98.7	98.7	0.026	0.015
(b) Second cycle						
Time (min)	**Replicate (%)**			**Average**	**SD**	**SE**
	1	**2**	**3**	**(%)**		
T_{72}	97.8	98.0	97.8	97.9	0.065	0.038
(c) Third cycle						
Time (min)	**Replicate (%)**			**Average**	**SD**	**SE**
	1	**2**	**3**	**(%)**		
T_{72}	98.6	98.5	98.5	98.6	0.064	0.037

Appendix 18: Raw data for the recycling study on Cu(II) ions removal by using Alg/TiO_2/Fe-2

(a) First cycle						
Time (min)	**Replicate (%)**			**Average (%)**	**SD**	**SE**
	1	**2**	**3**			
T_{120}	98.5	98.5	98.6	98.6	0.032	0.019
(b) Second cycle						
Time (min)	**Replicate (%)**			**Average (%)**	**SD**	**SE**
	1	**2**	**3**			
T_{120}	97.9	97.9	98.0	97.9	0.050	0.029
(c) Third cycle						
Time (min)	**Replicate (%)**			**Average (%)**	**SD**	**SE**
	1	**2**	**3**			
T_{120}	98.2	98.2	98.1	98.2	0.034	0.020

Appendix 19: Raw data for Pb(II) ions removal for the application of Alg/TiO_2/Fe-2 in MHM river water

(a) River water alone						
Time (min)	**Replicate (%)**			**Average (%)**	**SD**	**SE**
	1	**2**	**3**			
T_{72}	97.2	97.2	97.2	97.2	0.032	0.018
(b) Alg/TiO_2/Fe-2 under sunlight						
Time (min)	**Replicate (%)**			**Average (%)**	**SD**	**SE**
	1	**2**	**3**			
T_{72}	99.6	99.6	99.6	99.6	0.015	0.009
(c) Alg/TiO_2/Fe-2 under dark						
Time (min)	**Replicate (%)**			**Average (%)**	**SD**	**SE**
	1	**2**	**3**			
T_{72}	99.2	99.2	99.2	99.4	0.368	0.213
(d) Alg/TiO_2/Fe-2 under UV						
Time (min)	**Replicate (%)**			**Average (%)**	**SD**	**SE**
	1	**2**	**3**			
T_{72}	99.9	98.5	99.8	99.4	0.798	0.461

Appendix 21: Raw data for Cr(III) ions removal for the application of Alg/TiO_2/Fe-2 in MHM river water

(a) River water alone						
Time (min)	**Replicate (%)**			**Average (%)**	**SD**	**SE**
	1	**2**	**3**			
T_{72}	97.7	97.7	97.7	97.2	0.026	0.015
(b) Alg/TiO_2/Fe-2 under sunlight						
Time (min)	**Replicate (%)**				**SD**	**SE**

	1	2	3	Average (%)		
T_{72}	99.6	99.6	99.6	99.6	0.002	0.001
(c) Alg/TiO_2/Fe-2 under dark						
Time (min)	**Replicate (%)**			**Average**	**SD**	**SE**
	1	**2**	**3**	**(%)**		
T_{72}	99.7	99.7	99.7	99.7	0.003	0.002
(d) Alg/TiO_2/Fe-2 under UV						
Time (min)	**Replicate (%)**			**Average**	**SD**	**SE**
	1	**2**	**3**	**(%)**		
T_{72}	99.4	99.1	99.1	99.2	0.207	0.120

Appendix 22: Raw data for Cu(II) ions removal for the application of Alg/TiO_2/Fe-2 in MHM river water

(a) River water alone						
Time (min)	**Replicate (%)**			**Average**	**SD**	**SE**
	1	**2**	**3**	**(%)**		
T_{72}	97.8	97.8	97.8	97.8	0.008	0.005
(b) Alg/TiO_2/Fe-2 under sunlight						
Time (min)	**Replicate (%)**			**Average**	**SD**	**SE**
	1	**2**	**3**	**(%)**		
T_{72}	99.6	99.6	99.6	99.6	0.004	0.002
(c) Alg/TiO_2/Fe-2 under dark						
Time (min)	**Replicate (%)**			**Average**	**SD**	**SE**
	1	**2**	**3**	**(%)**		
T_{72}	99.7	99.7	99.7	99.7	0.014	0.008
(d) Alg/TiO_2/Fe-2 under UV						
Time (min)	**Replicate (%)**			**Average**	**SD**	**SE**
	1	**2**	**3**	**(%)**		
T_{72}	100.0	97.9	97.9	98.6	1.200	0.693